NASA CONTRACTOR REPORT

NASA CR-2046

INVESTIGATION OF THE APPLICABILITY OF THE FREE-WING PRINCIPLE TO LIGHT, GENERAL AVIATION AIRCRAFT

by Richard F. Porter, Ross G. Luce, and Joe H. Brown, Jr.

Prepared by
BATTELLE MEMORIAL INSTITUTE
COLUMBUS LABORATORIES
Columbus, Ohio 43201
for Langley Research Center

NATIONAL AERONAUTICS AND SPACE ADMINISTRATION • WASHINGTON, D. C. • JUNE 1972

1. Report No.	2. Government Accession No.	3. Recipient's Catalog No.
NASA CR-2046		

4. Title and Subtitle	5. Report Date
Investigation of the Applicability of the Free-Wing Principle to Light, General Aviation Aircraft	June 1972
	6. Performing Organization Code

7. Author(s)	8. Performing Organization Report No.
Richard F. Porter, Ross G. Luce, and Joe H. Brown, Jr.	

9. Performing Organization Name and Address	10. Work Unit No.
Battelle Memorial Institute Columbus Laboratories Columbus, Ohio 43201	760-71-03-01
	11. Contract or Grant No. NAS1-10174

12. Sponsoring Agency Name and Address	13. Type of Report and Period Covered
National Aeronautics and Space Administration Washington, D. C. 20546	Contractor Report
	14. Sponsoring Agency Code

15. Supplementary Notes

16. Abstract

A previous study indicated substantial gust-alleviation benefits for aircraft employing an unconventional wing, free to pivot about a spanwise axis forward of its aerodynamic center and subject only to aerodynamic pitching moments imposed by lift and drag forces and a trailing-edge control surface.

The investigation reported in this document is an extension of the previous study, with emphasis on the practical application of the free-wing concept to light, general aviation aircraft. Analytical work, supported by limited wind-tunnel experiments, was performed to evaluate the impact of selected design and certification constraints appropriate to the type of aircraft being considered.

17. Key Words (Suggested by Author(s))	18. Distribution Statement
Free-wing principle Light general aviation aircraft Aerodynamics Analytical work Wind-tunnel experiments	Unclassified - Unlimited

19. Security Classif. (of this report)	20. Security Classif. (of this page)	21. No. of Pages	22. Price*
Unclassified	Unclassified	120	$3.00

*For sale by the National Technical Information Service, Springfield, Virginia 22151

CONTENTS

CONTENTS (Continued)

INVESTIGATION OF THE APPLICABILITY OF THE FREE-WING PRINCIPLE TO LIGHT, GENERAL AVIATION AIRCRAFT

Richard F. Porter, Ross G. Luce, & Joe H. Brown, Jr.
BATTELLE
Columbus Laboratories

SUMMARY

A previous study indicated substantial gust-alleviation benefits for aircraft employing an unconventional wing, free to pivot about a spanwise axis forward of its aerodynamic center and subject only to aerodynamic pitching moments imposed by lift and drag forces and a trailing edge control surface. Although the primary benefit was found to be in the attenuation of normal load factor disturbances through symmetrical passive motion of the wing panels, rolling disturbances were also reduced by permitting differential freedom of the left and right wing sections.

The investigation reported in this document is an extension of the previous study, with emphasis on the practical application of the free-wing concept to light, general aviation aircraft. Analytical work, supported by limited wind-tunnel experiments, was performed to evaluate the impact of selected design and certification constraints appropriate to the type of aircraft being considered.

It is concluded that the free-wing concept can be applied to unsophisticated, low wing-loading light aircraft to provide ride quality, based upon normal load factor attenuation in turbulence, equal or superior to aircraft employing much higher wing loadings. Furthermore, all pertinent handling qualities and certification criteria can be met without recourse to stability augmentation, either active or passive.

The major concessions to practical constraints include: (1) the elimination of differential panel freedom for this class of aircraft, thereby precluding inherent attenuation of rolling disturbances, (2) the incorporation of a fixed wing-center-section between the free panels, and (3) the use of leading-edge slats for landing and takeoff.

INTRODUCTION

Background

The basic problem attacked in this investigation is the relatively poor ride quality of aircraft with low wing loadings and the quest for a practical

means of curing this deficiency for light, general aviation aircraft. Attention is focused on a unique design approach for the improvement of rough-air comfort, the free-wing concept.

Low wing loading has long been synonomous with poor ride quality in turbulence, a fact which has probably been a significant deterrent to more widespread acceptance of light aircraft as a practical means of transportation. The problem is compounded by the fact that light aircraft spend a major portion of their flight time at the lower altitudes where measureable turbulence is most likely to be encountered, even in good weather.

An increase in wing loading can be expected to produce ride improvement, but this approach is constrained by the need to maintain low minimum flying speeds. Not only is a low speed capability desirable from an operational standpoint for aircraft in this class, but Federal airworthiness standards (FAR Part 23) require a minimum speed of 61 knots or less for single engine aircraft. Even with well designed mechanical high-lift devices, it appears that a wing loading of 40 lb/ft^2 is an approximate practical upper limit; this may be compared to wing loadings of 90 to 110 lb/ft^2 typical of the commercial jet transport aircraft which have enjoyed wide acceptance by the traveling public.

An alternative approach to ride improvement is a gust-alleviation system. A review of work in this area is contained in Appendix C of this report; but, to summarize, these systems may roughly be classified as either active or passive in their mode of operation.

Active gust alleviation systems incorporate a sensing device, usually an angle of attack vane or accelerometer, which provides input signals to a control actuation system to relieve perturbations in rough air. Although such systems show great promise for certain applications, their potential for use in light civil aircraft is strongly inhibited by economic considerations and system complexity.

Passive gust alleviation systems rely upon pure aerodynamic and mechanical reactions to displace various portions of the airframe. Although most passive schemes have proven unsatisfactory, a noteworthy example is that of Hirsh (ref. 1). Although his system appears mechanically complicated, it has been successfully demonstrated in flight. The free-wing concept is also an example of a passive gust alleviation device; and it has also been flown, although in a somewhat different form than considered in this report, by Spratt (ref. 2).

The Free-Wing Concept

The basic concept of the free wing was disclosed in U.S. Patent No. 2,347,230, now expired, issued in 1944 to Mr. Daniel R. Zuck, who built a small prototype aircraft in 1945 as a private venture. This aircraft was never successcessfully flown, and the only analytical work known to have been performed to predict the dynamic behavior of such an aircraft is reported in Reference 3.

As conceived by Zuck, a free-wing aircraft differs from a conventional airplane in that the two panels of the fuselage-mounted wing are free to move independently about a spanwise axis and are controlled by means of trailing-edge control surfaces. Each wing panel is completely free to rotate about its spanwise axis, subject to aerodynamic moments but otherwise unrestricted by mechanical constraints. To provide static pitching stability, the axis of rotation is located forward of the chordwise aerodynamic center of the wing panel, as shown in Figure 1. The wing is brought to an equilibrium angle of attack through a balance of moments created by the trailing-edge surface, which is controlled by the pilot, and the torques produced by the lift and drag forces.

The gust alleviation feature of the free-wing is caused by the fact that a stable lifting surface tends to maintain a prescribed lift coefficient by responding to natural pitching moments which accompany changes in flow direction. While all stable aircraft tend to relieve the lift increment due to a vertical gust by pitching into the relative wind, the rapidity of the alleviating motion depends upon the pitching moment of inertia. Because of the greatly reduced inertia of the wing panel, compared to the aircraft as a whole, the free-wing concept produces significant reductions in turbulence responses.

A difficulty common to all gust alleviation systems, active or passive, is the fact that the aircraft cannot simply be made insensitive to angle of attack changes; for if it were, static longitudinal stability would be lost. Furthermore, the system must distinguish between angle-of-attack changes caused by turbulence and those commanded by the pilot. A strong argument for the free-wing concept is that it inherently avoids both of these problems; instead of reducing the static longitudinal stability of the aircraft, it employs it as the basic mechanism of alleviation. In addition, the equilibrium angle of attack is readily controlled by the pilot through displacement of the trailing-edge control surface.

Previous Analytical Work

The work reported in Reference 3 was conducted under Contract No. NAS2-5116, and is the only known analytical effort to predict the fundamental dynamic behavior of aircraft employing the free-wing principle. In that study, the complete set of equations of motion were developed. The controls-fixed set of equations described a system with eight degrees of freedom; six conventional variables to define the spatial position and orientation of the fuselage assembly, and two additional variables to define the respective left and right wing panel displacements with respect to the fuselage.

The complete set of equations were then linearized about a straight and level equilibrium flight condition, which permitted the separation of the equations into two uncoupled sets describing the lateral-directional and longitudinal motions, respectively. The characteristic roots of each set of equations was examined and conventional power spectral density techniques were used for turbulence response calculations.

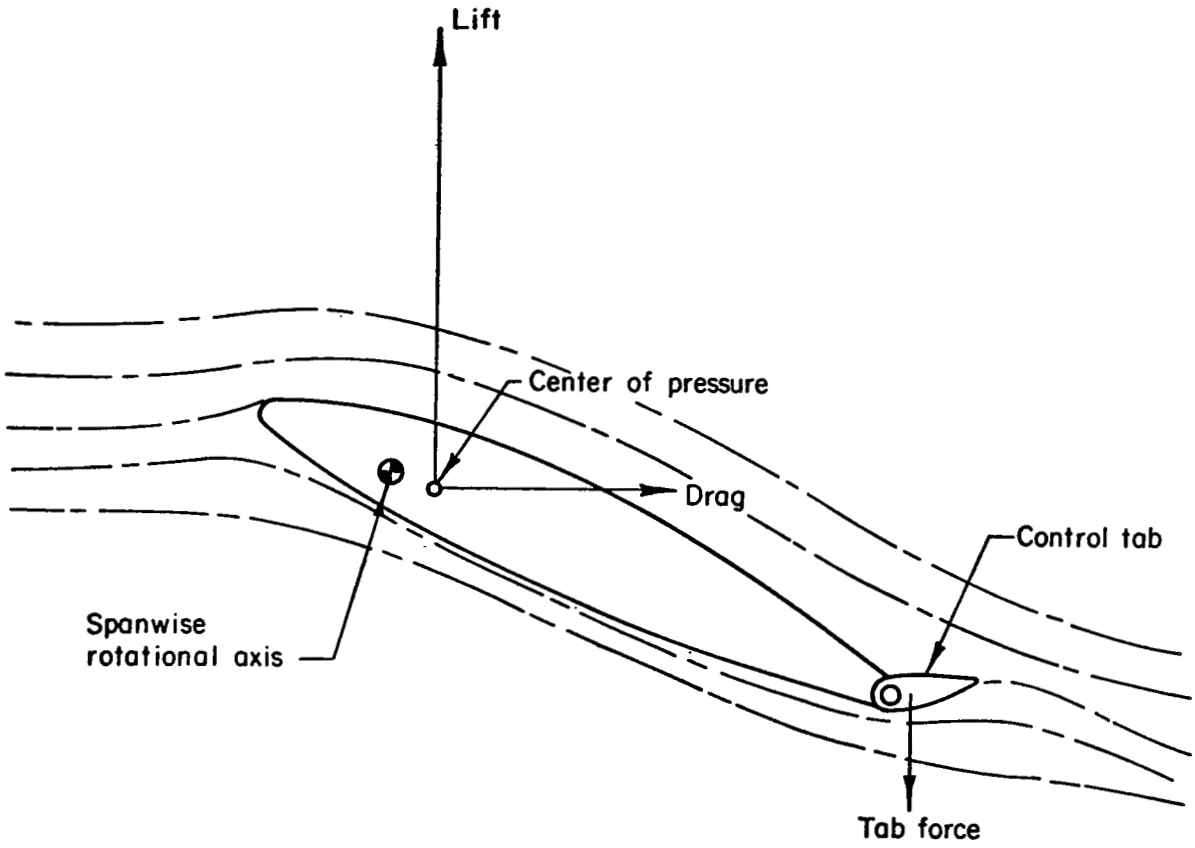

FIGURE 1. CROSS-SECTIONAL ILLUSTRATION OF THE FREE WING

The following conclusions were drawn from this earlier work:

(1) Most atmospheric turbulence effects were greatly reduced, particularly in the rms load factor (~62 percent reduction) and rolling disturbances (~25 percent reduction). On the other hand, the rms fuselage pitch rate was increased about 180 percent in comparison with equivalent fixed-wing aircraft.

(2) All stick-fixed modes of motion were stable except for the spiral mode, where the rate of divergence was found to be excessively high in the approach condition.

(3) The lateral-directional handling qualities were unsatisfactory because of the combination of low roll damping and spiral divergence.

(4) Artificial stability augmentation, in the form of a simple roll damper, provided excellent lateral control and turbulence penetration characteristics.

Purpose of This Investigation

The purpose of this study was to perform a realistic and comprehensive assessment of the practical aspects of implementation of the free-wing concept for light, general aviation aircraft.

Although the impressive gust alleviation benefits found in the previous study seemed to indicate a strong potential for light aircraft application, the scope had been limited to a first-order evaluation of the inherent linearized dynamic behavior of free-wing aircraft. No specific account had been taken of design features that might conflict with certification standards; maneuvering control force gradients were not examined; no nonlinear effects were included; the possible use of aero-mechanical stability augmentation schemes had not been treated; the attitude trim requirements of the fuselage assembly were not considered; and certain assumptions had been made with regard to unsteady aerodynamic phenomena and wing pitching moments due to sideslip. The present research program was designed to extend the previous work with specific treatment of the factors just mentioned.

Scope

In this study, attention was confined to variations of one specific hypothetical free-wing airplane based upon an existing conventional light aircraft. This work should not be construed as a complete design study, however, since only those parameters were explored whose influence is considered most relevant to the free wing application.

The investigation was analytical in nature, but supported by wind tunnel experiments on two physical models. One set of experiments was designed to verify the analytically predicted single degree of freedom motion of free-wing panels in pitch. The other model was used to provide an empirical determination of the wing pitching moment coefficient in sideslip.

The criteria for evaluating the acceptability of configuration variables included the Federal Aviation Regulations, Part 23, and the Military Handling Qualities Specification, MIL-F-8785B (ASG). It should be emphasized that only selected sections of these criteria were used; that is, those bearing directly on the fundamental question of the free-wing design acceptability.

SYMBOLS

The following symbols are used in the main body of this report; additional symbols are defined in each appendix, as required.

A_y = lateral acceleration, feet/sec^2

$\bar{c}$ = mean aerodynamic chord, feet

C_{ℓ_β} = slope of rolling-moment coefficient vs. sideslip angle

C_{m_β} = slope of right wing-panel pitching moment vs. sideslip angle

F_s = stick force, lb.

g = acceleration of gravity, feet/sec^2

I = nondimensional mass parameter

I_y' = moment of inertia of each wing panel about hinge axis, slug-ft^2

j = unit imaginary number, $\sqrt{-1}$

n = normal load factor, g units

P = area of free-wing panel, feet^2

U = true airspeed, feet/sec

α = angle of attack, radians unless otherwise specified

β = sideslip angle, radians unless otherwise specified

δ_e = longitudinal control surface deflection, radians unless otherwise specified

$\dot{\Psi}$ = yaw rate, radians/sec

$\ddot{\theta}$ = pitching acceleration, radians/sec

ρ = atmospheric density, slugs/ft^3

$\omega_{n_{SP}}$ = natural frequency of short-period mode, radians/sec.

DISCUSSION OF RESULTS

Wind-Tunnel Experiments

Dynamic Pitching Behavior of Free-Wing Panels.- For the previous work of Reference 3, reliance was placed upon linear analytical techniques for including unsteady aerodynamic effects on symmetrical wing pitching motion. Specifically, the first-order lag transfer function relating circulatory lift coefficient to angle of attack was obtained by a Laplace transformation of the time derivative of an exponential fit to the response time history following a step change in angle of attack. Appropriate additional forces and moments were added to account for the apparent mass effects, as described in Appendix B of Reference 3. From this, the conclusion was drawn that the reduced frequency and damping of the wing oscillatory pitch mode are dependent on only two parameters; the margin separating the hinge axis from the aerodynamic center, and a mass parameter given by,

$$I = \frac{8I_y'}{\rho \overline{Pc}^3} \tag{1}$$

For a single degree of freedom, in pitch, the characteristic equation of the system is a cubic; generally yielding one stable real root and a complex conjugate pair describing an oscillatory mode. The oscillatory mode is the one of primary interest because it is strongly related to the longitudinal frequency response of the aircraft to vertical gusts. The computed dimensionless roots of the oscillatory mode are shown in Figure 2.

Since no directly applicable experimental data could be found for comparison with the analytical results, and because of the importance of a realiable representation of wing dynamics in the longitudinal equations of motion of the complete aircraft, wind tunnel experiments were conducted to provide verification of the analytical technique. A complete description of the experimental program is contained in Appendix A, but the primary results are summarized here.

A dynamically scaled reflection-plane wing panel was mounted in the Battelle-Columbus subsonic wind tunnel. It was necessary to construct the basic model as light as practicable to obtain low mass parameter values, as given by Equation (1). The model was built up of balsa ribs and sheet covering with an aluminum tube serving as the hinge axis. Five discrete chordwise hinge axis positions were available by shifting the location of the aluminum tube with respect to the basic wing structure. The aluminum tube extended through the tunnel wall to the exterior, where discrete weights were mounted on moment arms to provide for variation of mass parameter and to establish the trim angle of attack through an unbalanced weight moment.

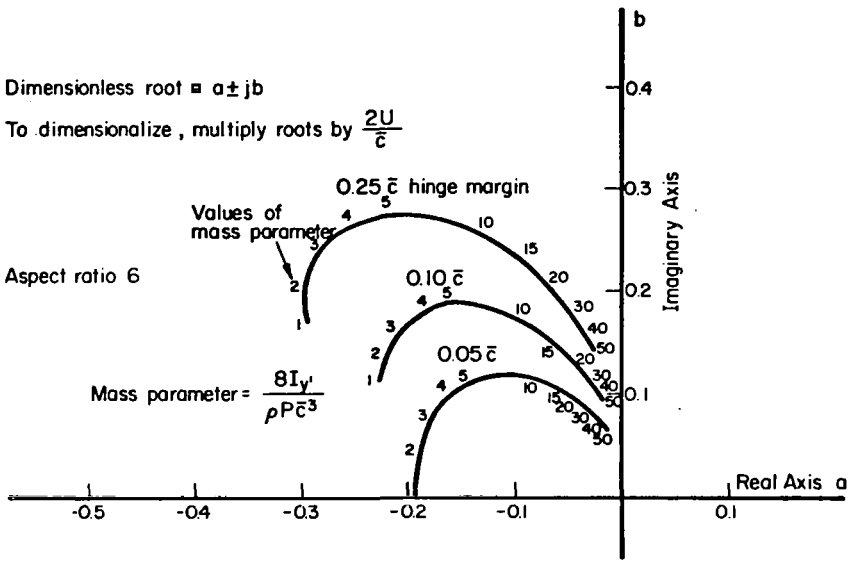

FIGURE 2. COMPUTED ONE-DEGREE-OF-FREEDOM OSCILLATORY MODE ROOTS

The test technique consisted of obtaining oscillograph recordings of recoveries from initial displacements for a variety of mass parameters, tunnel speeds, hinge axis locations, and equilibrium angles of attack in the linear aerodynamic range. The frequency and damping ratio of each datum point were then extracted using reduction techniques from Appendix III of Reference 4. Two methods were used; one based on the maximum slope of the recorded time history and one based on the transient peak ratio. The latter method was found to result in less scatter and all data presented were reduced by this method.

A summary of the experimental results and comparison with theory are shown in Figure 3.

It should be noted that for those points with relatively high damping (generally, for an aft hinge axis location and/or small mass parameter) it was difficult to extract a highly accurate damping ratio. It should also be noted that the panel motion is not, in actuality, simple second-order behavior. Even the analytical approximation is a third-order system and the stable aperiodic mode which accompanies the oscillation can significantly modify the initial transient response.

All factors considered, the degree of correlation between the experimental results and the theoretical predictions is judged to be quite adequate

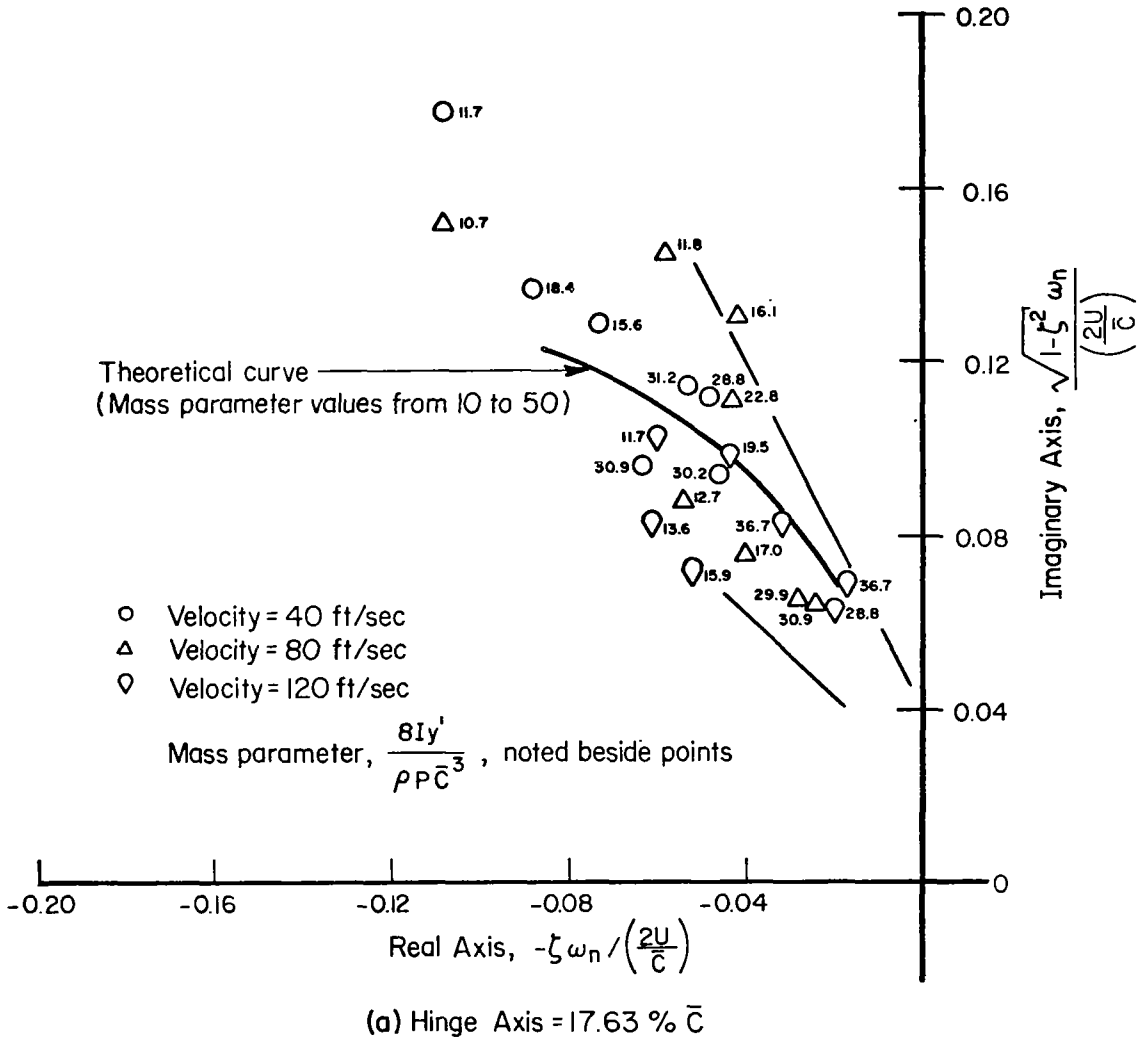

(a) Hinge Axis = 17.63 % $\bar{C}$

FIGURE 3. FREE WING MEASURED ONE DEGREE OF FREEDOM OSCILLATORY MODE ROOTS

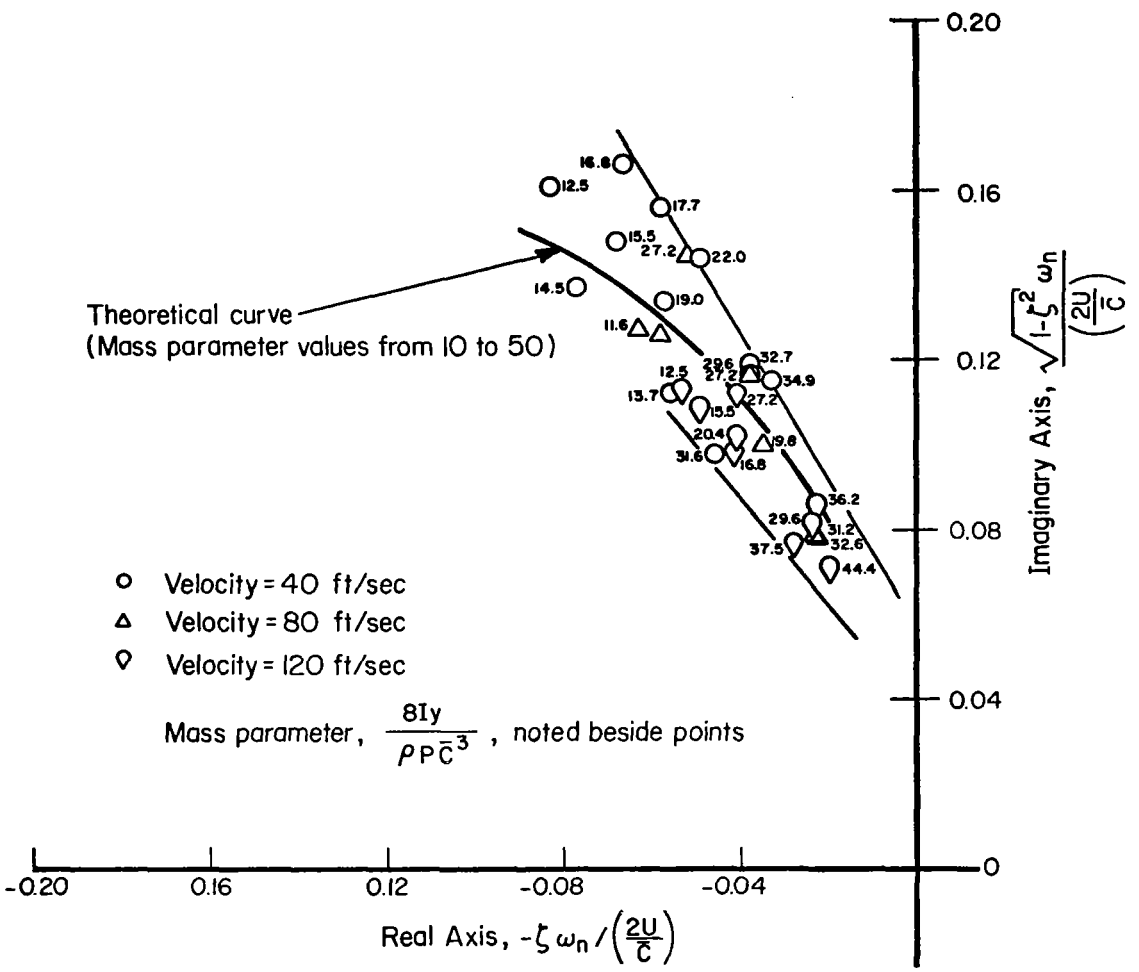

(b) Hinge Axis = 15.13 % $\bar{C}$

FIGURE 3. (CONTINUED)

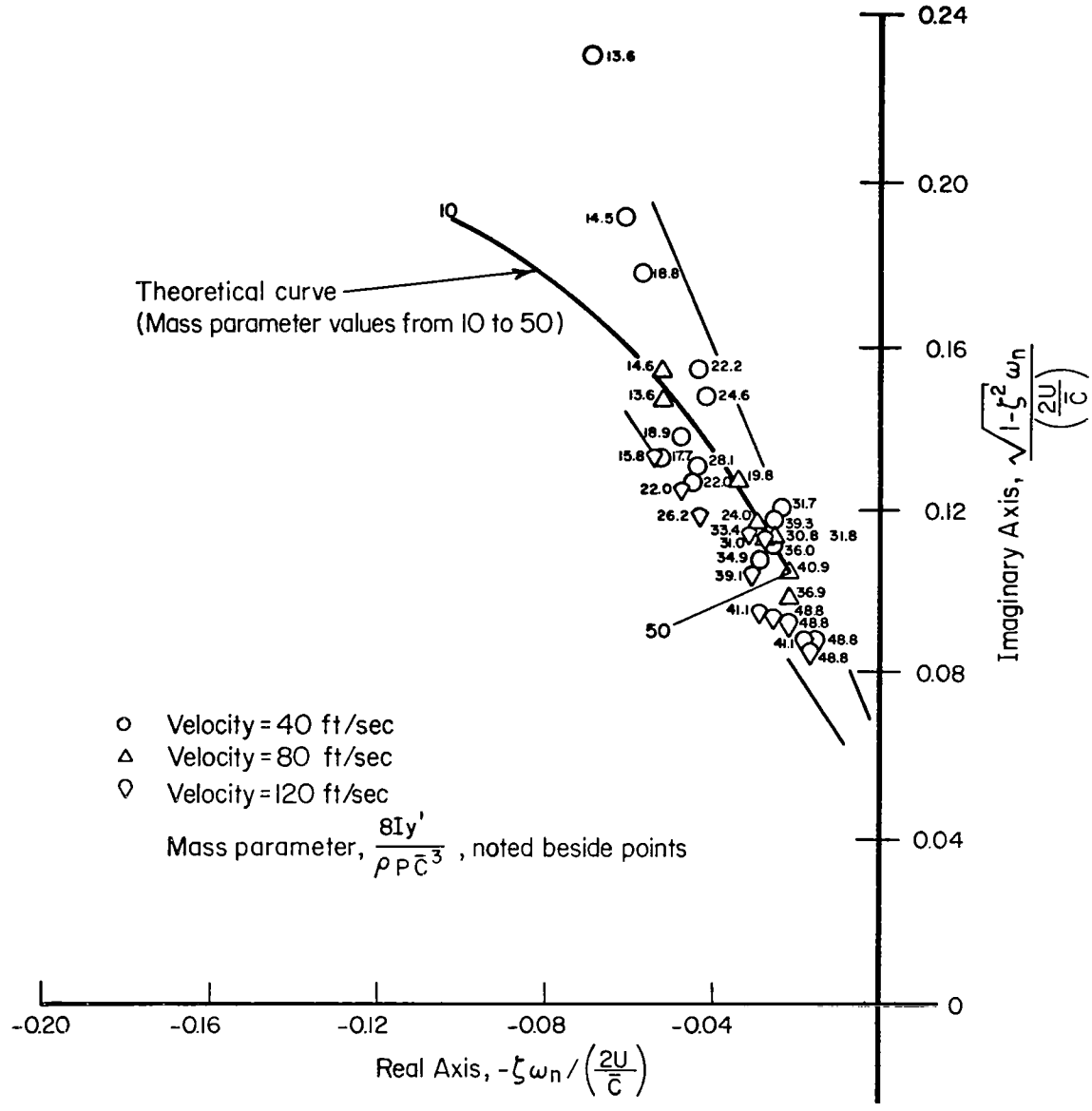

(c) Hinge Axis = 10.13 % $\bar{C}$

FIGURE 3. (CONTINUED)

for accepting the validity of the analytical model. From a qualitative standpoint, furthermore, all free motions that were observed were well damped with no tendency for static or dynamic instability, even when the wing was deliberately forced into a completely stalled condition by torques applied to the shaft exterior to the tunnel.

Asymmetric Panel Deflection in Sideslip.- If the wing has a positive dihedral effect with the wing panels restrained (negative C_{ℓ_β}), positive sideslip (to the right) will cause an increase in the lift on the right wing and a decrease on the left. Intuitively then, the incremental pitching moments about the hinge axis will be negative on the right wing and positive on the left, resulting in an asymmetric panel deflection in a direction which would reduce the dihedral effect. A determination of these pitching moments was beyond the simple lifting-line theory used in the previous study, so recourse was made to an arbitrary selected value of the pitching moment derivative, C_{m_β}, and a sensitivity analysis was performed to determine the importance of this unique derivative. The conclusion was reached that the most significant influence is on the spiral mode stability; this mode becoming more rapidly divergent as C_{m_β} assumes larger (negative) values.

Wind tunnel experiments were conducted to determine representative values of C_{m_β} and the results are summarized here. A more complete description is contained in Appendix A.

The experiment consisted of mounting, in the wind tunnel, an assembly composed of a typical fuselage with independent left and right panels, and taking static measurements of each wing panel deflection as functions of sideslip angle. Since only the equilibrium values of panel deflection were of interest, no dynamic scaling was required. The model was mounted on its side to eliminate the effects of weight imbalance about the hinge axis.

The panels were equipped with trailing-edge control surfaces to provide data at several trimmed angles of attack. The smoothed results are plotted in Figure 4 which shows the average ratio of incremental single panel deflection to sideslip angle as a function of wing lift coefficient. The displacements were equal and opposite for the left and right wing panels. These data are for a single hinge axis location computed to be 5.6 percent of chord forward of the aerodynamic center.

The extraction of the desired derivative, C_{m_β}, from these data is outlined in Appendix A. It is noteworthy that the value, so obtained, for the approach condition is an order of magnitude greater than that selected somewhat arbitrarily in the earlier study of Reference 3.

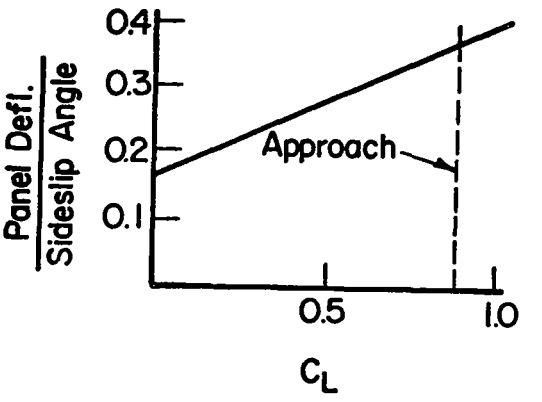

FIGURE 4. RESULTS OF SIDESLIP TESTS

Selected Practical Configuration

To provide a logical basis for the discussions which follow, the final selected practical configuration is briefly described in this section. This configuration is shown in Figure 5, while justification for many of the design features is given in more detail in later sections of the report.

Basic Configuration.- The aircraft selected for analysis is based upon an existing conventional light aircraft, the Cessna 182. The wing planform has been modified to a rectangular shape primarily for convenience in the analysis. The assumed gross weight is 2800 lbs, equal to the maximum weight of the 182. The airfoil is the NACA 23012 section, selected because of its relatively high maximum section lift coefficient and the wealth of pertinent empirical data contained in the literature. The wing area of the free-wing aircraft is slightly greater than that of the Cessna, being 184.4 ft^2 as opposed to 174 ft^2.

The high-wing configuration was selected because of the intuitive desirability of providing external support for the wings. The external strut arrangement is similar to that of the basic 182 aircraft and provides relief of bending moments on the inboard wing hinge bearings as well as greatly increased bending stiffness for flutter suppression. The need for external struts has not been established, however, since no structural or flutter analyses were performed. On the other hand, the strut arrangement might be carried further to an inverted "V" arrangement to relieve drag moments as well as moments due to lift forces on the wing panels.

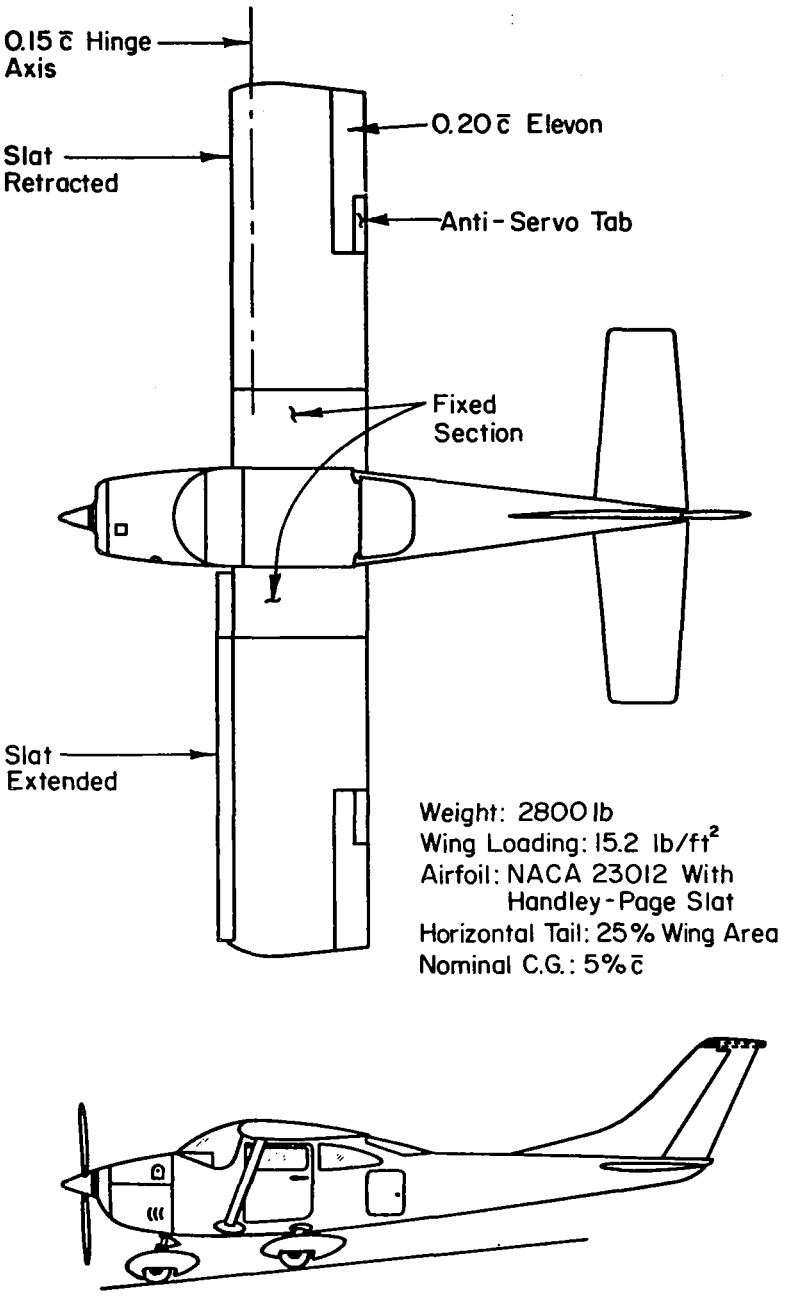

FIGURE 5. SELECTED CONFIGURATION

Fixed Center Section.- The fixed wing center section is a practical necessity to provide a convenient location for fuel tanks and to eliminate interference between cabin doors and wing panels while on the ground. In fact, FAR 23.807 states: "Emergency exits must be located to allow escape without crowding in any probable crash attitude". This requirement, in substance, demands the fixed center section to preclude any possibility of passengers being imprisoned in the cabin by wing panel deflections.

Retractable Leading-Edge Slats.- FAR 23.49 (b)(i) requires a minimum speed capability of 61 knots (CAS) or less for single engine aircraft certificated in the Normal, Utility, or Acrobatic categories. Since the trailing-edge control surfaces are deflected upward for trim, the maximum trimmed lift coefficient is less than that of a conventional wing of the same planform. Trailing-edge, high-lift flaps cannot be used directly unless some additional mechanism is developed to overcome the powerful negative pitching moments. The aircraft has a wing loading of 15.2 pounds per square foot, so compliance with the airworthiness standards would require a maximum trimmed lift coefficient of not less than 1.21. It appears unlikely that values much in excess of 1.0 are achievable for a basic free wing trimmed by trailing-edge control surfaces.

Fortunately, a literature search revealed considerable data on leading-edge slats used with the selected NACA 23012 airfoil section. The Handley Page slat seems particularly attractive. This device not only yields a very substantial increase in section lift coefficient, but causes an apparent forward shift in aerodynamic center location, thereby reducing the trim control deflection. With this device, the maximum trimmed lift coefficient was computed to be in excess of 1.46, reducing the minimum speed to an acceptable 55.5 knots.

Structurally Coupled Free-Wing Panels.- The left and right free-wing panel of the final suggested configuration do not have differential freedom but are mechanically constrained to pitch only in unison. Although the analysis indicates a possibility of retaining differential freedom with the aid of passive mechanical stability augmentation devices, the benefits, for this type of aircraft, are not judged to be worth the additional complexity. With the panels retrained to symmetrical displacements only, the longitudinal gust alleviation benefits remain and the lateral-directional handling qualities, stability, and turbulence responses are identical to an equivalent fixed-wing aircraft.

Control Surfaces.- The control surfaces are sized to provide sufficient power to bring the wing panels to maximum lift coefficient with the leading-edge slats in either the retracted or extended position. They are 20 percent of chord in depth and cover half of the span of the free panels. Their outboard position enables them to be used as conventional ailerons for lateral control. An antiservo tab, geared one-to-one with control surface displacement, is required to bring the maneuvering stick force gradient to an acceptable value.

Horizontal Tail Size.- The previous study of Reference 3 had indicated the possibility of using only a small horizontal stabilizing surface at the aft end of the fuselage to provide angle of attack stability for the fuselage assembly. This choice was reevaluated in this study and the final selection was a horizontal tail slightly larger than the Cessna 182 (in percent of wing area). This choice was motivated by the inclusion of the fixed center-section of the wing and the requirement to provide independent fuselage attitude trim throughout the speed and center of gravity range of the aircraft.

Aircraft Center of Gravity.- The usable center of gravity range is 1.2 feet (22.5 percent of chord), approximately the same as the Cessna 182. The nominal center of gravity is more forward than most conventional aircraft, being located at the 5 percent chord point.

Balanced Wing Panels.- The analyses to follow indicates the necessity of providing static balance, about the hinge axis, for the wing panels. Two methods were considered for achieving this: internal balance weights inside the wing leading edge, or extended balance weights on moment arms protruding forward of the wing, in small, faired nacelles.

With the internal ballast, a weight penalty totaling about 200 lb is incurred. This is reduced to about 88 lb for external masses on one foot extension arms. These mass balance requirements were computed using basic wing mass distribution similar to the Cessna 182. It is expected that careful design, using the extended ballast could reduce the weight penalty to about 40 lb.

Lateral-Directional Handling Qualities

Effects of Differential Panel Freedom.- Were it not for the adverse effect on lateral-directional handling qualities, the results of the previous study indicated two primary advantages of independent left and right wing panels. These were (1) a significant reduction in roll disturbances in turbulence and (2) very powerful roll control even at the lowest airspeeds.

Unfortunately, the same mechanism which yields these advantages is also the primary contributor to the inherently unsatisfactory lateral control characteristics. The factor referred to here is the low effective roll damping due to the tendency of each wing panel to pitch into the local relative air flow caused by a rolling rate. It may seem paradoxical that the low effective roll damping is accompanied by a reduction in roll disturbances in turbulence, but this is because a major contributor to lateral perturbation is the spanwise gradient of vertical gust velocity, and this "rolling gust" disturbs the airplane in proportion to the aerodynamic roll damping coefficient. If the effective aerodynamic roll damping is small, the forcing function is reduced.

Another significant effect of differential panel freedom is the reduction of effective dihedral caused by asymmetric panel displacements in sideslip. This is objectionable for two reasons: (1) the tendency for spiral divergence is aggravated and (2) the steady sideslip characteristics are such that lateral control displacement must be held away from the direction of slip to maintain a constant bank angle. The latter tendency is in contradiction to both FAR 23.177 (a)(2) and Section 3.3.6.3 of MIL F-8785B(ASG).

Modal Characteristics and Turbulence Responses.- The characteristic lateral-directional modes of motion were computed using the equations of motion given in Appendix B, for two flight conditions: approach (72 knots CAS, sea level, slats extended), and cruise (125 knots CAS, 6500 ft, slats retracted). For purposes of comparison, computations were made both with and without differential panel freedom.

TABLE 1. COMPARISON OF BASIC FREE-WING CHARACTERISTIC ROOTS WITH AND WITHOUT DIFFERENTIAL PANEL FREEDOM

	Approach		Cruise	
	Differential Freedom	No Differential Freedom	Differential Freedom	No Differential Freedom
Dutch Roll	-.651±j1.97	-.252±j1.72	-.906±j2.70	-.446±j2.56
Spiral	.857	.00615	.854	-.00673
Roll Mode	-.190	-3.87	-.268	-5.99
Asymmetric Panel Mode	-45.5,-7.26	--	-30.8±j16.1	--

From the standpoint of characteristic modes, the kindest thing that can be said of differential panel freedom is that it seems to improve the dutch-roll damping. This is far outweighed by the adverse effects of the spiral and roll mode roots.

The dominant problem here is the extremely rapid spiral divergence. The rate of divergence is practically the same at both flight conditions, with the time to double amplitude being less than .81 seconds. This is well below the standards of Section 3.3.1.3 of MIL-F-8785B(ASG), which specifies a minimum acceptable time to double amplitude of 4 seconds. For the approach condition, the recommended value is at least 12 seconds and for cruise, 20 seconds. With differential freedom removed, the spiral mode is stable in the cruise configuration and the benign instability in approach has a time to double amplitude of 163. seconds.

Aside from the spiral instability, the roll mode time constant (the reciprocal of the root) can only meet Level 3 standards* with differential freedom permitted. With no differential freedom, Level 1 standards are exceeded.

A comparison of responses to continuous turbulence is given in Table 2. These responses were computed for the combined effects of uncorrelated side and rolling gusts using the power spectral density techniques described in Appendix E of Reference 3. The output spectra were trancated to include frequency components only within the temporal frequency range from 0.3 to 40 radians/sec. The rms values are based upon integrating the output spectra in this interval.

TABLE 2. COMPARISON OF TURBULENCE RESPONSES (UNIT INTENSITY)

	Approach		Cruise	
RMS Variable	Differential Freedom	No Differential Freedom	Differential Freedom	No Differential Freedom
Roll angle, deg.	.418	.465	.503	.314
Yaw angle, deg.	.200	.404	.106	.237
Roll rate, deg/sec	.465	.563	.623	.425
Yaw rate, deg/sec	.183	.444	.190	.385
Lateral displacement, ft	1.13	1.22	1.24	.871
Lateral load factor, g's	.00791	.0081	.0103	.00654

The unexpected observation from Table 2 is that, for the cruise condition, the turbulence responses are substantially larger for the differential freedom case, except for yawing motion. This is contrary to the results in Reference 3, where reductions in roll disturbances were noted for both approach and cruise.

*MIL-F-8785B(ASG) defines three levels of acceptability:

Level 1: Flying qualities clearly adequate.
Level 2: Flying qualities adequate to accomplish the mission...but some increase in pilot work load or degradation of mission effectiveness exists.
Level 3: Flying qualities such that the airplane can be controlled safely but pilot workload is excessive or mission effectiveness is inadequate, or both.

The adverse effect of differential freedom on rolling disturbances was traced to the influence of the side gust component acting through $C_{m\beta}$. In Figure 6, the roll rate PSD function is plotted for two types of input disturbances: the complete uncorrelated rolling and sideslip gusts, and with the sideslip gusts omitted. With no differential freedom, most of the disturbance is caused by the rolling gust. Differential freedom should relieve this, but the $C_{m\beta}$ effect makes the wing panels very susceptible to the sideslip gust component with the adverse effect we have noted.

To summarize, the unaugmented aircraft with differential panel freedom has unacceptable rates of spiral divergence; unsatisfactory roll damping; unacceptable steady sideslip control requirements; and, for the cruise condition, substantially degraded lateral turbulence response characteristics. Without differential panel freedom, on the other hand, the lateral-directional behavior is identical to a geometrically similar fixed-wing aircraft, and is satisfactory.

Lateral-Directional Stability Augmentation.- In the previous work of Reference 3, an active stability augmentation system (SAS) was simulated which fed back a roll rate signal to displace the lateral controls. This simple roll damper was found to be very effective in providing very good lateral-directional control characteristics and in further reducing the turbulence responses.

In the current investigation, using the experimental values of $C_{m\beta}$, such a system is inadequate because it does nothing to improve the unacceptable steady sideslip characteristics caused by the negative dihedral effect.

It is clear that the role of an active SAS, in a civil aircraft of the type being considered, must be limited to providing an improvement in deficiencies which, uncorrected, are not totally unsatisfactory. This is not the situation here. The analysis indicates that it is questionable whether the basic unaugmented aircraft, with differential panel freedom, could be safely controlled by a human pilot. It follows that an attempt to correct such gross deficiencies by an active SAS would place this aircraft in the category of a Control Configured Vehicle (CCV).

Since an active SAS is inappropriate, attention was focused on several passive mechanical devices which could, conceivably, be made as reliable as the basic airframe structure. These mechanisms are discussed in the following paragraphs.

Differential Torsion Spring.- Since the differential freedom of the left and right panels is the basic cause of the deficiencies, it is logical to explore the effect of partially restraining this motion by a simple torsion spring. In principle, the torsional stiffness of such a spring could be increased to the point where no differential freedom existed, for all practical purposes. In this analysis, however, the meaningful range of spring stiffness

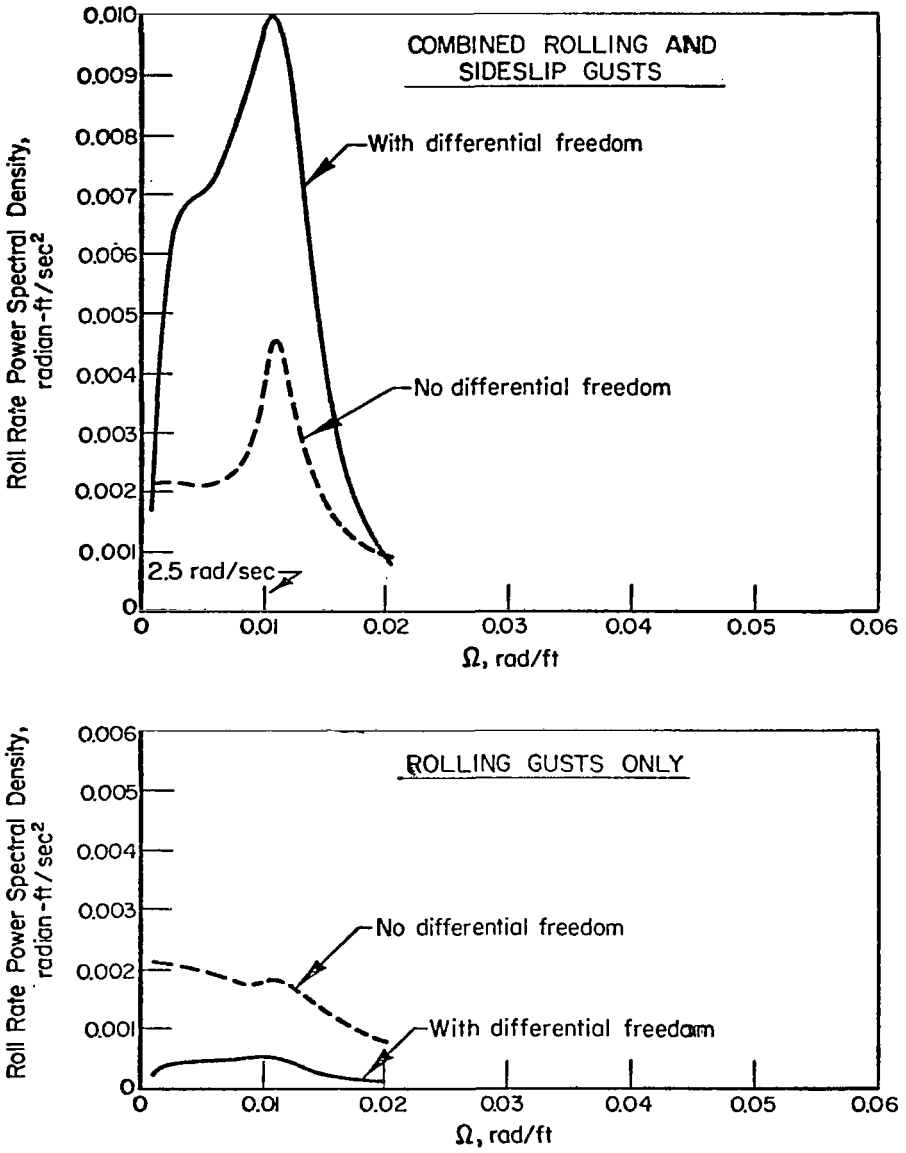

FIGURE 6. COMPARISON OF ROLL RATE SPECTRA SHOWING EFFECT OF SIDESLIP GUST COMPONENT

Cruise Configuration

was reduced because unsteady aerodynamic effects were not explicitly treated for asymmetric panel motion. Consequently, the range of spring stiffness was confined to values which did not yield extremely high frequencies of oscillation for the asymmetric panel mode.

For the approach condition, a modest torsional spring stiffness of 55.4 ft-lb/degree gave good results; with the spiral mode equalling the Level 2 standards of MIL-F-8785B(ASG), the static sideslip control characteristics being satisfactory, and the turbulence responses being superior to the aircraft without differential freedom. Unfortunately, this same spring constant was inadequate for the cruise condition, since the aerodynamic moments are proportional to dynamic pressure.

The torsional spring device was not pursued further because it would be necessary to design the spring to provide acceptable aircraft behavior at high dynamic pressures, up to the design dive speed of the airplane. Consequently, at the lower dynamic pressures, where lateral gust alleviation is most required (see Table 2 for the case of No Differential Freedom), the responses would tend to those of the rigid wing.

Differential Panel Displacement-Aileron Interconnect.- A mechanical linkage was simulated to provide a control surface deflection, on each panel, to oppose differential displacement of the wing panels. This device tends to improve both the spiral and roll modes while causing modest deterioration of the dutch roll damping. Unfortunately, for gearing ratios beneficial to the modal characteristics, the steady sideslip lateral control displacements required by the pilot are of the wrong sign, failing Section 3.3.1.3 of MIL-F-8785B(ASG).

Differential Panel Displacement-Rudder Interconnect.- A mechanical linkage was simulated to provide a rudder displacement proportional to differential wing panel movement. This did not seem to have any particular merit. Depending on the sign of the interconnect, one can either improve the spiral or roll modes slightly, but at the expense of the other.

Lateral Bobweight-Aileron Interconnect.- A pendulous mass, situated at the airplane center of gravity, was simulated to provide lateral control hinge moment proportional to the sensed lateral acceleration (including the gravity component). The sensed acceleration is given by,

$$A_y = U(\dot{\Psi}+\dot{\beta}) - g\varphi \quad . \tag{2}$$

This quantity is nearly proportional to sideslip angle, at a given dynamic pressure, and therefore provides an opportunity to counteract the C_{m_β} pitching moment without resorting to a sideslip vane.

Increasing the gain of this mechanical feedback tends to stabilize the spiral mode and improves the roll convergence, but reduces the damping of the dutch roll mode. In fact, for the approach case, the dutch roll became dynamically unstable before the other modes were adequately improved.

Lateral Bobweight With Differential Torsion Spring.- Lastly, a combination was simulated, consisting of the pendulous mass linked to aileron and the differential torsion spring. The gain of the acceleration feedback is .315 degrees of control deflection per ft/sec^2 of lateral acceleration, for the cruise condition. For approach, the gain was increased to reflect the reduction in control hinge moment at the lower dynamic pressure. The magnitude of this gain was limited to prevent the dutch roll damping from deteriorating below that of the rigid wing aircraft at either flight condition. The spring constant is the aforementioned 55.4 ft. lb/degree.

The results were good for both the approach and cruise conditions, as shown in Table 3, which includes a comparison of rms turbulence responses with those of the rigid wing airplane.

TABLE 3. EFFECT OF COMBINED LATERAL BOBWEIGHT AND TORSION SPRING AUGMENTATION

	Approach	Cruise
Roll Mode Time Constant	.352 sec	.471 sec
Spiral Mode Time to Double Amplitude	19.5 sec	19.2 sec
Reduction in RMS Response		
Roll angle	6.8%	11.7%
Yaw angle	2.0%	2.5%
Roll rate	13.4%	29.4%
Yaw rate	3.4%	2.0%
Lateral Displacement	2.8%	6.6%
Lateral Acceleration	5.9%	6.0%

The roll mode time constant is superior to the Level 1 requirements of MIL-F-8785B(ASG) which specifies maximum values of 1.4 seconds for cruise and 1.0 second for approach for this class of airplane. The spiral mode, though unstable in both configurations, is only slightly below the Level 1 standards which specify a time to double amplitude of 20 seconds or more. An additional, and important, benefit of this SAS configuration is that the steady sideslip lateral control displacement has the proper sign, meeting Section 3.3.1.3 of MIL-F-8785B (ASG).

The encouraging results obtained must be tempered by the understanding that the analysis was idealized in several respects. For example, the detailed dynamic behavior of the pendulous mass-control surface mechanical system was not included; and the effects of extraneous sensed lateral accelerations caused by rudder deflection, or placement of the bobweight off the actual airplane center of gravity, were not examined. In addition, this system would require, in practice, the incorporation of separate auxiliary control surfaces to prevent the annoyance of motion feedback to the pilot's lateral control system.

Conclusions Regarding Differential Panel Freedom.- The limited analysis just discussed has shown the possibility that passive mechanical stability augmentation can provide acceptable handling qualities and reduced lateral-directional turbulence responses for aircraft with differential wing panel freedom. Nevertheless, it is concluded that differential freedom is not justified on the basis of the benefits derived versus the complexity involved, for unsophisticated light aircraft of the type being considered.

This conclusion is strengthened by the fact that other means are available for improving the lateral turbulence behavior of the aircraft without differential panel freedom; specifically, the simple, fail-safe, low-cost wing-leveling devices currently in use on several light aircraft. The failure of such a system would not present a flight safety problem since the stability characteristics are acceptable without it, provided the wing panels do not have differential freedom.

Longitudinal Handling Qualities

Characteristic Modes.- The linear longitudinal set of equations, including control system dynamics, is given in Appendix B. The characteristic equation is a tenth degree polynomial, generally yielding four oscillatory modes and two aperiodic roots. For the approach case, one of the oscillatory modes, appearing primarily in wing panel deflection, splits into two aperiodic roots because of the reduced effective hinge margin with slats extended.

The characteristic stick-free modes of the nominal configuration are given in Table 4.

The characteristic modal behavior and other handling qualities criteria were investigated for the cruise and approach conditions over a range of values of key configuration parameters. These parameters included: horizontal tail size, wing panel imbalance, airplane center of gravity position, control surface imbalance, and longitudinal control system bobweight mass. The handling qualities criteria were chosen from MIL-F-8785B(ASG), and are intended to include all of those standards which are intimately affected by the free-wing design. Specific criteria are discussed separately in the following paragraphs.

TABLE 4. STICK-FREE CHARACTERISTICS ROOTS FOR NOMINAL CONFIGURATION

Mode	Approach	Cruise
Phugoid	-0.275±j.367	-.0224±j.191
Fuselage Short-Period	-3.02±j3.10	-4.56±j6.52
Symmetric Wing Panel	-11.1, -13.7	-23.2±j7.82
Control System	-15.6±j19.5	-27.7±j5.10
Aperiodic	-5.24, -32.9	-85.1, -26.1

Phugoid Stability.- The phugoid damping ratio is governed almost exclusively by the location of the wing panel center of gravity with respect to the hinge axis. The effect is most in evidence at the approach condition, where, with the wing panel c.g. placed .75 ft aft of the hinge axis, the phugoid damping goes to zero. Forward panel c.g. locations are beneficial resulting in lower phugoid frequency and an improved damping ratio.

The beneficial effect of slightly forward panel c.g. locations is fortunate since, if the panels are balanced in the cruise condition, extension of the slats will cause a slight forward displacement of the wing c.g.

Section 3.2.1.2 of MIL-F-8785B(ASG) requires a phugoid damping ratio of at least .04 for Level 1. For the case of balanced wing panels, the phugoid damping ratio in the approach configuration is .075, and for cruise, .116.

Short-Period Damping.- The damping ratio of the short-period mode, which appears pr marily as a pitching oscillation of the fuselage assembly, is affected by two parameters; the horizontal tail size, and the airplane center of gravity location. Figure 7 represents the upper half of the complex plane of the characteristic roots, and contains a map of short-period roots as functions of these two parameters in the cruise condition. Also shown is the corresponding root for an equivalent fixed-wing aircraft with center of gravity at 25 percent of mac., and the constraint boundary representing the Level 1 standard of section 3.2.2.1.2 MIL-F-8785B(ASG).

It can be seen that, although the short period damping ratio is reduced by the free-wing concept, compliance with the criterion is not difficult. The horizontal tail size and nominal c.g. (5 percent mac) were chosen partly on the basis of these data.

With regard to variation of the center of gravity from nominal, Figure 8 contains root loci for both the approach and cruise configuration. It may be concluded that the short-period damping standard can be met for both flight regimes throughout the center of gravity range of the airplane.

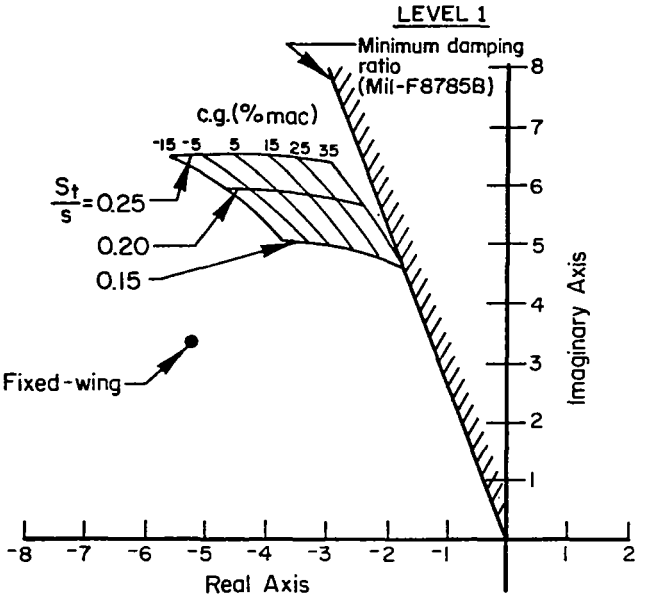

FIGURE 7. EFFECT OF RELATIVE HORIZONTAL TAIL SIZE AND AIRPLANE CENTER OF GRAVITY ON SHORT-PERIOD MODE

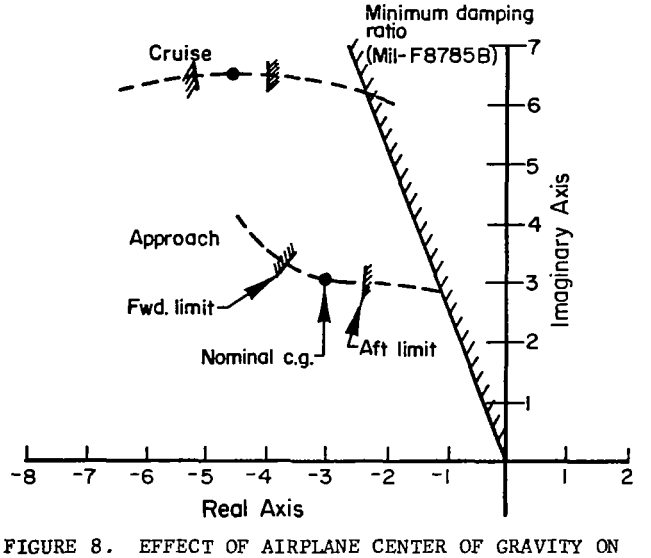

FIGURE 8. EFFECT OF AIRPLANE CENTER OF GRAVITY ON SHORT-PERIOD, STICK-FREE

Maneuvering Sensitivity.- In Section 3.2.2.1.1 of MIL-F-8785B(ASG), upper and lower bounds on short-period frequency are specified as functions of normal load factor divided by angle-of-attack change, where this ratio is determined by the response to a step elevator input. This criterion cannot be applied, as presented, to the free-wing aircraft because the short-period mode is not the primary mechanism for load factor changes; instead, the load factor response is governed by the wing panel mode, while the short period is largely restricted to the pitching motion of the fuselage assembly.

The criterion as stated, specifies for Level 1, for the most demanding flight phases,

$$.28 \leq \frac{\omega_{n_{SP}}^2}{(n/\alpha)} \leq 3.6 \quad . \tag{3}$$

Fortunately, for our purposes, the background information contained in Reference 4 demonstrates that the specified quantity of Equation 3 is equivalent, for conventional aircraft, to the ratio of initial pitching acceleration to the final steady-state load factor increment. With this in mind, the criterion can be transformed to,

$$.28 \leq \frac{\left|\frac{\ddot{\theta}}{\delta_e}\right|_{t=o+}}{\left|\frac{n}{\delta_e}\right|_{SS}} \leq 3.6 \quad . \tag{4}$$

Compliance with this criterion was then checked, directly, by examining time histories of responses to step longitudinal control displacements. For approach the value of the criterion is .6 sec^{-2}, while for cruise, it is 1.31 sec^{-2}. Both are well within the boundaries of Equation 4.

The existence of this criterion is further substantiation of the beneficial effect of fuselage pitching response to wing panel displacement. It might be thought that the removal of mechanical coupling between the free-wing panels and the fuselage would make the fuselage assembly insensitive to wing angle of attack. This is not the case, nor would it be desirable. The primary mechanism of the coupling is the change in downwash at the horizontal tail in response to changes in wing lift coefficient. The resulting pitching of the fuselage is not only essential to the pilot in anticipating the load factor increment, but also provides the pilot with the ability to damp the long-period phugoid motion by manipulating the controls in response to pitch attitude cues, as demonstrated in Reference 3.

Maneuvering Control Forces.- MIL-F-8785B(ASG) places limitations on the maneuvering control forces required for both steady maneuvers and for sinusoidal load factor responses at all frequencies.

For wheel controllers, the minimum force gradient for steady maneuvers is given in Table V of Reference 4. It is,

$$\left(\frac{F_s}{n}\right)_{min} = \frac{45}{n_L - 1} \quad . \tag{5}$$

Equation 5 applies down to a minimum of 6 lb/g. The aircraft under consideration would be certificated in the normal category, which requires a limit maneuvering load factor of +3.8 g's.

From the same source,

$$\left(\frac{F_s}{n}\right)_{max} = \frac{120}{n_L - 1} \quad . \tag{6}$$

The limits of acceptable stick force for the subject aircraft are, then:

$$16. \leq \frac{F_s}{n} \leq 43. \text{ lb/g} \quad . \tag{7}$$

The factors which influence the stick force gradient are: airplane center of gravity location, wing panel imbalance, control surface imbalance, and the presence of a bobweight effect in the longitudinal control system components mounted in the fuselage. These factors are discussed in the following paragraphs.

Airplane Center of Gravity.- If the center of gravity is in a forward location, the angle of attack on the wing center section is reduced in a pull-up maneuver by the action of the mass moment of the fuselage acting about the hinge axis. The reduced center section lift requires a greater free-panel displacement to attain a prescribed normal load factor, consequently the control surface deflection and the stick force are both increased. For aft c.g. locations, the trend is reversed and the stick force per g is reduced.

The smallest stick force gradient occurs at the aft airplane c.g. limit in the approach configuration, since extension of the leading edge slats effectively reduces the hinge margin and decreases the control surface deflections.

With the plain control surfaces sized to bring the airplane to maximum lift coefficient, the stick force gradient was found to be unacceptably low,

about 2.0 lb/g. For this reason, an anti-servo tab was simulated to provide an effective increase in C_{h_δ}. Using data from Appendix B.5 of Reference 5, an anti-servo tab running one third the control span and 30 percent of the control surface chord and geared 1 to 1 with control deflection, raised the stick force gradient to acceptable values. With this device, the force gradient at the nominal c.g. for approach is 16 lb/g, and varies ±1.25 lb/g at the fore and aft c.g. limits, respectively.

In cruise, the stick force gradient is appreciably higher, varying from 28.5 lb/g at the aft limit to 34.9 lb/g at the forward limit. Both are well below the maximum acceptable value of 43 lb/g.

Wing Panel Imbalance.- The location of the wing panel center of gravity with respect to the hinge line has a powerful effect on the stick force gradient in maneuvering flight. The stick force gradient changes about 1 lb/g for every inch of panel c.g. travel, in the approach configuration.

As mentioned previously, the panel c.g. will be slightly forward with slats extended, if the panels are balanced in the clean configuration. This is beneficial because of the relatively low force gradients in the approach condition.

The variation of force gradient with panel c.g. is approximately the same in cruise as in the approach configuration.

Control Surface Imbalance.- An imbalanced control surface with c.g. aft of the control hinge increases the stick force per g slightly, but not significantly. The most noticeable effect from this analysis was an increase in the frequency of the wing panel oscillatory mode accompanied by a slight reducting in damping ratio.

Although mass balancing of the control surfaces was not found to be critical in this study, a flutter analysis might indicate the desirability of balanced control surfaces.

Bobweight.- As expected, a bobweight increases the stick force gradient but reduces the damping ratio of the fuselage short-period mode. The deliberate use of mass imbalance, in the fuselage-mounted components of the control system, is not recommended.

In addition to the steady-state stick force gradient, Section 3.2.2.3.1 of MIL-F-8785B(ASG) requires that the amplitude of stick force per g for sinusoidal inputs be not less than 6 lb/g at all frequencies. In the discussion of Reference 4, it is implied that the phugoid mode is disregarded. For this reason, the airspeed degree of freedom was removed in the computations used to apply this criterion.

The dynamic stick for per g is presented in Figure 9 for the critical case of aft airplane center of gravity for both approach and cruise. These data indicate that Section 3.2.2.3.1 is satisfied.

Conclusions Regarding Longitudinal Handling Qualities.- From this investigation, it is concluded that the free-wing aircraft can be developed to match the Level 1 standards of MIL-F-8785B(ASG). A further significant conclusion is that the wing panels should be balanced about the hinge axis with the slats retracted. This feature is needed to prevent degradation of the phugoid damping and the control force gradients in maneuvering flight.

Inertial Coupling Effects on Wing Panels

All of the analysis discussed to this point has used a linear representation of the airplane, with complete separation of longitudinal and lateral-directional behavior. On the other hand, it is well known that large simultaneous angular rates about more than one axis can result in substantial coupling effects between these motions.

Except for their possible influence on transient past-stall motions, inertial coupling phenomena are usually significant only with respect to very maneuverable, high-density aircraft. Nevertheless, because of the unique pitch freedom of the free-wing panels, it seemed prudent to examine the possibility of dangerous inertial pitching moments on the wing in large displacement maneuvers. The details of this investigation are contained in Appendix D, but are summarized here.

The complete nonlinear equations describing the pitching motion of the wing panels was examined to estimate the probable relative magnitude of each term in normal maneuvers. It was concluded that angular rates consistent with routine maneuvers in light aircraft would not generate significant inertial pitching moments unless large wing-panel center of gravity displacements were permitted. Since large panel c.g. offsets are not to be expected for other reasons, only those large angular rates associated with autorotational maneuvers (spins and snap rolls) were considered further.

Although it is most unlikely that a free-wing aircraft could be spun, because of the inherent stall resistance of the trailing-edge controlled wing panels, it was assumed that the aircraft was executing a spinning maneuver and the influence of the inertial and aerodynamic pitching moments was computed. A total rotational rate of one revolution per second was assumed, with the aircraft center of gravity displaced ten feet from the axis of the spin.

Considering the inertial terms alone, two effects dominate; the gyroscopic term which depends upon the difference between the yaw and roll moments of inertia of the panels, and those terms dependent upon panel imbalance about

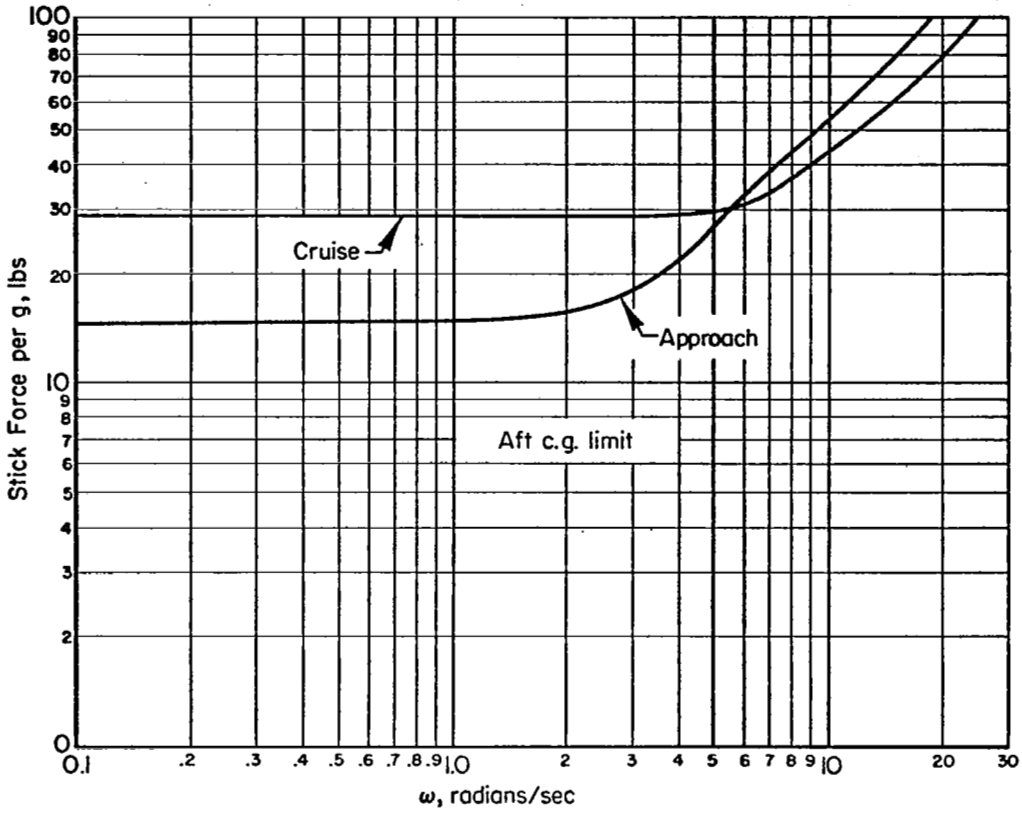

FIGURE 9. DYNAMIC STICK FORCE PER g

the hinge axis. The latter contribution could be quite large, if permitted, and constitutes another compelling reason to provide static balance for the wing panels. Both of these terms provide identical pitching moments to the left and right wings, so their influence exists regardless of whether or not differential panel motion is permitted. These terms, singly and in combination, tend to rotate the wing panels into a plane such that the longitudinal (chordwise) axis of the wing is normal to the axis of spin. The leading edge of the wing panel would be pointed either toward or away from the spin axis depending on the sign of the wing panel c.g. offset.

Fortunately, the aerodynamic pitching moment tends to dominate, even for this rapid spin rate and the low assumed airspeed (59 knots). The influence of the aerodynamic pitching moment is to cause the wing panels to align with the axis of the spin. For an assumed mass imbalance of one slug-foot per panel, the combined effects of inertial and aerodynamic terms yielded equilibrium angles of attack below the stall with relatively small control deflections.

Whether or not the absence of corrective control would sustain the spin was not examined because only modest control surface deflections would be required to bring the wing out of stall and stop the autorotation. In all cases, the direction of control travel is into the attached flow side of the surface, so the control deflection is effective in providing substantial corrective pitching moments.

If the wing panel is balanced, the equilibrium angle of attack for zero control deflection would be zero since the remaining inertial term vanishes when the panels are aligned with the spin axis, and the aerodynamic moment dominates at all other angles of attack.

The conclusion is reached that nonlinear coupling is only significant in a violent maneuver of the assumed type. Furthermore, maneuvers of this sort can only persist if autorotation is present. Since it appears that the wing can always be brought out of stall through modest control movement, no uncontrollable situation can reasonably be expected.

Takeoff and Landing

Static Low-Speed Characteristics.- Considering flight through the complete speed range of the aircraft, it is desirable to provide an independent attitude trim capability for the fuselage assembly. Intuitively, the fuselage attitude should be trimmed to minimize the combined profile and induced drag at any selected lift coefficient. The trim stabilizer setting would, of course, depend on the center of gravity location.

Figure 10 shows the variation of fuselage attitude and wing panel deflection (with respect to the fuselage) for the two extreme airplane c.g. locations. These data are for a fixed fuselage trim setting, selected to yield zero panel deflection at 121 knots EAS., with the airplane c.g. at the aft limit. At the approach speed of 72 knots the wing panel deflection would be about 5.5 degrees, increasing to perhaps 9.5 degrees at touchdown, for the aft limit c.g. With the same fuselage trim setting, but the forward limit c.g., the approach speed wing panel deflection would be over 11 degrees and would rise to about 17 degrees at touchdown. It is noteworthy, however, that even for the out-of-trim condition with forward c.g., the fuselage attitude at minimum speed is over 8 degrees nose-up. This natural tendency for nose-up attitudes at low speed should make inadvertent premature nose-wheel contact with the runway unlikely.

If the stabilizer setting is adjusted to yield zero panel deflection, the fuselage angle of attack depends only slightly on airplane center of gravity as shown in Figure 11.

A peculiarity of the free-wing aircraft is the fact that the maximum wing lift coefficient is not a fixed value, but depends on the free panel deflection relative to the center section. Using section data from Reference 6 for the NACA 23012 with Handly Page slat extended, the maximum section lift coefficient is about 2.0. These nonlinear section data were used in a lifting-line computer program to compute the maximum trimmed wing lift coefficient. To be conservative, this value was determined by restricting the maximum local lift coefficient to 1.9. Since the spanwise lift distribution depends on panel deflection, so does the maximum trimmed wing lift coefficient. Figure 12 depicts three lift distributions which yielded the same maximum local lift coefficient. The wing panel deflections are zero and ±.1 radian (5.73 degrees). The maximum trimmed wing lift coefficients for these three cases are given in Table 5.

TABLE 5. EFFECT OF PANEL DEFLECTION ON MAXIMUM WING LIFT COEFFICIENT AND TRIM CONTROL DEFLECTION

Panel Deflection	Maximum Trimmed Wing Lift Coefficient	Control Deflection
-5.73°	1.28	-21.8°
0.°	1.46	-24.0°
+5.73°	1.50	-25.0°

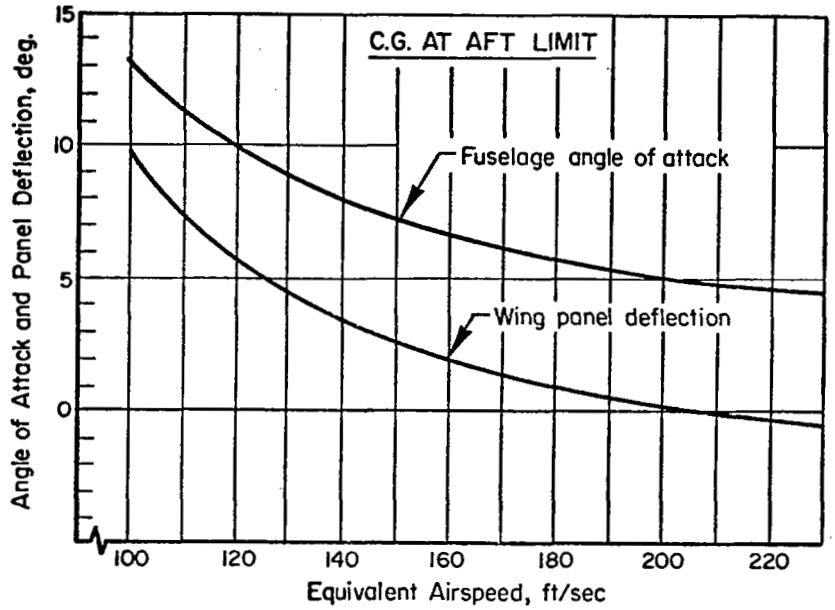

(a) c.g. of Aft Limit

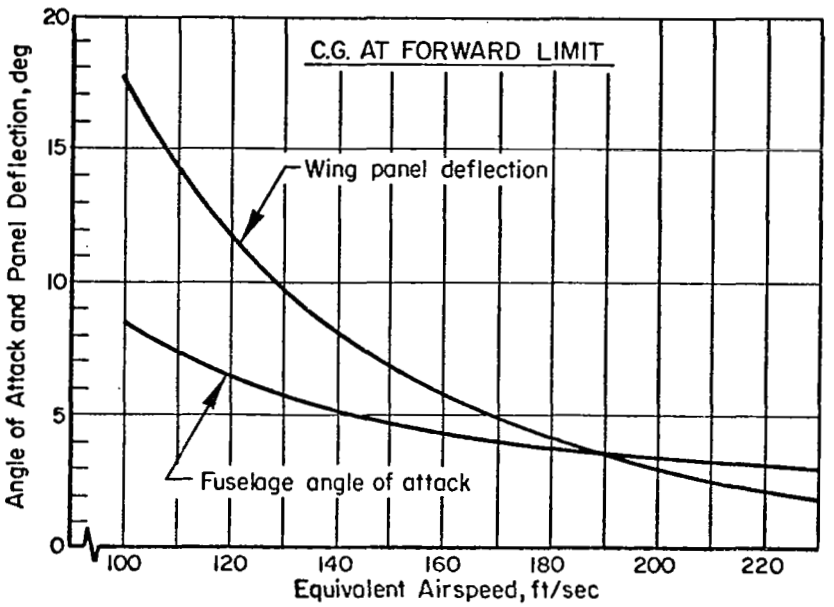

(b) c.g. at Forward Limit

FIGURE 10. TRIM ANGLES FOR FIXED STABILIZER SETTING

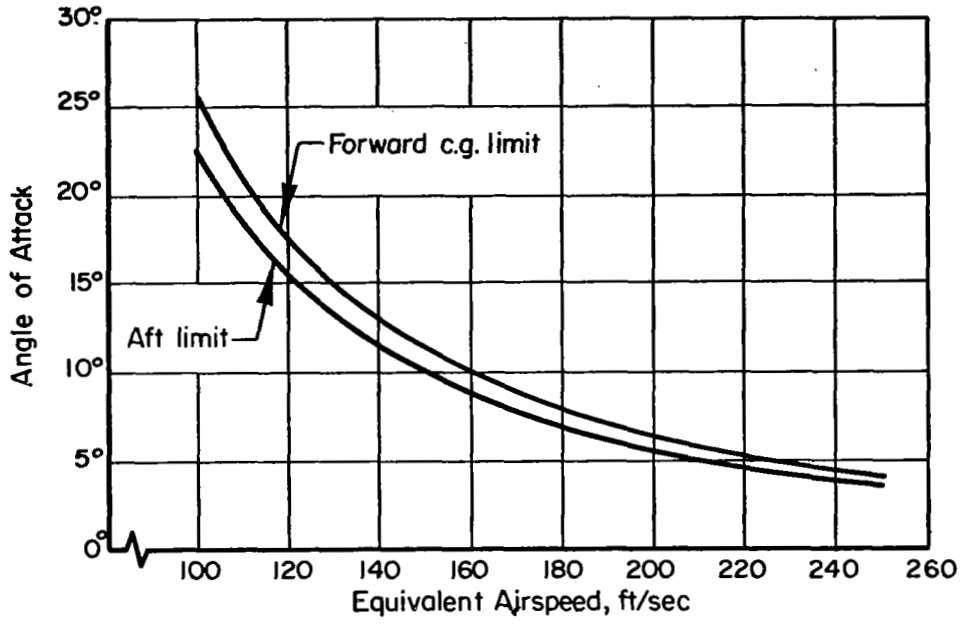

FIGURE 11. FUSELAGE ATTITUDE FOR ZERO PANEL DEFLECTION

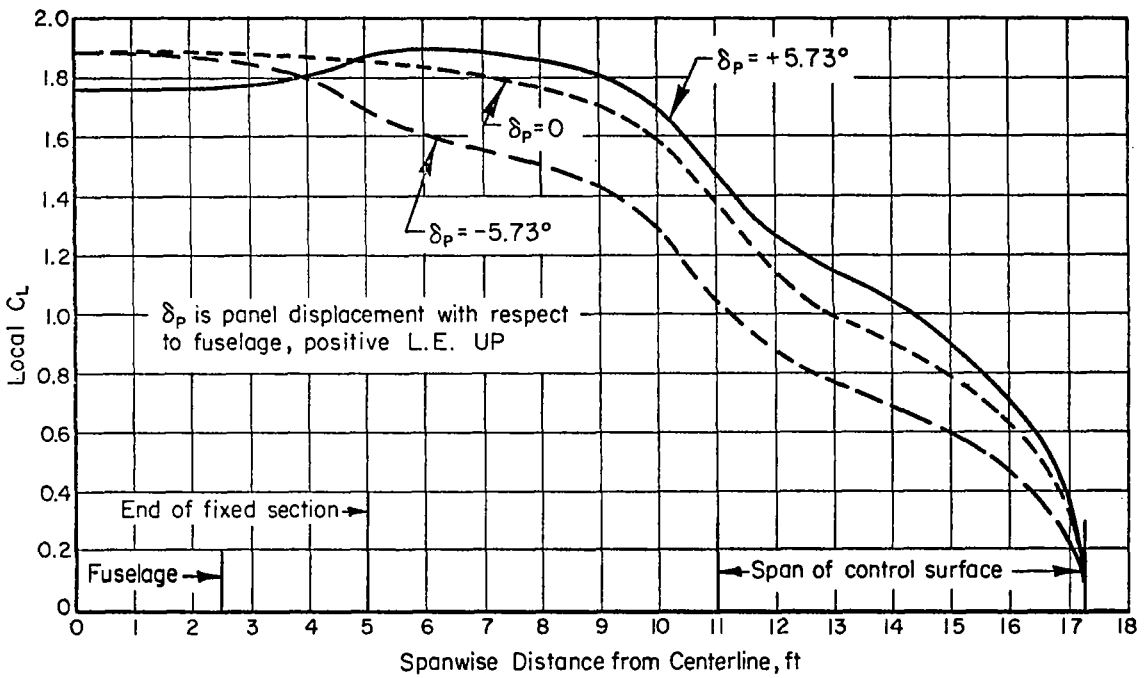

FIGURE 12. LIFT DISTRIBUTIONS YIELDING SAME MAXIMUM LOCAL C_L

Takeoff and Landing Dynamics.- The subject of lift-off and touchdown dynamic behavior required a cursory examination because of the unique pitch freedom of the fuselage assembly and the possibility of undesirable transient motions during these phases.

The reduction in downwash at the horizontal tail, due to ground effect, was included; using the expression for downwash increment given in Appendix B.7 of Reference 5. No effect on wing pitching moment was included, since information in Reference 7 indicates a negligible direct effect on wing pitching moment if the ratio of wing altitude to chord length is greater than 1.2. For the aircraft under study, the ratio is over 1.1, so the effect was disregarded.

Takeoff Motion.- Using the equations of motion given in Appendix B, several time histories were computed to depict the takeoff maneuver following an abrupt wing panel deflection. The speed was assumed constant at 65 knots. To provide an initial disturbance, the initial conditions were such that no weight was on the landing gear. This could represent a disturbance caused by runway undulations. A step longitudinal control input was applied at zero time to bring the wing panels from a zero lift condition to $C_{L_{max}}$.

No unusual motions were observed for any of the simulated takeoffs. Figure 13 is a typical history. The fuselage motion is well damped and is qualitatively similar to that of a conventional airplane. This case was with balanced wing panels.

Landing Motion.- Figure 14 is a time history of a relatively smooth landing with an initial sink rate of slightly over 2.0 ft/sec. The wing panels were balanced, the nominal c.g. location was used, and the speed was held constant at 65 knots. The longitudinal control was maintained at a constant value throughout the maneuver. Although it appears that the wing panel is responding to the landing impact, it must be remembered that the panel deflection is measured with respect to the fuselage. Consequently, only the fuselage attitude is disturbed by the landing gear reactions, but this motion makes it appear that the panel is also disturbed.

With the assumed constant speed, the nose wheel does not touch the runway; and the motion converges to one in which the main gear is supporting only a part of the airplane weight with wing lift providing the difference. It may be conjectured from this that it would be easier to hold off the nose wheel with the free-wing design than with a conventional light airplane. In a conventional aircraft, the pitch-down transient caused by main gear contact reduces the lift on the entire wing and it is sometimes difficult to prevent the nose gear from contacting the runway almost immediately after main gear touchdown.

The effect of airplane center of gravity position was examined by simulated landings at both c.g. limits. In addition, the initial rate of sink was set at 6.0 ft/sec to depict hard landings. The time histories are given in

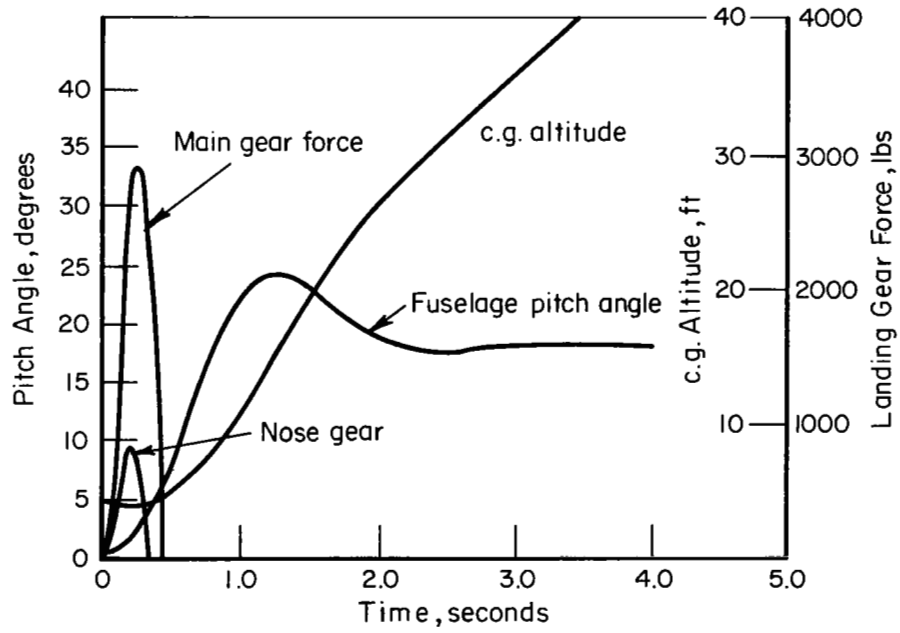

FIGURE 13. COMPUTED TAKEOFF HISTORY

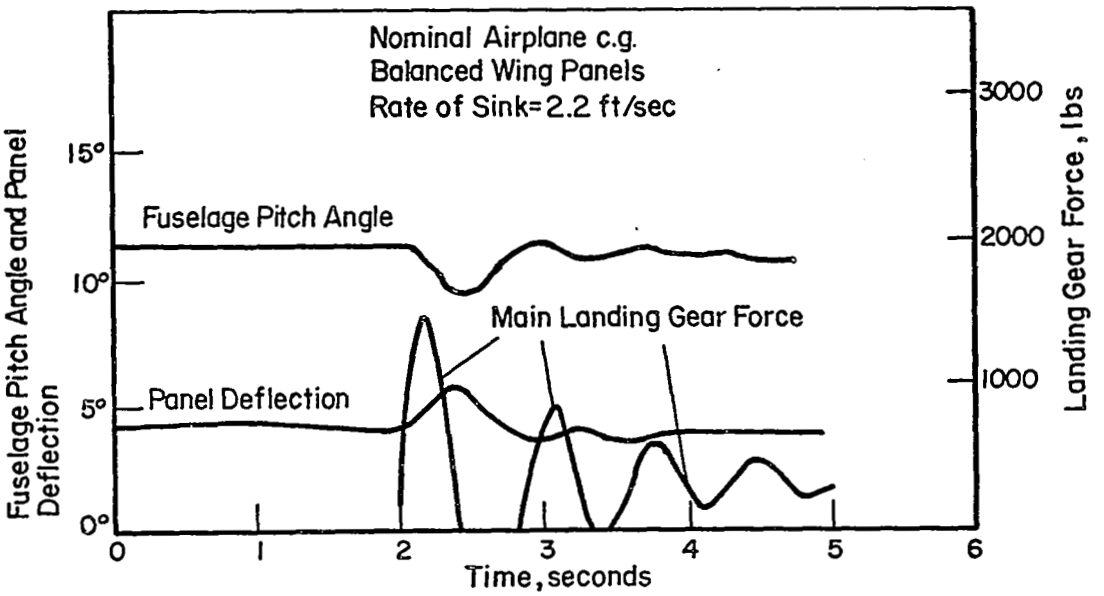

FIGURE 14. LANDING TIME HISTORY, LOW SINK RATE

Figure 15, for the balanced wing panel condition. The fuselage stabilizer trim was identical for both landings, and this is reflected in the lower pitch attitude of the forward c.g. case. In this case, the nose wheel contacted the runway briefly during the initial transient, but remained off the runway in the subsequent motion. With the aft c.g. position, two bounces are observed but the nose wheel remains clear of the runway.

Additional simulations were performed to examine the effect of wing panel unbalance. Two relatively soft landings are shown in Figure 16 for panel c.g. displacements one foot fore and aft of the hinge axis, respectively.

With the panel c.g. forward of the hinge axis, the landing is actually improved slightly; as may be seen by comparing Figures 16(a) and 14. The tendency for the panel deflection to decrease, in this case, immediately reduces the lift and inhibits possible bouncing.

The opposite is true of the case shown in Figure 16(b) with the panel c.g. one foot aft of the hinge line. It would appear practically impossible to perform a no-bounce landing in this condition because of the tendency for the panel angle of attack to increase in reaction to the landing impact. The situation is analogous to that found in earlier "tail-dragger" light aircraft, but is compounded by the much more rapid pitching response of the wing panels as compared to the aircraft as a whole.

The behavior of the aircraft during landing constitutes another reason for not permitting the wing panel c.g. to lie aft of the hinge axis. Aside from this, the landing of the free-wing aircraft appears to present no special problems; at least for the case examined here with no differential panel freedom.

Gust Alleviation and Ride Comfort

We arrive now at the "raison d'etre" of the free-wing concept; the gust alleviating behavior and the effects of this alleviation on the ride quality of the aircraft. It will be seen that although the structural load alleviation is very substantial, the primary benefit is an improvement in ride quality.

Discrete Vertical Gust Response.- A series of time histories was computed in which the nominal free-wing and equivalent fixed-wing aircraft were subjected to a discrete "1-cosine" gust of varying wave length. Figure 17 shows the ratio of peak load factor increments and illustrates the fact that the free-wing is most effective at the longer wave lengths. FAR 23.333(c)(2)(i) specifies a 25 chord length gust of this shape for compliance with the structural gust load criterion. At the cruise condition shown, the response of the free-wing aircraft is 54 percent of the response of its fixed-wing counterpart. At the longer wave lengths, the free-wing load factor increment is even more dramatically reduced, approaching 22 percent of the conventional airplane value.

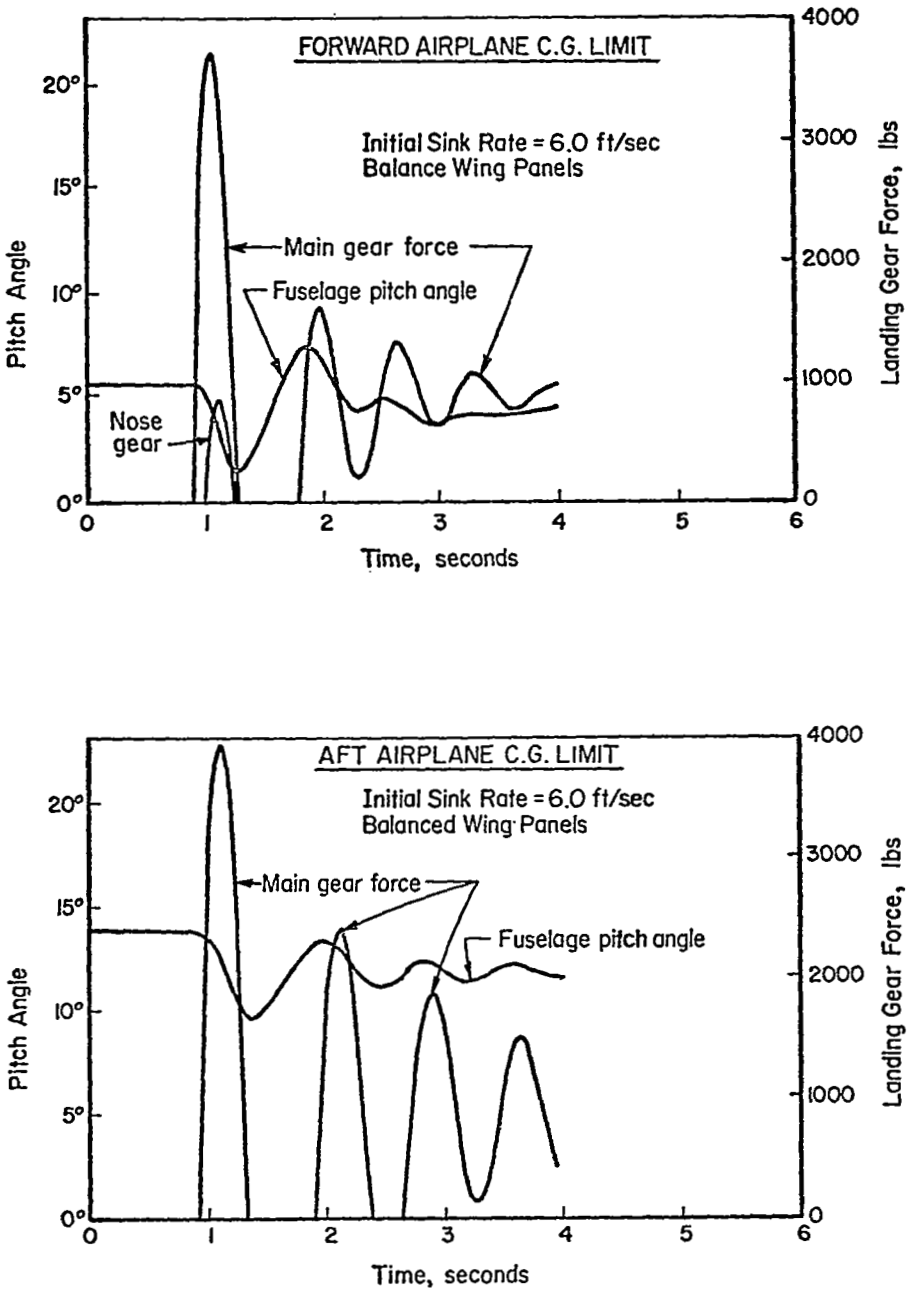

FIGURE 15. EFFECT OF AIRPLANE C.G. ON HARD-LANDING MOTION

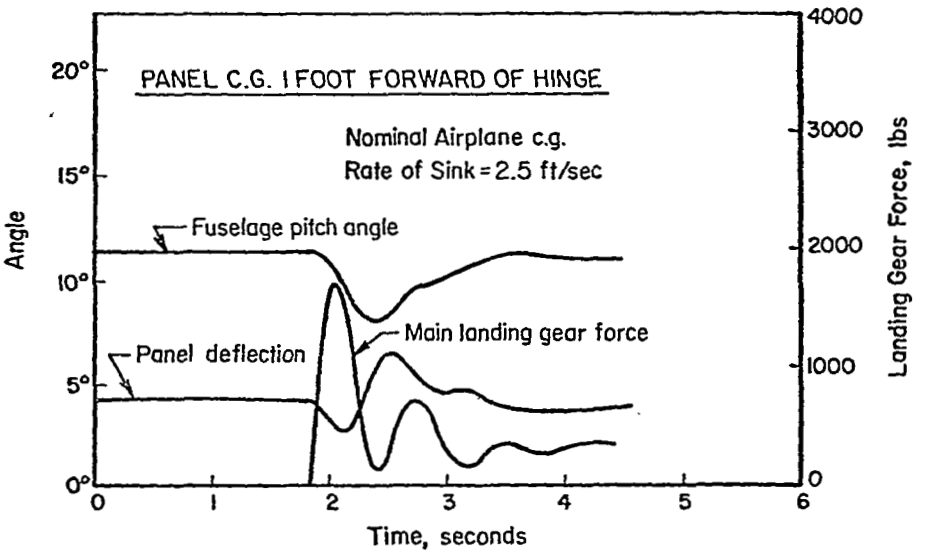

(a) Panel c.g. 1 Foot Forward of Hinge

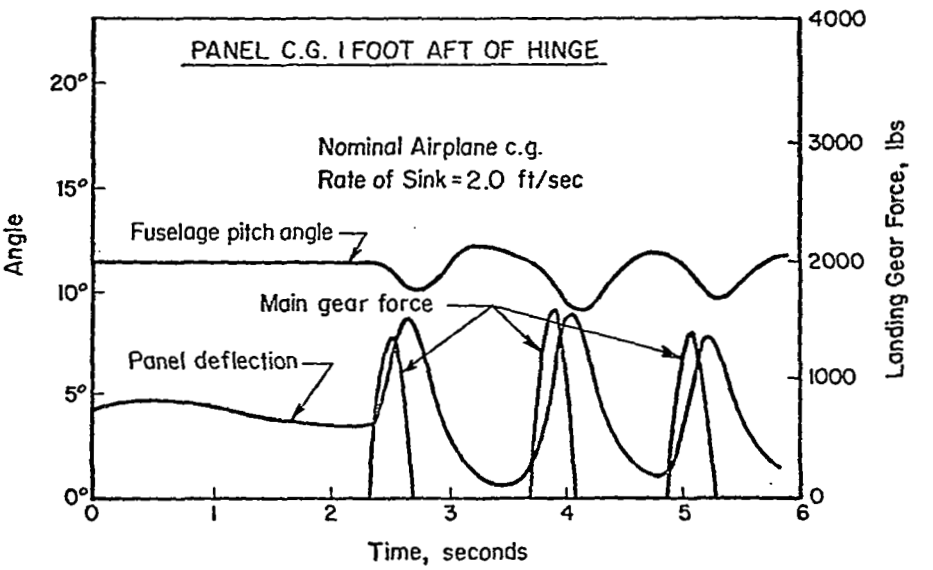

(b) Panel c.g. 1 Foot Aft of Hinge

FIGURE 16. EFFECT OF WING PANEL IMBALANCE ON LANDING DYNAMICS

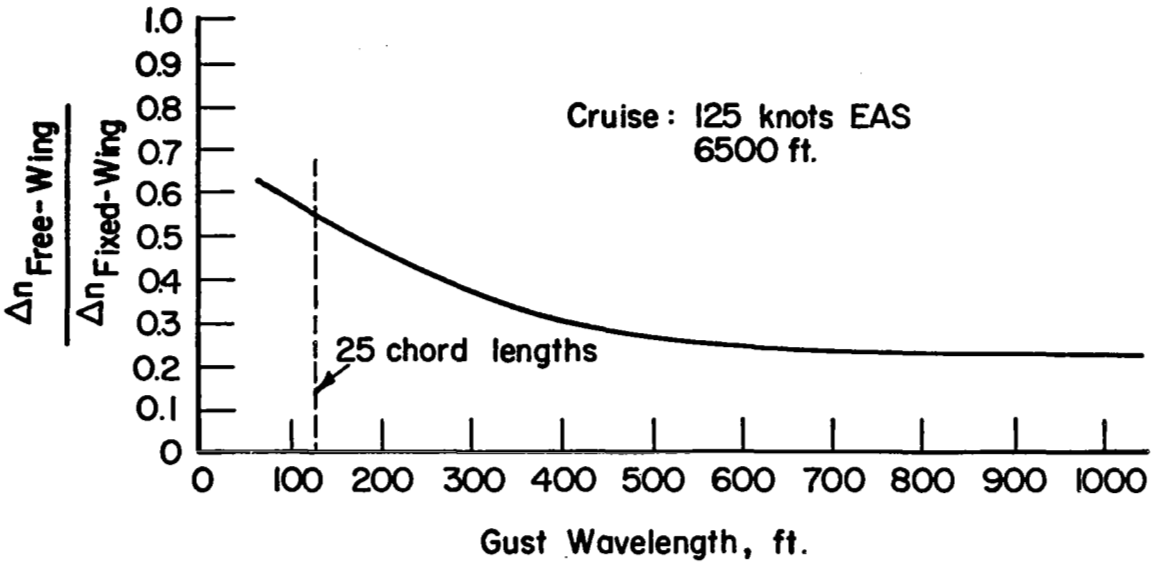

FIGURE 17. COMPARISON OF RESPONSES TO DISCRETE 1-COSINE GUSTS

Response to Continuous Turbulence.- The trend toward greater gust alleviation at long wavelengths is supported by the reaction to continuous turbulence. Figure 18 shows the load factor power spectral density as a function of temporal frequency for both aircraft. At this cruise condition, a 25 chord length gust would correspond to a frequency of about 11 radians/second. Clearly, the primary benefit of the free-wing is in evidence of the lower frequencies (longer wavelengths).

A comparison of rms responses to unit turbulence intensity is given in Table 6 for the free-wing airplane and the equivalent fixed-wing aircraft at the same cruise condition. The stick-fixed responses are shown since they are practically identical to the stick-free results and no stick-free data were generated for the fixed-wing airplane.

TABLE 6. COMPARISON OF RMS RESPONSES TO UNIT TURBULENCE INTENSITY

Variable	Free Wing	Fixed Wing
Normal load factor, g's	.00844	.0184
Pitch rate, deg/sec	.266	.112
Pitch acceleration, deg/sec	2.28	1.24
Wing panel displacement, deg	.0529	--

The most significant item in this comparison is the fact that the rms load factor for the fixed-wing aircraft is 2.18 times as great as the free-wing airplane. Stated another way, the free-wing provides a 54 percent reduction in rms load factor response.

The data in Table 6 were computed on the assumption that the wing balance weight is carried internally in the leading edge. If the ballast were positioned one foot forward of the leading edge in small, faired nacelles to reduce the weight penalty, the pitching moment of inertia would be increased by 36 percent. Fortunately, calculations indicate that the normal load factor response would increase only by about 2 percent, rms, while the other rms values would be virtually identical. Since the wing pitching moment of inertia is very much smaller than that of the entire aircraft, for reasonable wing mass placement, the load alleviation appears to be relatively insensitive to the specific wing mass distribution.

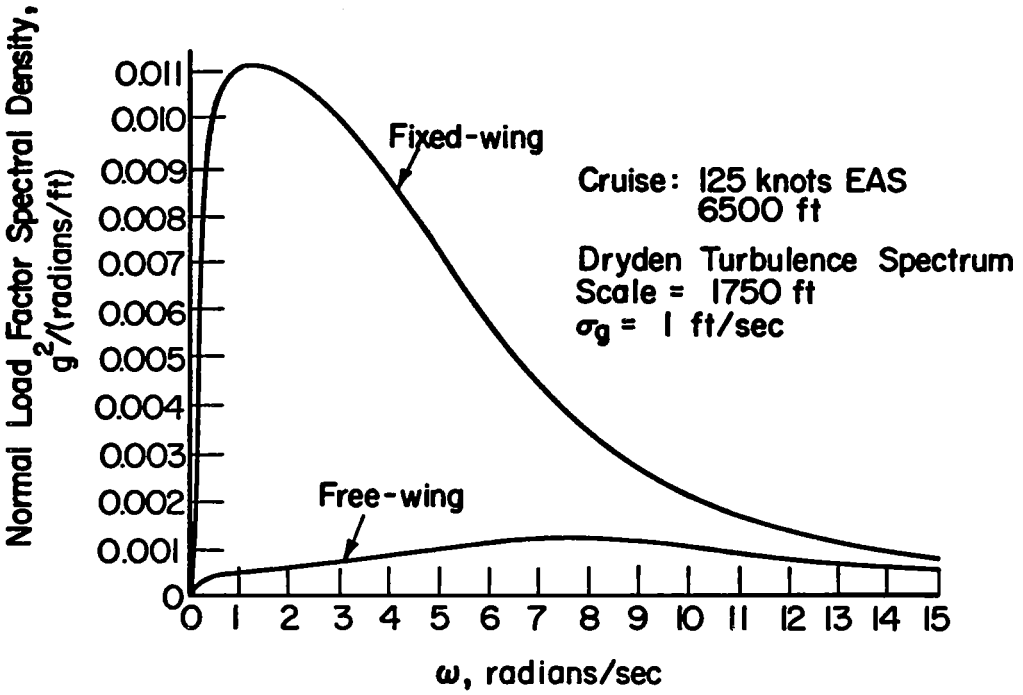

FIGURE 18. RESPONSES TO CONTINUOUS TURBULENCE

An interesting observation is the surprisingly small rms wing panel displacement required to provide the alleviation. Even in relatively heavy turbulence, say 10 ft/sec rms, the rms panel displacement would be only a little over one half of a degree.

On the adverse side, the pitch rate and pitch acceleration responses are approximately doubled as compared to the fixed-wing airplane. The significance of this is not known since no quantitative ride quality criteria are available which explicitly account for pure angular rates. If subsequent experimentation should find this objectionable, it would be expected that a simple pitch damper could reduce these motions.

Ride Comfort Criteria.- Although the quantitative measure of ride quality is in its infancy, a literature search revealed two criteria which were then applied to the free-wing light aircraft. These are discussed in the following paragraphs.

Boeing Low-Wing-Loading STOL Criterion.- In Reference 8, a relatively simple criterion of acceptable ride quality was employed. This criterion, based on experience with commercial jet transport aircraft, states that an rms load factor of .11 g's is acceptable with a probability of exceedance of 10^{-3} or less.

To apply this criterion at a given flight condition, the turbulence intensity required to achieve .11 g's rms is computed and then the probability of encountering turbulence of the computed intensity is estimated. For our purpose here, the Probability of Exceedance data contained in Reference 4 was used. These data are for nonstorm turbulence and are believed to be appropriate for light aircraft operations.

As an additional point of reference, another aircraft was used to compare with the light aircraft. This was a hypothetical rigid jet transport with a wing loading of 90 lb/ft^2, chosen because aircraft of this type are known to have acceptable ride quality.

The light aircraft were considered in cruise flight at 125 knots EAS at an altitude of 6500 feet. The jet transport was assumed to be flying at the same altitude, but at the realistic operational speed of 250 knots EAS.

A comparison of the three aircraft appears in Table 7.

TABLE 7. PROBABILITY OF EXCEEDING .11 g's RMS

	RMS Gust Intensity Required	Probability of Exceedance
Free-wing light aircraft	13.3 ft/sec	$\sim 1.5 \times 10^{-7}$
Fixed-wing light aircraft	6.0 ft/sec	5.1×10^{-3}
Jet Transport	8.45 ft/sec	$.18 \times 10^{-3}$

It is seen that the free-wing light aircraft is far superior to the acceptable standard of this criterion. In fact, the probability of encountering nonstorm turbulence of 13.3 ft/sec rms is vanishingly small and is off the scale of the data presented in Reference 4. The figure of 1.5×10^{-7} was determined by a rough extrapolation of the given data.

The fixed-wing light aircraft does not meet the stated criterion, exceeding .11 g's rms over five times as frequently as permitted. This fact is a demonstration, incidentally of the extreme nonlinearity involved in relating rms responses to subjective ride comfort. Although the fixed-wing version of the light aircraft has a load factor response only slightly over twice as great as the free-wing, the free-wing aircraft is about four orders of magnitude superiod from the standpoint of this particular ride quality criterion.

The jet transport, as might be expected, exceeds the standards of the criterion, experiencing the acceptable rms load factor only about one fifth as often as permitted. Nevertheless, the free-wing light plane is actually superior to the jet transport by a substantial margin, according to the criterion.

Grande's Subjective Discomfort Index.- An interesting approach to the quantitative measure of subjective discomfort is given by D. L. Grande in References 9 and 10. Data were obtained by subjecting flying personnel to sinusoidal accelerations of various frequencies and amplitudes. Using the concensus of subjective opinions, tolerance spectra were obtained for ratings of "Mildly Annoying", "Extremely Annoying", and "Alarming". By inverting these tolerance spectra, the relative discomfort per g at various frequencies is obtained. Figure 19 shows the discomfort spectrum for the "Mildly Annoying" rating. For the purposes of this investigation, the magnitude of the discomfort index was truncated at the lowest frequencies because no data were presented in that region in the cited references.

The main point of interest is the sharp rise in discomfort at frequencies below 2 or 3 cycles per second. This region might be called the airsickness band. This is especially significant when it is recalled that the primary alleviation effect of the free-wing is in the lower frequencies as illustrated previously in Figure 18.

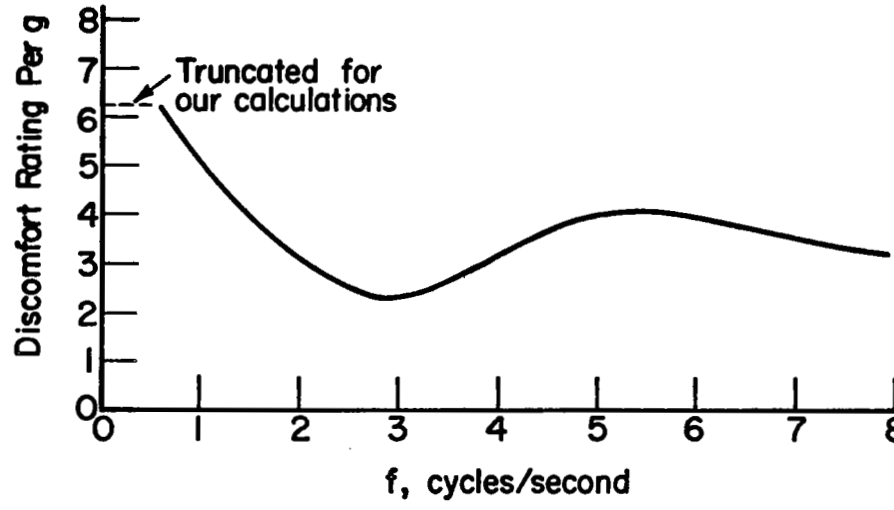

FIGURE 19. DISCOMFORT SPECTRUM

Using Grande's analytical technique, the discomfort spectrum is squared, multiplied by the normal load factor PSD function of Figure 18, and integrated to obtain a subjective discomfort index per unit turbulence intensity. It is then possible to compute the turbulence intensity which would cause the rms discomfort index to equal unity, yielding the subjective rating designated by the discomfort spectrum being used.

Using this technique, a turbulence intensity of slightly less than 7 ft/sec rms would yield the "Mildly Annoying" rating for the fixed-wing light aircraft in cruise. By contrast, a turbulence level of 19 ft/sec rms would be required to reach the same degree of discomfort in the free-wing airplane. When one considers the relative likelihood of encountering turbulence intensities of these magnitudes, the results are dramatic. Although intensities of 7 ft/sec or more could be expected occasionally in fair weather cumulous clouds and might be encountered in clear air about 1 percent of the time at the lower altitudes (ref. 4), the probability of encountering a turbulence level of 19 ft/sec is virtually zero in any conditions other than thunderstorm activity.

Special Mechanical Design Considerations

A free-wing light aircraft design based upon the results of this study would require special mechanical and structural design considerations not encountered with conventional aircraft. These factors were not explicitly treated in the current study since they would most appropriately be addressed in a more specific and detailed design study; nevertheless, some general comments are offered in the following paragraphs.

Mechanical Stops on Panel Displacement. With externally supported panels, at least, the wings are obviously not free to rotate through a complete 360 degrees. It would be necessary to ensure enough freedom to preclude the possibility of encountering a mechanical stop for all reasonable combinations of speeds, center of gravity locations, fuselage stabilizer settings, and maneuvers. This would not seem to be a particularly difficult design problem, and the effects of limited panel deflection on aircraft behavior were not examined in this study.

As a practical matter, it would be necessary to provide a gust lock device for the wing panels while the aircraft is parked on the ground. Candidate systems might be in the form of an external clamping device or an internal pin arrangement, such as used in conventional aircraft to protect the control system from gusty surface winds. Since the wing panels, themselves, are a major component of the longitudinal control system, the provisions of FAR 23.679, concerning control system locks, would be mandatory.

Aeroelastic Phenomena.- With regard to static elastic deformations, two effects are of primary interest: the torsional stiffness of the interconnecting structure in resisting differential panel deflections and the rearward bending of the hinge axis caused by drag loads.

The first of these, the torsional stiffness of the panel interconnect, is important because of the possibility of reduced aileron effectiveness, or reversal, at high dynamic pressures. In the event that the required interconnect torsional stiffness creates a serious weight penalty, two possibilities exist to relieve the differential wing torsion: auxiliary control surfaces, mounted inboard on the wing and mechanically linked to respond to differential panel deflection; and the use of spoilers for lateral control instead of differential motion of the primary trailing-edge control surfaces.

The rearward static bending of the hinge axis must be considered since it would be essential to insure adequate clearance, from the hinge axis to the trailing edge, to prevent mechanical interference between the free panels and the fixed center section.

With regard to dynamic aeroelastic phenomena, the influence of bending stiffness on flutter speed would require examination for the particular case at hand where the wing has zero structural stiffness in symmetric torsion. Although no insurmountable flutter problem would be anticipated for a low-speed aircraft, the unique pitch freedom would demand some attention.

Conclusions

From the results of this investigation, the following conclusions may be drawn:

(1) The free-wing concept can be applied to unsophisticated low wing loading light aircraft to provide ride quality, based on normal load factor attenuation, equal or superior to aircraft employing much higher wing loadings. Compared to similar light aircraft in cruise flight, reductions of about 54 percent can be realized in the rms load factor increments in continuous turbulence.

(2) For free-wing aircraft without differential wing panel freedom, all pertinent handling qualities and certification criteria can be met without recourse to stability augmentation, either active or passive.

(3) Differential pitch freedom between the left and right wing panels should not be permitted for aircraft in this class; although it appears that passive mechanical devices can be applied to correct the serious lateral deficiencies which accompany such freedom.

(4) Leading edge slats are necessary for takeoff and landing to compensate for the inherent low maximum trimmed lift coefficients obtained with trailing-edge control surfaces.

(5) The free-wing panels should be balanced about the spanwise hinge axis with leading edge slats retracted. A ballast weight penalty is incurred which might range from about 1.5 to 7.0 percent of the aircraft gross weight, depending on the detailed design.

REFERENCES

(1) Hirsch, René: Gust Absorption on Aircraft and Results of Flight Tests of an Experimental Device. DOCAERO, No. 105, July 1967, pp 41-56.

(2) Townsend, Lew: Movable Wing Controls Flying Boat. The AOPA Pilot, vol. 12, no. 9, Sept. 1969.

(3) Porter, Richard F. and Brown, Joe H., Jr.: Evaluation of the Gust-Alleviation Characteristics and Handling Qualities of a Free-Wing Aircraft. NASA CR-1523, 1970

(4) Chalk, C. R., et al: Background Information and User Guide for MIL-F-8785B(ASG), Military Specification--Flying Qualities of Piloted Airplanes. AFFDL-TR-69-72, 1969

(5) Etkin, Bernard: Dynamics of Flight, John Wiley and Sons, Inc., New York 1959.

(6) Schuldenfrei, Marvin,J.: Wind-Tunnel Investigation of an NACA 23012 Airfoil With a Handley Page Slat and Two Flap Arrangements. NACA WR L-261, 1942.

(7) Saunders, G. H.: Aerodynamic Characteristics of Wings in Ground Proximity. Canadian Aeronautics and Space Journal, June 1965.

(8) Anon.: Low-Wing-Loading STOL Transport Ride Smoothing Feasibility Study--Final Report. The Boeing Company, Wichita, Kansas, NASA CR-111819, 1971

(9) Grande, D. L.: Some Effects of Random Turbulence on Weapon-System Performance. Aerospace Engineering, Oct. 1962.

(10) Grande, D. L. and Schowalter, N. D., Jr.: Some Effects of Stability on Low-Altitude Ride Quality. AIAA Journal of Aircraft, vol. 2, no. 5, September-October 1965.

APPENDIX A

SUPPORTING WIND TUNNEL EXPERIMENTS

Introduction

This appendix is a discussion of the experimental program that was conducted in the Battelle-Columbus Laboratories' Subsonic Wind Tunnel. Included is a description of the design and fabrication of the models, calibration test, wind tunnel test procedure, and data analysis and results.

The experimental program was designed to obtain a limited amount of data that could be used to substantiate some of the assumptions used in the theoretical analysis. Two models were designed and fabricated to study the pitch damping characteristics and the yawing effects on freely mounted wing panels.

The "Pitch Model" was a reflection plane model that was mounted horizontally within the wind tunnel test section. This model was used to study the damping characteristics in the pitch direction for various pitch inertias, pitch axis locations and free stream velocities. The other model, "Yaw Model", was a scaled-down version of a Cessna 305A aircraft. The wing panel sections of this model were capable of freely rotating independently about the 15 percent pitch axis. This model was used to study yaw effects on panel angle of attack. The model was installed with the wing pitch axis vertical in the test cabin to eliminate gravity effects on the wing panels and to allow an increase in the overall size of the model.

The pitch model was tested at the three wind velocities of 50, 80, and 120 fps, and three pitch axes locations of 10.13, 15.13, and 17.63 percent chord. The model inertia was varied from 2.35×10^{-3} to 1.0×10^{-2} slug-ft^2 which corresponded to mass parameter values, as defined by Equation (1) of this report, ranging from approximately 10 to 45. The yaw model was tested at wind velocities of 80, 120, and 180 fps. The trim angle was varied from 0 to $\pm$ 6.0 degrees. The pitch axis location for the yaw model was at 15 percent chord.

Various calibration tests were conducted to ensure that the models were aerodynamically similar to the respective full-scale systems. Airfoil force and moment data obtained during the program were compared with published information for the airfoil cross-section, which was used, the NACA 0015. A limited amount of data was obtained with tufts on the surface of the models to identify any local separation regions and to define stall angle of attack.

Because of the lead time involved, the models were designed at the very beginning of the total research program. Consequently, neither model is an exact duplicate of the final configuration selected in the overall investigation. To be specific, both models used the NACA 0015 airfoil, while the selected free-wing design employs the NACA 23012 section. In addition, neither model incorporated the short, fixed center section found necessary in the main effort of the investigation. Because of the general nature of the study, it is not believed that these discrepancies seriously impair the applicability of the experimental results.

A total of 230 test points were obtained for both models, not including repeated data. Repeated test points were run to examine the repeatability of the results.

Scaling Parameters

The scaling parameters used to design the wind tunnel test models are discussed in this section. The parameters that were used can be categorized in general as aerodynamic static and dynamic scaling parameters. Dynamic similarity of the test models with full-scale systems is essential if the wind tunnel test results are to be useful in predicting the characteristics of full-scale systems.

The procedure followed was to select an airfoil shape (with simple geometry) which had previously been tested so that its steady-state aerodynamic characteristics were well established. Using a simple geometry would also simplify fabrication. Based on these considerations, the NACA 0015 profile was chosen. The 15 percent thick airfoil was chosen because of structural reasons that will become apparent in the model design section.

Although aerodynamic scaling with regard to wind tunnel testing is a common practice, it is necessary to examine the scaling parameters in light of the specific test goals of this program. In the experiments to be performed in this program, the pitch motion of freely mounted wing panels about selected hinge axes was to be studied. For such tests it was necessary to consider the following characteristics of the NACA 0015 profile: (1) lift and drag coefficient data, (2) moment coefficient, and (3) aerodynamic center.

The lift and drag characteristics for the NACA 0015 airfoil were obtained from Reference A-1. These results indicate the influence of Reynolds number on the lift and drag coefficients that were measured during various wind tunnel experiments. If the test Reynolds number is in the range of 3×10^5 to 3.5×10^6 and the airfoil angle of attack is less than 10 degrees, the lift and drag coefficients are independent of Reynolds number. Aerodynamic moment and aerodynamic center is also independent of Reynolds number for the conditions mentioned above. Based on this information and the fact that aerodynamic similarity is required, the test Reynolds number should not be less than 3.0×10^5. Since the wind tunnel is limited to a

speed range of 25 to 250 ft/sec, the minimum Reynolds number condition defines a minimum model size.

The aerodynamic data of Reference A-1 were used for comparison with data obtained from steady-state tests that were performed during this study. These test results are discussed in the Calibration section.

The vortex system generated at the tip of a finite wing will alter the aerodynamic characteristics of the wing. Corrections due to finite wing effects on the lift-curve slope are presented in Equation (1)

$$a = \frac{a_o}{1 + a_o(57.3)/\pi e\, AR} \quad , \qquad \text{(A-1)}$$

where a is the finite wing lift-curve slope, a_o is the two-dimensional lift-curve slope, e is the span efficiency factor and AR is aspect ratio. The span efficiency factor for a rectangle planform is 0.953.

The steady-state similarity parameters discussed above apply to both of the models to be used in this study. The model to be used to study the aerodynamic pitch damping characteristics must also be dynamically scaled to simulate the motion of a full-scale wing. The scaling parameter used for this purpose was derived in Reference A-2. The dynamic scaling parameter is referred to as mass parameter and is given by the following equation:

$$\bar{I} = \frac{8Iy}{\rho Sc^3} \quad , \qquad \text{(A-2)}$$

where Iy is the panel pitch moment of inertia about the pitch axis, S is the panel planform area, c is chord length, and ρ is ambient (free-stream) density.

To simulate the dynamic behavior of an actual wing, the mass parameter term should be duplicated in the wind tunnel model. Typical full-scale values of the mass parameter term are given in Reference A-2 and range from about 5 to 50. In the design of the pitch model, this term strongly influenced the model design.

The primary difficulty in the design and fabrication of the pitch model was to obtain sufficiently low values of the mass parameter. By keeping the structure as light as practicable, values as low as 10 were achieved. This value represents an approximate upper limit of those computed for actual light aircraft wing panels.

Wind Tunnel Wall Correction Factors

The reason for determining the relationships for tunnel wall corrections is two-fold. During the design stages of the wind tunnel model, the correction factors are useful in establishing overall model size limitations. Secondly, if the correction factors for a particular model are large, then appropriate corrections to the wind tunnel data should be made. This section will include discussions of the general tunnel wall correction factors, the correction factors for the "pitch model", and a subsection on the "yaw model" correction factors.

Tunnel Wall Interference

Since an early investigation of tunnel wall interference effects by Prandtl, much research has been done on studying the influence of tunnel walls. The results of these studies are reported in an AGARD report by Garner, Rogers, Acum, and Maskell (Ref. A-3). Pope (Ref. A-4) also gives a complete account of wall interference effects. The information presented in this section was obtained from these two references. Most of the working relationships were obtained from Reference A-4.

The interference of tunnel walls is due to the fact that the flow about the model is confined during tunnel testing, but in actual flight the flow is not confined. The confinement leads to two basic types of errors, (1) the variation of stream conditions due to model blockage, and (2) the effects on the streamline curvature. The first type of error is referred to as blockage interference and usually arises due to the volume occupied by the model and its wake. Streamline curvature effects are known as lift interference since they are usually associated with circulation or vorticity around the model.

Solid blockage velocity effect for wings and bodies is given by the following equations, respectively:

$$\epsilon_{sbw} = \frac{\Delta v}{V_m} = \frac{K_1 \tau_1 (\text{wing volume})}{C^{3/2}} \qquad \text{(A-3)}$$

$$\epsilon_{sbB} = \frac{\Delta v}{V_m} = \frac{K_3 \tau_1 (\text{body volume})}{C^{3/2}} \quad , \qquad \text{(A-4)}$$

where ϵ_{sb} is the incremental velocity due to solid blockage, and K_1 and K_3 are body-shape factors given in Figure 6:15 of Reference A-4 as a function of body thickness ratio; τ_1 is a factor depending on the tunnel test section shape, and model-span to tunnel-width ratio as shown in Figure 6:16 of the same reference. For bodies of revolution a model-span to tunnel-width ratio equal to zero is generally assumed: C is the test section area, V_m is indicated air velocity.

Wing volume and body volume can be estimated using the following relationships:

$$\text{wing volume} = 0.70\ tcb, \tag{A-5}$$

where t is wing thickness, c is chord length, and b is span;

$$\text{body volume} = 0.45\ \ell d^2 \quad , \tag{A-6}$$

where ℓ is length and d is maximum diameter of the body. Solid blocking for a wing-body combination is simply the sum of each component as determined from the above relationships.

The incremental velocity due to wake blockage is given as

$$\epsilon_{wb} = \frac{\Delta v}{V_m} = \frac{1}{4}\,(S/C)C_{D_\infty} \quad , \tag{A-7}$$

where S is wing area and C_{D_∞} is drag coefficient.

The drag increments due to wake blockage for a wing and/or body are given by

$$\Delta C_{D_w} = \frac{K_1 \tau_1 (\text{wing volume})}{C^{3/2}}\ C_{D_m} \quad , \tag{A-8}$$

$$\Delta C_{DB} = \frac{K_3 \tau_1 (\text{body volume})}{C^{3/2}}\ C_{D_m} \quad . \tag{A-9.}$$

The total blockage correction then is:

$$\epsilon = \epsilon_{sb} + \epsilon_{wb} \quad . \tag{A-10}$$

Before showing how these correction factors are used, the correction factors associated with lift interference will be discussed. It is shown in Reference A-4 that angle of attack corrections due to streamline curvature effects, $\Delta\alpha_{sc}$, can be expressed as;

$$\Delta\alpha_{sc} = \tau_2 \delta (S/C) C_L \quad , \tag{A-11}$$

and the total correction to angle of attack, $\Delta\alpha$, is expressed as

$$\Delta\alpha = (1 + \tau_2)\ \delta\ (S/C)\ C_L \quad , \tag{A-12}$$

where δ is referred to as the boundary correction factor and is given as a function of wing-effective-span to tunnel-width-ratio and tunnel-shape in Figure 6.30 and 6.32 of Reference A-4 for uniform and elliptical wing loading, respectively.

An effective wing span is used to account for the rolling-up of the wing tip vortex system. The effective wing span, b_e, is given by

$$b_e = \frac{b + b_v}{2} \quad , \tag{A-13}$$

where b_v/b is the vortex-span to wing-span ratio from Figure 6:23 of Reference A-4.

The term τ_2 in Equations A-11 and A-12 is a function of tail-length to tunnel-width ratio and tunnel shape. Figure 6:34 of Reference A-4 provides data for various values of effective wing-span to tunnel-width ratios. The "tail length" is defined as one-quarter of the wing chord length.

Equation A-11 for $\Delta\alpha_{sc}$ can be simplified if linearity is assumed for small values of "tail length" to tunnel-width ratio.

The resulting equation is

$$\Delta\alpha_{sc} = \frac{c}{4B}\left(\frac{d\tau_2}{d(\ell_t/B)}\right)\delta\ (S/C)\ C_L \quad , \tag{A-14}$$

where for a particular test facility both B and $\left(\frac{d\tau_2}{d(\ell_t/B)}\right)$ will be known constants. This eliminates τ_2 from the correction equation and expresses $\Delta\alpha_{sc}$ in terms of model chord length.

The additive lift correction due to lift interference, $\Delta C_{L_{sc}}$, is

$$\Delta C_{L_{sc}} = -\Delta\alpha_{sc} a \quad , \tag{A-15}$$

where a is the wing lift curve slope. The additive correction to the moment coefficient, $\Delta C_{m_{sc}}$, is

$$\Delta C_{m_{sc}} = -0.25\Delta C_{L_{sc}} \quad . \tag{A-16}$$

For these tests it was more convenient to correct just the angle of attack rather than the angle of attack and lift. To make angle corrections, τ_2 should be determined by using c/2 as a tail length, instead of c/4. For a linear approximation as in Equation A-14, $\Delta\alpha_{sc}$ is doubled when tail length is assumed equal to c/2. The moment correction will then be

$$\Delta C_{m_{sc}} = 0.125\Delta\alpha_{sc/2} a \quad . \tag{A-17}$$

The following is a summary of the tunnel wall correction factors and how they are used to correct tunnel conditions and model data.

$$\text{tunnel velocity:} \quad V = V_m(1 + \epsilon) \quad , \tag{A-18}$$

where $\epsilon = \epsilon_{sb} + \epsilon_{wb}$ and V_m is indicated tunnel velocity.

$$\text{dynamic pressure:} \quad q = q_m(1 + 2\epsilon) \quad , \tag{A-19}$$

$$\text{Reynolds number:} \quad R = R_m(1 + \epsilon) \quad , \tag{A-20}$$

$$\text{lift coefficient:} \quad C_L = C_{L_m} (1 - 2\epsilon) - \tau_2 \Delta\alpha \, a \quad , \tag{A-21}$$

where $\Delta\alpha = \delta(S/C) \, C_L$.

$$\text{angle of attack:} \quad \alpha = \alpha_m + [\delta(S/C)C_L] \, (1 + \tau_2) \quad , \tag{A-22}$$

pitching moment coefficient:

$$C_{m_{1/4}} = \left[C_{m_{1/4}}\right]_m (1 - 2\epsilon) + 0.25 \, \tau_2 \Delta\alpha a \quad , \tag{A-23}$$

drag coefficient:

$$C_D = C_{Dm} (1 - 2\epsilon) - \Delta C_{Dw} - \Delta C_{DB} + \delta(S/C)C_L^2 \quad . \tag{A-24}$$

Pitch Model

In this subsection, the tunnel wall interference relationships that were defined in the previous section are used to estimate the magnitude of the correction factors associated with various model sizes in the Battelle-Columbus Subsonic Wind Tunnel. The tunnel has a test section that is 55 inches in height and 39 inches wide. This gives a total test section area of $C = 14.9 \ ft^2$.

The pitch model was a reflection plane model mounted on the side wall of the tunnel. The tunnel wall corrections for a reflection plane model can be treated as though the entire model was in a tunnel of double the width of the existing tunnel. Usually a slightly lower lift curve slope and slightly higher induced drag will be determined from a reflection plane model compared to a complete model because of vortex shedding in the root boundary layer adjacent to the tunnel wall.

The airfoil shape being used for this model was an NACA 0015 airfoil. The profile drag coefficient for this airfoil at a lift coefficient of 0.8 is approximately 0.015. The drag coefficient at approximately 10 degrees angle of attack is used because this gave maximum wake blockage errors and also because this was the maximum angle of attack used with this model.

The tunnel parameter terms, K_1 and τ_1, for the 15 percent thick wing for an effective tunnel width-to-height ratio of 1.42 are given by

$$K_1 = 1.04 \quad ,$$

$$\tau_1 = 0.87 \quad .$$

τ_1 can be assumed constant over a wing-span to tunnel-width ratio of zero to 0.8 for a tunnel width-to-height ratio of 1.43 (which corresponds to the BCL tunnel).

Substituting these values into Equations A-3 and A-7 results in the following equations for solid model and wake blocking.

$$\epsilon_{sbw} = 0.83 \times 10^{-3} \, c^2 b \quad , \tag{A-25}$$

$$\epsilon_{wb} = 1.26 \times 10^{-4} \, cb \quad . \tag{A-26}$$

These give the total velocity increment in percent of tunnel velocity, due to solid model and wake blocking as;

$$\epsilon = (0.083c + 0.0126) \, cb \quad . \tag{A-27}$$

Figure A-1 is a plot of the blockage errors that will exist for the 15 percent-thick airfoil for various wing chord lengths and spans. The dashed line represents a wing whose semi-span is 80 percent of the tunnel width.

The lift interference error for various size models was estimated by using Equation A-22 to correct only the angle of attack as a function of model size and wind tunnel shape. This can be rewritten in terms of percent angle. The resulting expression is

$$\frac{\Delta\alpha}{\alpha} = 10^2(1 + \tau_2) \, \delta \, (S/C) \, \frac{C_L}{\alpha} \quad . \tag{A-28}$$

The linear approximation is used to express τ_2 and since corrections are only made to angle of attack, a value of c/2 is used for tail length. Here, τ_2 is given by

$$\tau_2 = \frac{c}{2B} \frac{d\tau_2}{d(\ell_t/B)} \quad , \tag{A-29}$$

where $\frac{d\tau_2}{d(\ell_t/B)}$ is equal to 2.5 for the tunnel shape parameter, $\lambda = 0.705$. Substituting this value for τ_2 into Equation A-28 and simplifying gives

$$\frac{\Delta\alpha}{\alpha} = 515 \, (1 + 1.25 \, \frac{c}{B}) \, \delta \, (S/C) \quad . \tag{A-30}$$

From Figure A-1, the lift curve slope for this profile is approximately 0.09 over the linear range.

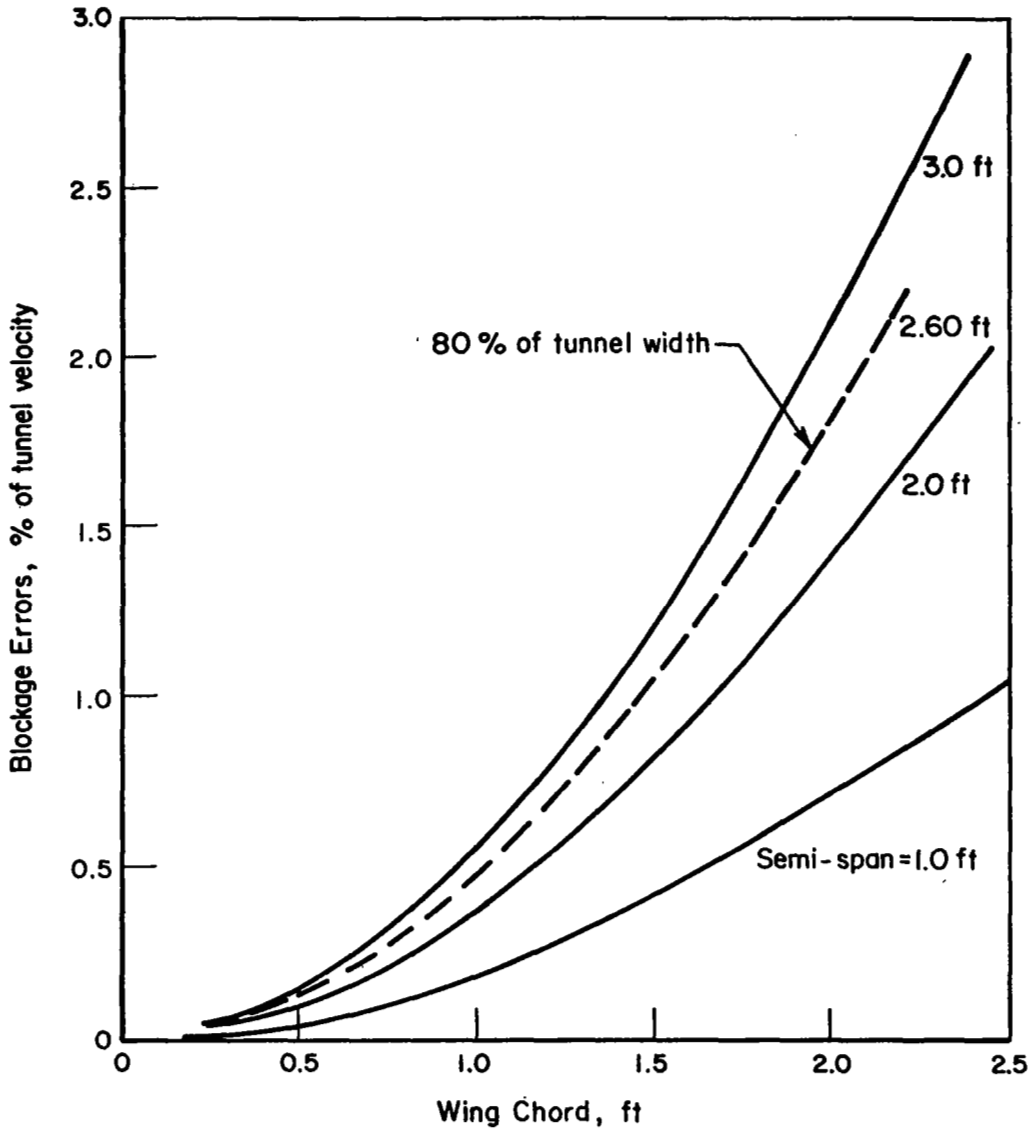

FIGURE A-1. BLOCKAGE ERRORS DUE TO TUNNEL WALL INTERFERENCE

The vortex span width for this wing is approximately equal to 0.86 of the geometric span for wing aspect ratios between 4 and 8 and a taper ratio of 1.0. Therefore, the effective span is $b_e = 0.93b$. From Figure 6:30 of Reference A-4 for a tunnel shape factor of $\lambda = 0.705$ and effective span-to-tunnel width ratios less than about 0.70, the boundary correction factor, δ, is approximately equal to a constant value of 0.118. Substituting for δ, C and B in Equation A-30, gives the following:

$$\frac{\Delta\alpha}{\alpha} = 2.04\ (1 + 0.385c)\ cb \quad . \tag{A-31}$$

Figure A-2 is a plot of the angle error in percent of angle for various size models. The dashed line represents a model with a semi-span of 80 percent of the tunnel width. Various values of wing aspect ratio are shown cross-plotted in Figure A-12 for corresponding values of wing span and chord.

From Figure A-2 for a wing with an 0.75-ft chord and an aspect ratio of 6.5, the angle of attack correction would be 9.5 percent. This would approximately represent an angle of attack error of 1.0 degree at 10 degrees. Since the angle of attack has been corrected totally, with tail length defined as c/2, there would not be any correction to the lift coefficient. Therefore, the errors indicated in Figure A-2 would be representative of total errors.

The correction to moment coefficient can be estimated using Equations A-17 and A-14 and, once again, assuming a linear relationship for τ_2. The resulting equation for the moment correction is

$$\Delta C_{m_{sc}} = 0.89 \times 10^{-4} c^2 b\alpha \quad . \tag{A-32}$$

An approximate expression for the pitching moment coefficient about the 15 percent chord location for the NACA 0015 airfoil section is given by

$$C_{m_{15\%}} = 0.077\ C_L \quad . \tag{A-33}$$

Assuming that the aerodynamic center for this wing is at the 22.5 percent chord, and using 0.09 for the lift curve slope, the equation for pitching moment coefficient is

$$C_{m_{15\%}} = 6.94 \times 10^{-3} \alpha \quad . \tag{A-34}$$

If Equation A-34 is divided into Equation A-32, the relative percent error in the moments about the 15 percent chord station can be estimated for various model sizes by

$$\frac{\Delta C_{m_{sc}}}{C_{m_{15\%}}} = 1.29\ c^2 b \quad . \tag{A-35}$$

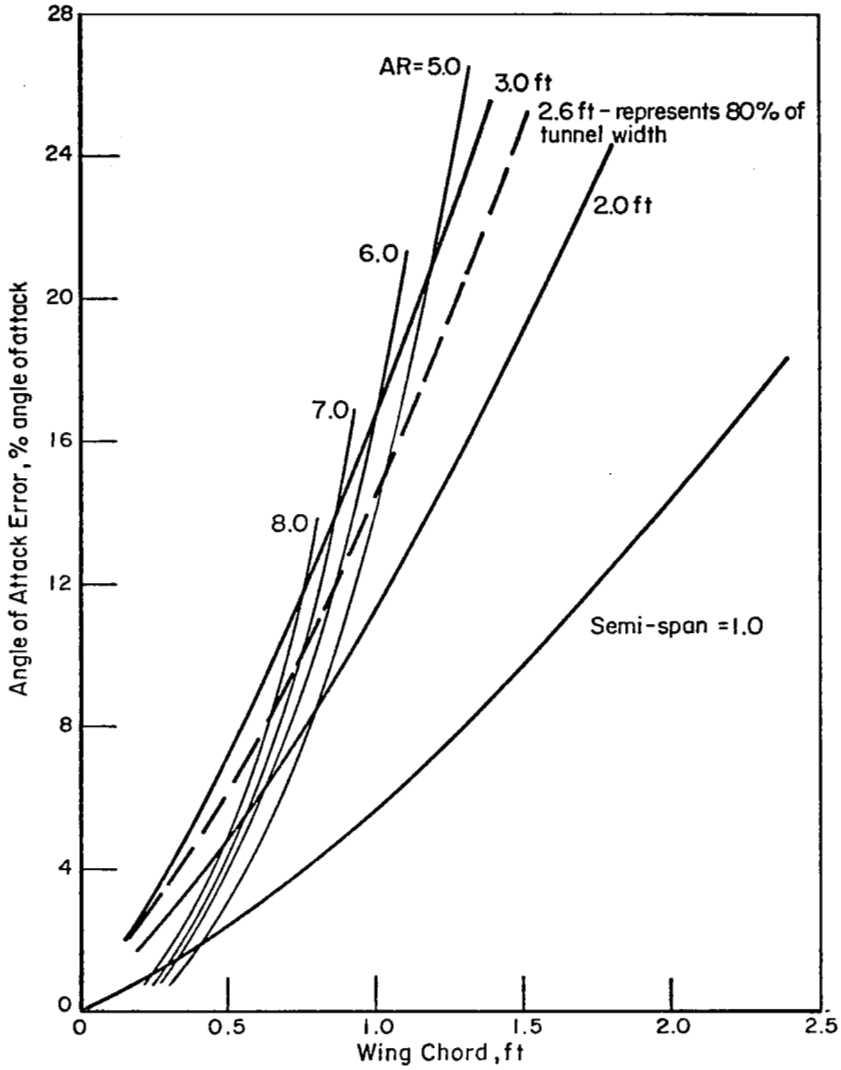

FIGURE A-2. ANGLE OF ATTACK ERRORS DUE TO TUNNEL WALL INTERFERENCE FOR VARIOUS SIZE PITCH MODELS

Figure A-3 represents the error in pitching moment coefficient about the 15 percent chord pitch axis for various model sizes. For a model with a 1-foot chord and a span of 80 percent of the tunnel width, the moment correction would be approximately 6.5 percent of the pitch moment value.

Moment correction factors for different pitch axis locations can be estimated from Figure A-3 by multiplying by the ratio of the static margin for the 15 percent chord pitch axis to the new pitch axis static margin. For instance, for pitch axis locations of 10 percent and 20 percent chord multiply the results of Figure A-3 by 0.60 and 2.75, respectively, to obtain an estimated moment correction factor.

Based on the correction factor data for the pitch model, it was found that a model could be built and tested in the tunnel while still keeping the correction factors less than 10 percent. From blockage considerations, it appeared that these errors could be kept less than 1/2 percent of the stream values for model sizes up to 1.0 foot in chord length.

Yaw Model

Tunnel wall interference for the yaw model are discussed in this subsection. The analysis follows the same procedure that was carried out for the pitch model corrections in the previous subsection. The yaw model consisted of two freely mounted wing panels and a fuselage section. The panels were each independently free to pitch about the 15 percent chord axis.

The wind tunnel model was a scaled-down version of a Cessna 305A (L-19) aircraft, except the wings for the wind tunnel model were rectangular. They were designed using a NACA 0015 profile with a rectangular planform. In order to increase the size of the model and eliminate gravitational effects, this model was mounted in a vertical position in the tunnel. The tunnel shape parameter for this type of model installation is calculated on the basis that the tunnel height is now the tunnel width and the tunnel width becomes tunnel height. Therefore, the tunnel height-to-width ratio is equal to 0.71. The test section area, C, is 14.9 ft^2.

Some approximate geometric values for this aircraft are listed below:

$$AR = 6.70$$

$$\ell_{b/C} = 4.65$$

$$d_{max}/C = 0.77$$

where ℓ_b and d_{max} are body length and maximum diameter. The tunnel parameters K_1, K_3, and τ_1 for this model are:

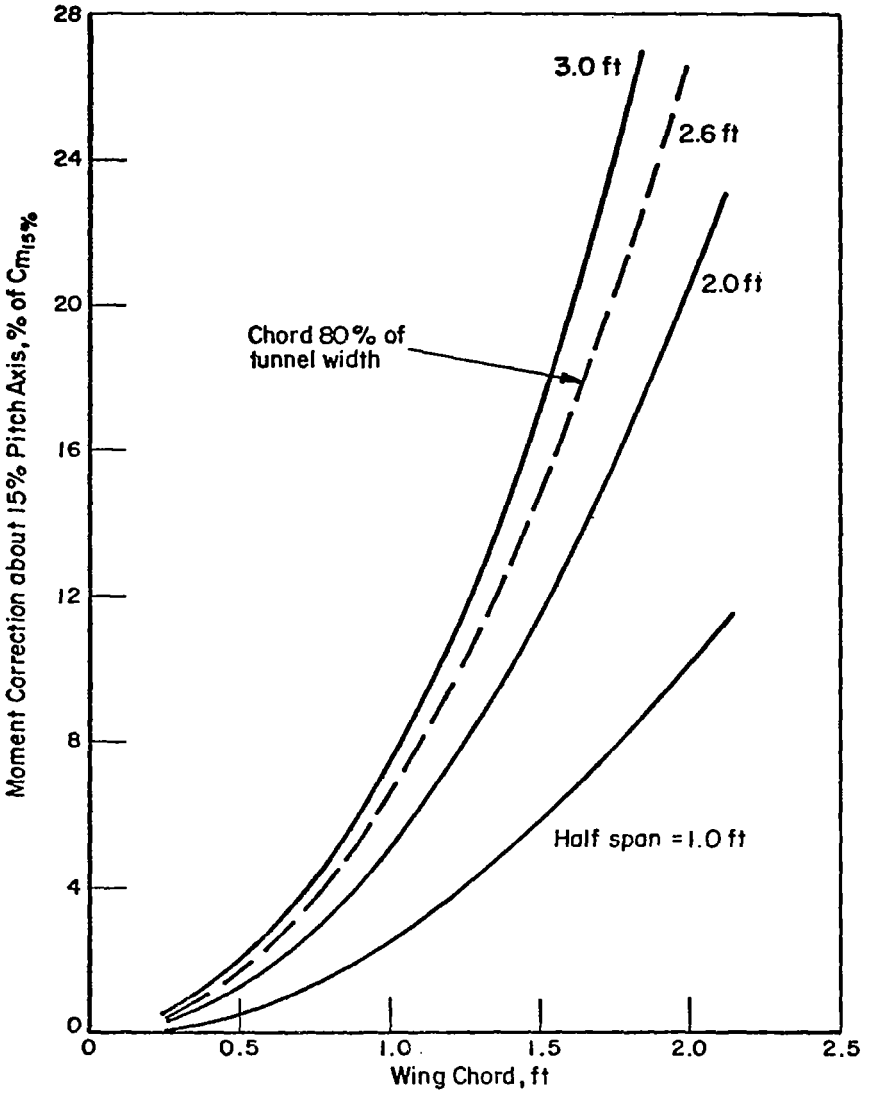

FIGURE A-3. PITCHING MOMENT COEFFICIENT ERRORS FOR PITCH AXIS AT 15% CHORD VERSUS MODEL SIZE

$$K_1 = 1.04$$

$$K_3 = 0.93$$

$$\tau_{1w} = 0.87$$

$$\tau_{1b} = 0.87 \quad .$$

The volume of the wing and body was approximated by the following equations:

$$\text{wing volume} = 0.105\ c^2 b \ , \text{ and}$$

$$\text{body volume} = 1.24\ c^3 \quad .$$

These volumes are based on the geometric similarity parameters listed above for this aircraft. Substituting the above results into Equations A-3 and A-4 gives the solid blockage corrections expressed in terms of wing chord length and span for the wing and body,

$$\epsilon_{sbw} = 1.65 \times 10^{-3}\ c^2 b \ , \text{ and} \qquad \text{(A-36)}$$

$$\epsilon_{sbB} = 1.74 \times 10^{-2}\ c^3 \quad . \qquad \text{(A-37)}$$

The wake blockage for the wing and body are expressed as

$$\epsilon_{wb} = 2.52 \times 10^{-4}\ cb \ , \text{ and} \qquad \text{(A-38)}$$

$$\epsilon_{wb} = 0.0173\ c^2 \quad . \qquad \text{(A-39)}$$

Summing the blockage factors for the wing-body combination gives the following results for percent error in tunnel velocity:

$$\epsilon = (0.165c + 0.0252)\ cb + (1.74c + 1.73)c^2 \ , \qquad \text{(A-40)}$$

Figure A-4 is a plot of the blockage correction factors for various size yaw models.

Using Equation A-31, an estimate of the angle errors or correction that must be applied to the tunnel data was obtained. Since the tunnel parameters are approximately equal and the airfoil shape is similar, the results obtained in Figure A-2 can be used, if some of the parameters are redefined. Figure A-5 is a replot of Figure A-2 for the parameters appropriately redefined and also for an additional wing span value of 4 feet. The angle correction factors in

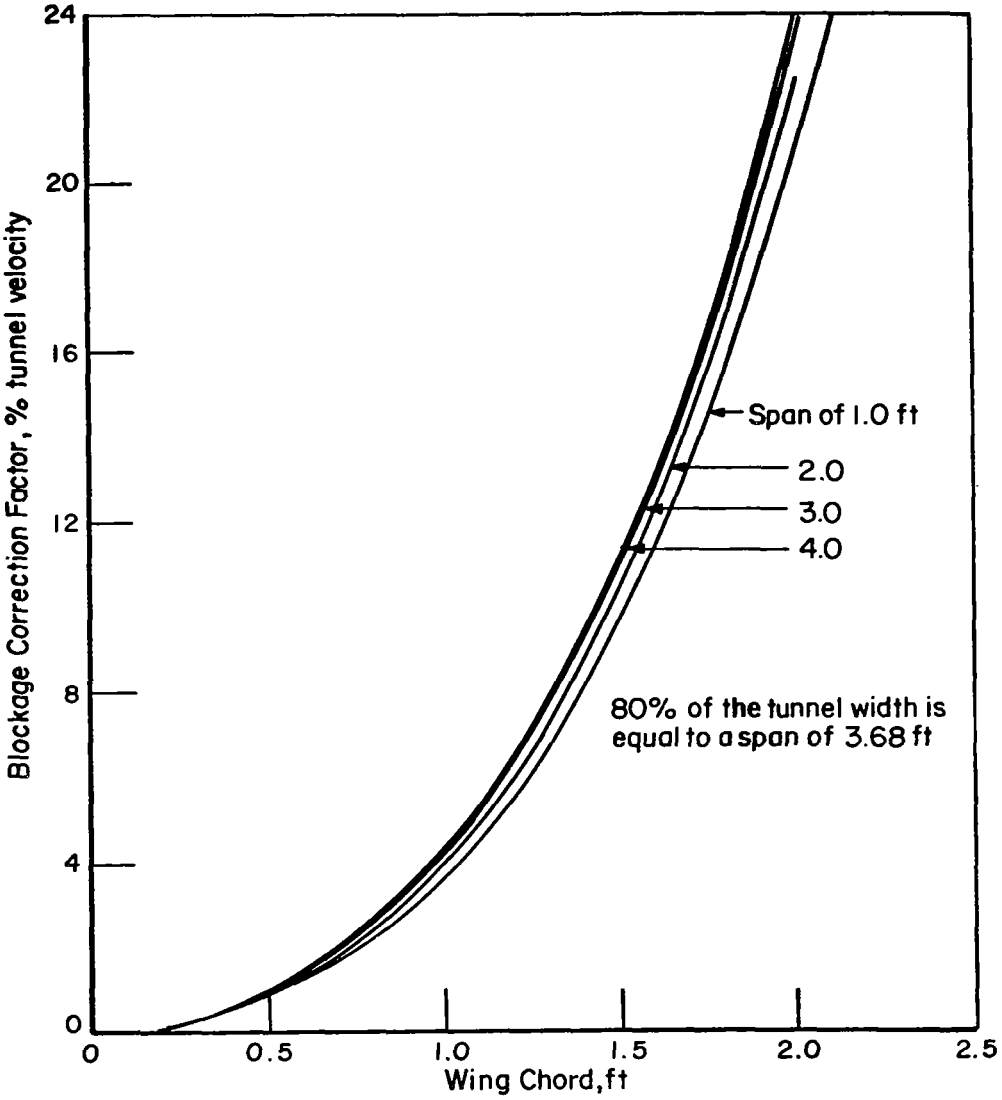

FIGURE A-4. BLOCKAGE CORRECTION FOR VARIOUS SIZE YAW MODEL

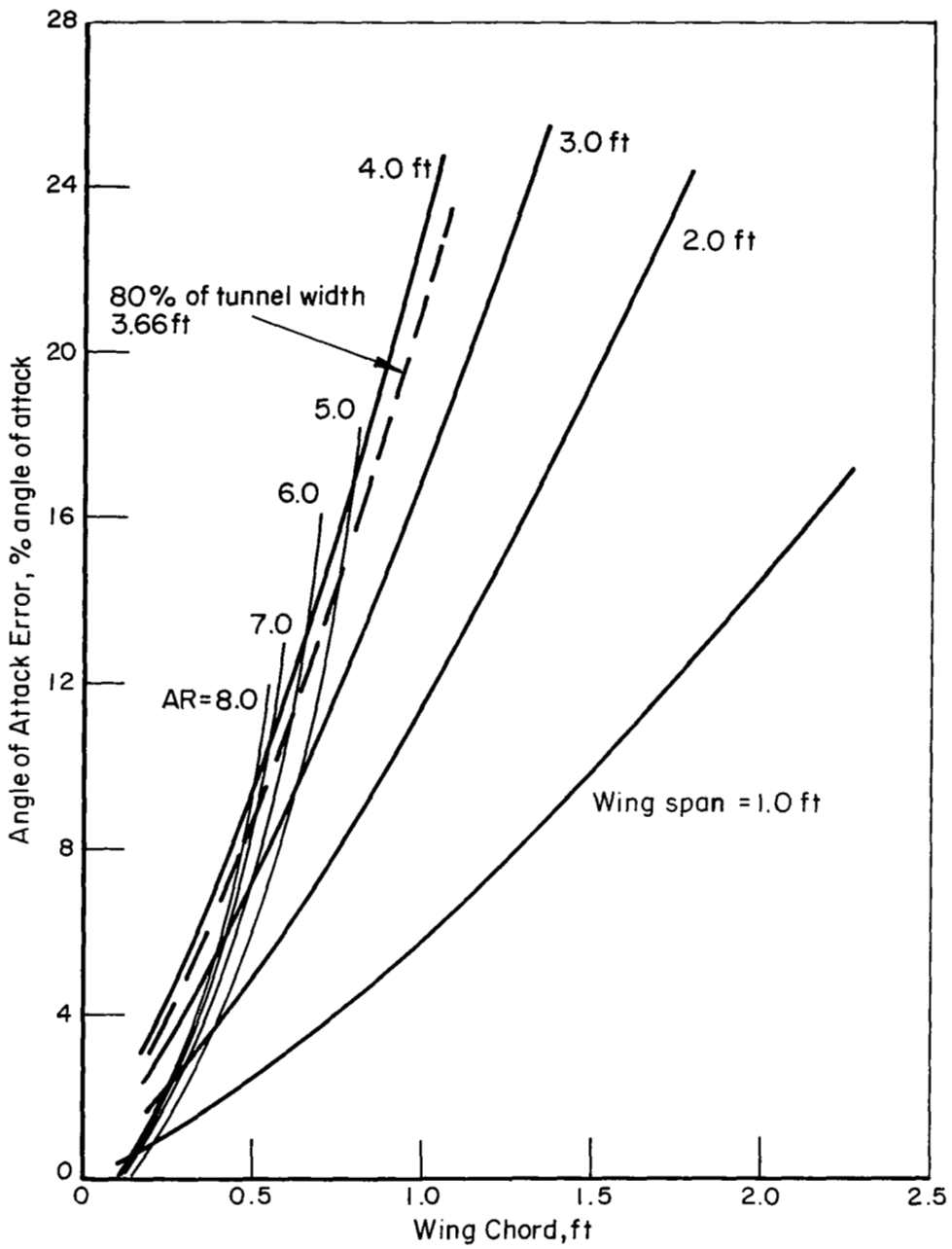

FIGURE A-5. ANGLE OF ATTACK ERRORS DUE TO TUNNEL WALL INTERFERENCE FOR VARIOUS SIZE YAW MODELS

Figure A-5 are based on a "tail length" of c/2, therefore, the lift coefficients do not have to be corrected for lift interference.

The aerodynamic moments were corrected using Equation A-35. Once again, since the model was similar, basically the same tunnel shape parameter holds, so the results of Figure A-3 can be used. Some of the parameters in Figure A-3 must be redefined as in the angle correction data. Since this model had a fixed hinge axis at the 15 percent chord location, the error in moment at this location is given by Equation A-35 in terms of model size.

Figure A-6 is a plot of the moment correction data for the yaw model. Based on the results of angle errors for various model sizes, and on the geometric constraint placed on the yaw model, the moment coefficient correction data was determined for model sizes up to a chord length of one foot.

Design and Fabrication of Model

Details concerning the design and fabrication of the wind tunnel models are presented in this section. Information presented in the sections on "Scaling Parameters" and "Wind Tunnel Correction Factors" are used in this section to define various limits that were placed on the specific design of each model. Specific details of each model are discussed in the subsections entitled "Pitch Model" and "Yaw Model".

Pitch Model

The pitch model was designed as a reflection plane model having an NACA 0015 section and a rectangular planform. This model was mounted to rotate freely in pitch about selected hinge axes.

From a construction standpoint, a large model is preferred. The principal constraint on model size was the desirability of achieving an aspect ratio (full span) of 6.5, representative of light aircraft, while keeping the model span to not more than 80 percent of the tunnel width.

A reflection plane model span of approximately 30 inches and a chord length of 9 inches was selected on the basis of these considerations. Since it was previously established that the Reynolds number should not be less than 3.0×10^5, a tunnel speed of 75 ft/sec was required to achieve aerodynamic similarity to full-scale wings. This tunnel speed value includes the effect of the tunnel turbulence factor of 1.08.

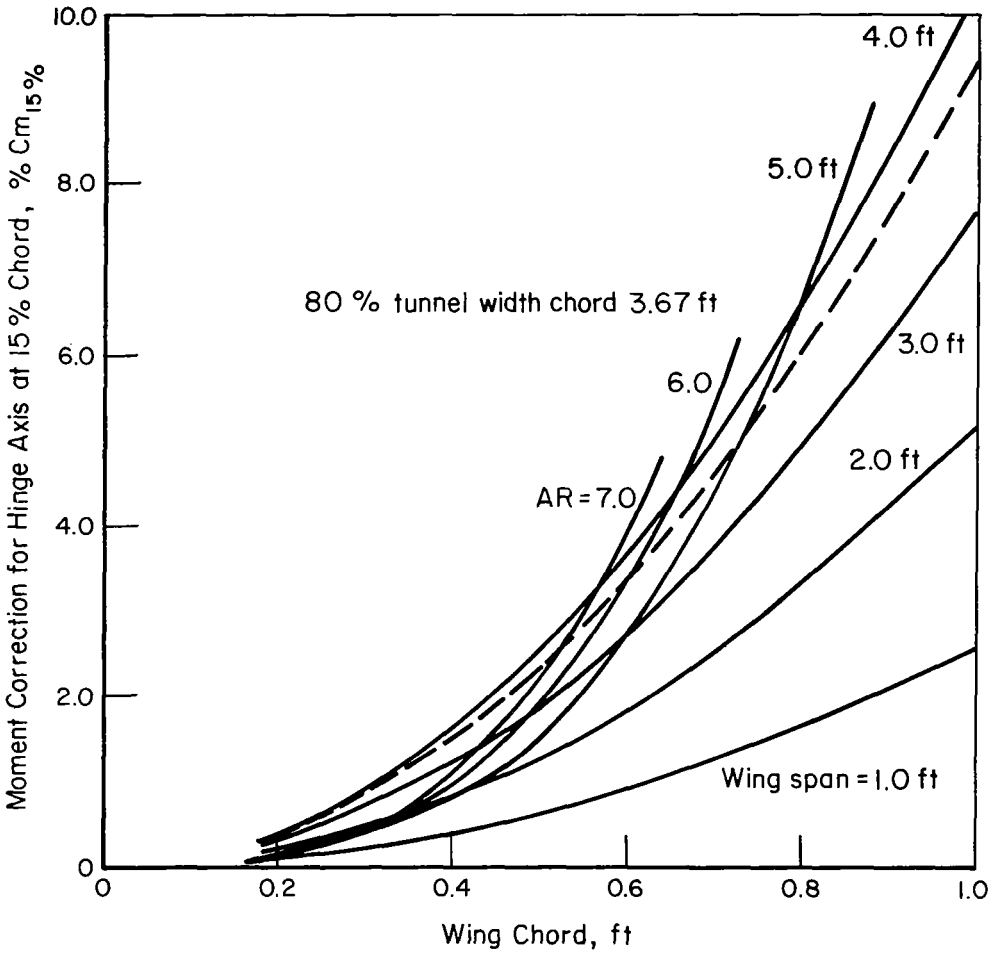

FIGURE A-6. PITCH MOMENT COEFFICIENT ERRORS FOR 15% CHORD HINGE AXIS FOR YAW MODEL OF VARYING SIZE

To achieve dynamic similarity in the oscillation experiments, the mass parameter defined by Equation A-2 must be duplicated. For a model with a 9-inch chord length, a mass parameter as low as 10 requires a ratio of pitch moment of inertia to planform area of not more than 1.25×10^{-3} slug-ft^2/ft^2.

It was determined that a solid wing panel, even if constructed of balsa-wood, would have excessive pitching inertia about a representative pitch axis at 15 percent chord. As a result, a structure was designed with balsa leading and trailing edges, ribs, stringers, and sheet skin.

An aluminum tube was designed into the model to reinforce the wooden structure and to act as the hinge axis of the wing. The tube ran approximately the full span of the model and extended 6 inches outside the rib at the root of the wing. The tube size was 5/8-inch in diameter with a 60-mil wall. The support tube was attached to the wooden structure at three locations--0, 50, and 95 percent span. The ribs at these locations were increased in size from 1/8-inch to 1/2-inch thick. The tube was joined to the wooden ribs with mounting brackets that were permanently bolted to the ribs. Rigid attachment was accomplished with pins that extended through the aluminum tube and brackets. Details of the attachment brackets are shown in Figure A-7. The holes in the metal mounting brackets are for setting various pitch axis locations. The holes correspond to nominal pitch axis locations of 10, 12.5, 15, 17.5, and 20 percent chord. The model was supported in the wind tunnel by placing the 5/8-inch aluminum tube (which extended from the root of the wing) through the tunnel wall and into a 3/4-inch aluminum tube that was permanently mounted to the model support mechanism on roller bearings outside the tunnel test cabin. The 5/8-inch tube and 3/4-inch tube were pinned together eliminating any relative motion between them. An additional support point was built into the model at the 75 percent span. This support was basically a bearing and housing that slipped over the 5/8-inch aluminum tube. The bearing housing was designed so that four wires could be attached to it and brought outside the tunnel for rigid support. The wires were not attached to the tunnel due to tunnel vibration.

The bearings in the model and on the support frame outside the tunnel were low friction roller bearings that can withstand normal loads of up to 250 pounds, for extended periods. The loads experienced by the bearings during the test were well below this value.

The components used to vary the inertia and center of gravity location of the model were located outside the tunnel on the 3/4-inch tube that acted as the model support. Since these components were outside the tunnel, it was possible to make inertia and center of gravity changes during testing. The inertia of the model was varied with two weights that could be placed at desired distances from the pitch axis. Two weights were used at equal distances from the pitch axis to vary model inertia so that the system center of gravity would not be changed. With the addition of the weights, the model inertia could be increased from 1.2×10^{-4} to 4.3×10^{-3} slugs/ft^2 in a selective fashion. A disk shaped piece of lead was used to vary the model's center of gravity. This weight was supported on the same

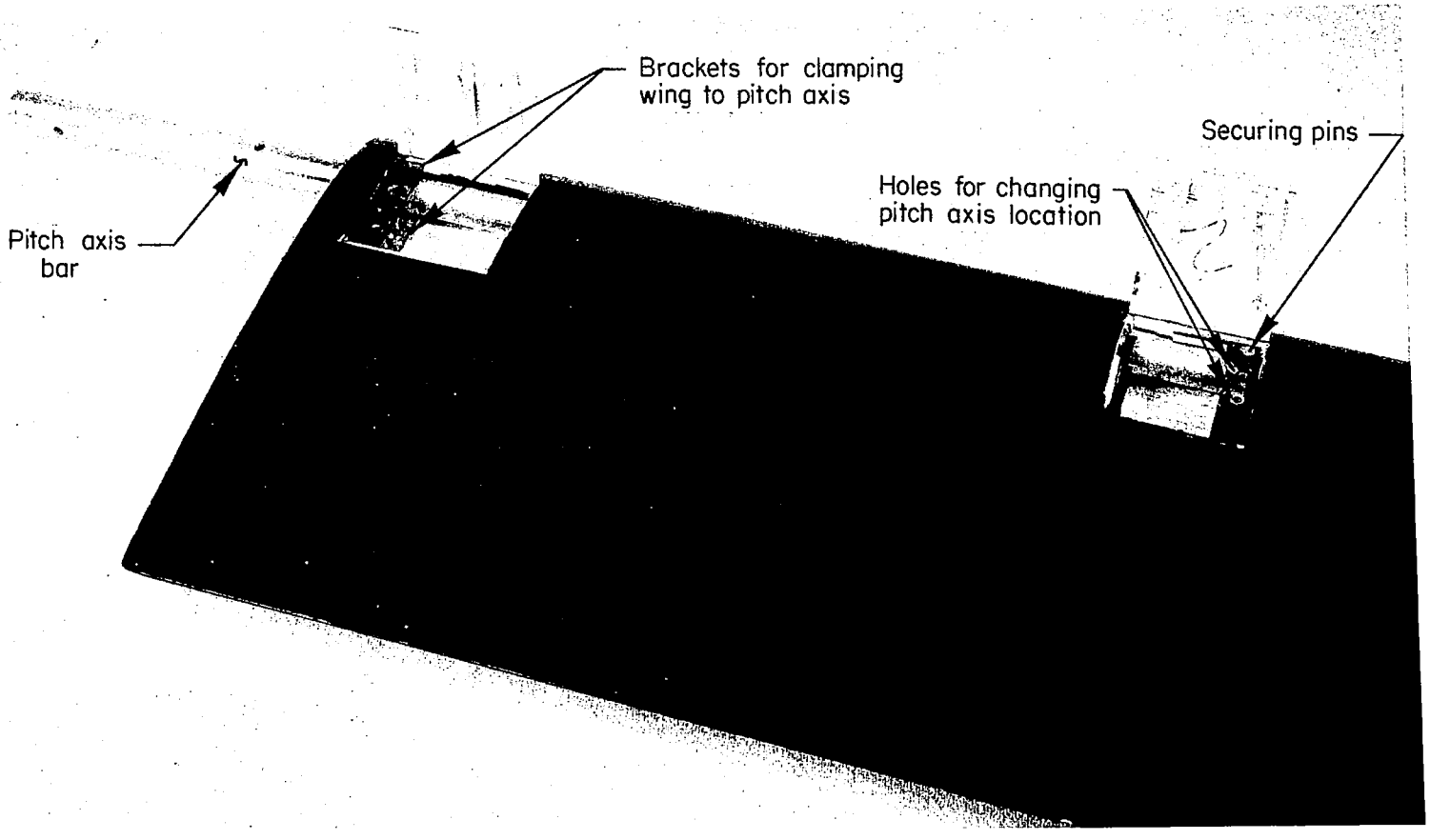

FIGURE A-7. DETAIL OF PITCH BAR ATTACHMENT

rod which was used to support the inertia weights. Although this weight was for changing center of gravity, its use also adds to the system inertia.

Angle of attack was measured with a potentiometer that was attached to the end of the 3/4-inch support tube. A 3-turn potentiometer was used that had a linearity specification of 0.1 percent over the full range of the potentiometer.

Yaw Model

The purpose of the yaw model was to measure the influence of yaw angle on angle of attack of the freely mounted semi-span panel sections. The model was designed so that each semi-span section could rotate independently about a common hinge axis. As in the previous subsection, the information presented in the Scaling Parameter and Wind Tunnel Correction Factors section was used to establish various geometric boundary conditions. Since the purpose of the yaw model was for determining static condition of angle of attack, dynamic scaling was not necessary. Aerodynamic similarity of the model was ensured based on the same Reynolds number consideration as for the pitch model.

This model was designed to be mounted vertically in the wind tunnel. The advantages in installing the model vertically were: (1) a bigger model could be used in the tunnel (the height of the test section is greater than the width of the test section), and (2) gravity forces on the freely mounted wing panels were eliminated.

The wing cross-section and planform for this model were the same as for the pitch model. Therefore, the aerodynamic characteristics outlined in the previous section for the pitch model also apply to this model. A minimum test Reynolds number condition of 3.0×10^5 existed to ensure that the aerodynamic forces were properly simulated.

The model span was to be no greater than 44 inches which corresponds to 80 percent of the tunnel height. Based on a span of 44 inches and an aspect ratio of 7.0, the wing chord was about 6 inches. The tunnel corrections for a model with a 6-inch wing chord were less than 10 percent in angle of attack, and the moment correction was less than 3 percent.

The fuselage section of this model was scaled from a Cessna 305A (L-19) aircraft. The scale factor was approximately 1 inch on the model represented 1 foot on the full-scale aircraft.

Figure A-8 shows the various components of this model. The hinge axis was at the 15 percent chord location. Tabs were designed into the wing so that various trim angles could be set aerodynamically. The tabs were maintained at specified angles with rods that extended through the tabs. Small potentiometers

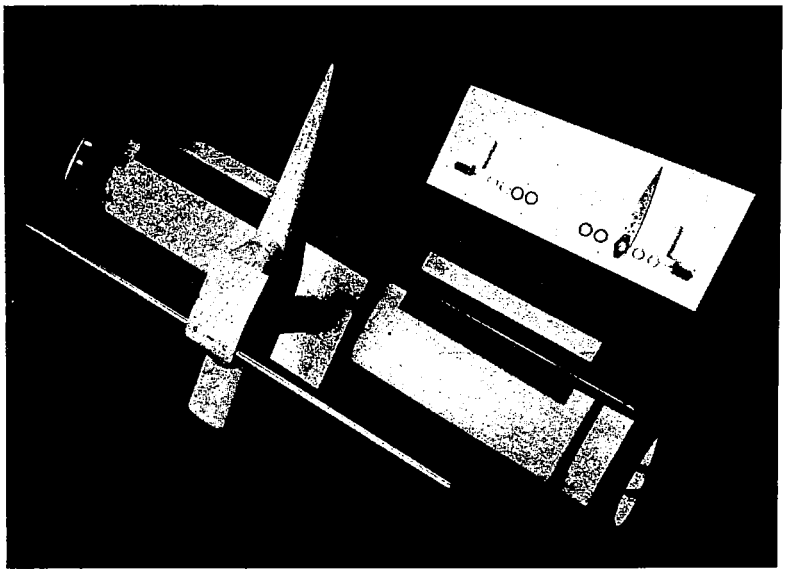

FIGURE A-8. COMPONENTS OF YAW MODEL

were mounted in the wing tips to measure angle of attack. Figure A-9 is a detailed picture of the potentiometer attachment. The potentiometer wiper shaft was locked to the main pitch bar and a bracket was used to rigidly attach the potentiometer body to the wing cross-section. The electrical wires to the potentiometers were run inside the pitch axis tube from the center of the fuselage, where the wires were brought to the outside of the tunnel through the model support tube.

The model was attached to a flat plate which, in turn, was welded to a cylindrical tube that acted as the main support. The tube extended outside the test cabin through a hole in the cabin wall. The tube was attached to the tunnel model support mechanism on roll bearings so that the tube could rotate about its axis (to allow variation in yaw angle).

On the main support tube outside the tunnel, a pointer and protractor were arranged so that yaw angles could be visually set and recorded during a run. The scale was such that it could be read accurately to 0.25 degrees.

Calibration Test

Prior to performing the wind tunnel tests, various calibration tests were performed. These tests included the calibration of the potentiometers, vacuum test of the pitch model to measure the inertia and friction forces of the bearings, tuft studies of both models to visually observe flow irregularities, and steady-state aerodynamic force measurements. Included in this section is an overall estimate of the total error band for these data, based on the calibration tests and instrumentation used.

Pitch Model

The pitch inertia for this model was estimated originally by summing the theoretical values of the various model components about the 15 percent chord axis. Since wing inertia was an important quantity in these tests, it was decided that an experimental evaluation of the model inertia be obtained to verify the theoretical calculation. During the inertia test, it was possible to also obtain estimates of the pitch damping due to bearing friction. Although the model was designed to have minimum bearing friction, an estimate of the frictional damping was desirable to compare to the aerodynamic damping and ensure that such effects were small.

Prior to performing the vacuum test the potentiometer for measuring angle of attack was calibrated. The potentiometer was found to be linear to within 1.0 percent over an angle of attack range of $\pm$ 10 degrees.

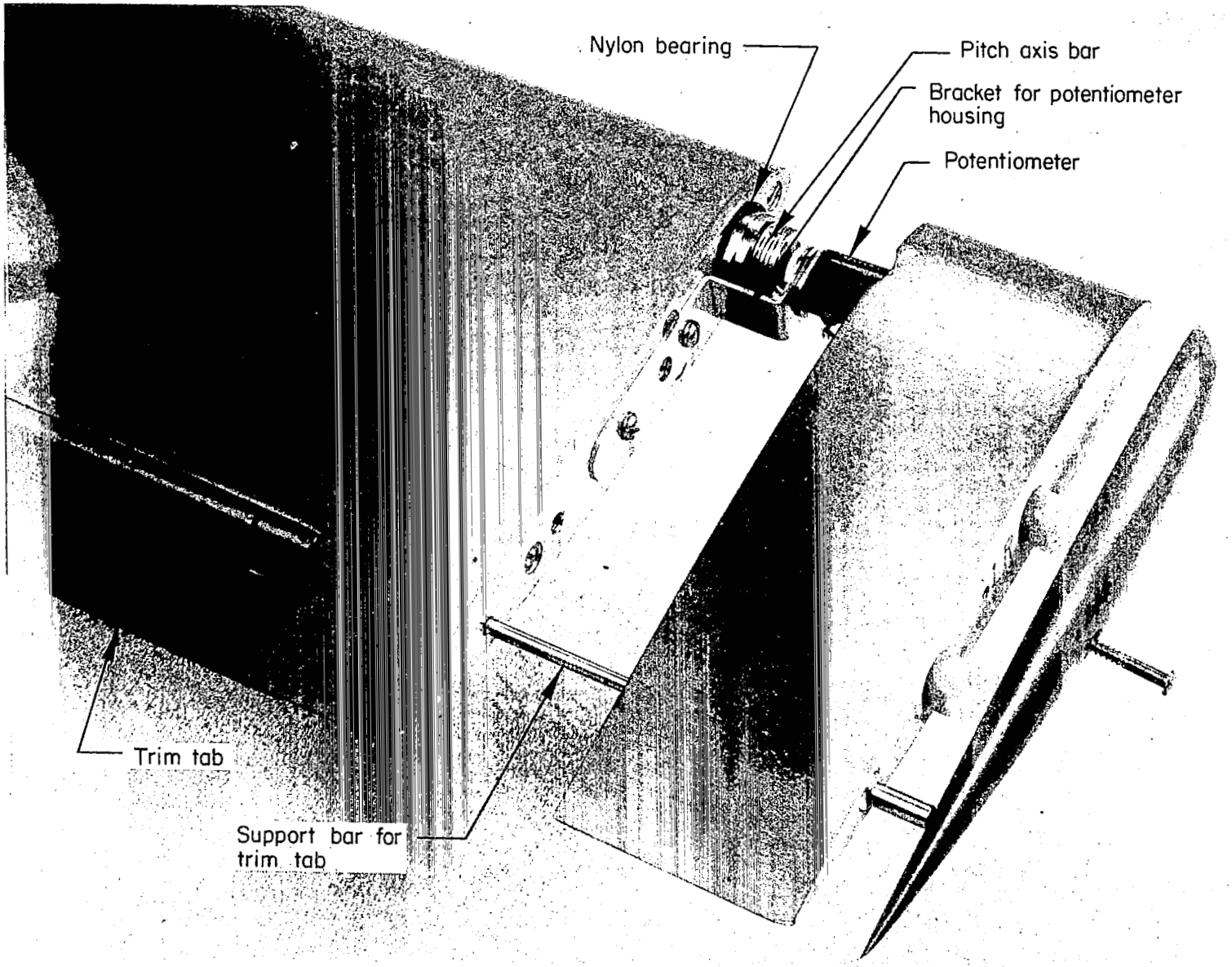

FIGURE A-9. DETAIL OF POTENTIOMETER ATTACHMENT

The wing and support plates were placed in a vacuum chamber for the inertia tests to eliminate the influence of air circulation about the wing. The pressure in the chamber was maintained at 1/2 mmHg. The wing was set up in a pendulum fashion with the pitch axis at the 15 percent chord location. The governing equation of motion for this system is well known and given by

$$I_y\ddot{\theta} + mg\bar{\ell} \sin \theta + Fsgn\dot{\theta} = 0 \quad , \tag{A-41}$$

where I_y = inertia about pitch axis

θ = angular displacement

m = mass of wing

F = torque due to friction

$\bar{\ell}$ = distance between pitch axis and center of gravity

g = gravitational constant .

Equation A-41 is the simple pendulum equation of motion with the additional damping term, $Fsgn\dot{\theta}$, to account for constant frictional torque. Based on the solution of Equation A-41, the following expressions for pitch inertia and frictional torque can be obtained:

$$I_y = \frac{mg\bar{\ell}}{\omega^2} \quad , \text{ and} \tag{A-42}$$

$$F = \frac{\delta mg\bar{\ell}}{4} \quad , \tag{A-43}$$

where ω is natural frequency and δ is amplitude decay per cycle.

The natural frequency and amplitude decay were measured during the experimental test. The center of gravity was determined by placing the model on a set of knife edges. The center of gravity was found to be at the 32.6 percent chord location for this configuration (pitch axis at 15 percent chord). The lead weight used to counterbalance the model weighed 1.02 lbs. Table A-1 lists the distances from the pitch axis where this weight was to be located to ensure that the center of gravity coincides with the pitch axis.

The inertia of the system was changed in the same manner as during the wind tunnel tests. Data were taken with the inertia weights at 2 and 6 inches from the pitch axis and with no weights. Table A-2 lists the natural frequencies and amplitude decays that were measured. The inertia and frictional torque values that were calculated from these data are also included in the table. The agreement between model inertia obtained from theoretical predictions and experimental results is within 2 percent. The inertia difference for the no weight and weight at 6 inches is in excellent agreement with predicted changes (see note in Table A-2). The experimentally measured values of inertia were used in the data analysis.

TABLE A-1. WEIGHT LOCATION FOR MODEL CENTER OF GRAVITY TO COINCIDE WITH PITCH AXIS

Pitch Axis Location, Percent Chord, Xp	Weight Location From Pitch Axis, -Vs (in.)
10.13	2.58
12.63	2.29
15.13	2.00
17.63	1.72
20.13	1.43

The frictional torque values determined from the test results are much less than the predicted aerodynamic moments associated with this model. For example, the aerodynamic moment about a pitch axis located 7.5 percent chord from the center of pressure would be 0.38 lb. inches, for an angle of attack of one degree and a velocity of 50 ft/sec. If the frictional torque values are substituted into the equation for aerodynamic moment, the resulting angle of attack due to this moment about zero angle is $\pm$ 0.18 degree. This implies that for the velocities of interest the angle of attack deviation due to frictional torque should be less than $\pm$ 0.18 degree.

TABLE A-2. VACUUM TEST RESULTS

Run Configuration	Measured Natural Frequency, ω cps	Measured Inertia (I_y), Slug ft^2	I_y/S	Amplitude Decay Rate	Frictional Torque lb.-in.
No weights	1.37	2.48×10^{-3}	1.35×10^{-3}	0.130	0.066
Weights at 2 inches	1.21	3.08×10^{-3}	1.68×10^{-3}	0.127	0.064
Weights at 6 inches*	0.81	6.90×10^{-3}	3.78×10^{-3}	0.124	0.063

* From theoretical calculation, the addition of weights at 6 inches from pitch axis should increase inertia by 4.3×10^{-3} slug ft^2. The difference in inertia for these two configurations is 4.42×10^{-3} slug ft^2.

The wing was also checked for twist deformations. Once again, the pitch axis was set at 15 percent chord during these tests. Total twist angles were measured by rigidly supporting the wing tip and applying moments at the support bar used to vary inertia. The results of this test indicated that the twist angle was less than 3/4 of a degree for predicted maximum aerodynamic moments. The results were used to correct the static-aerodynamic data that were obtained for this wing.

The flow field over the upper surface of the wing was observed visually by attaching tufts to the surface. The tufts were used to define the onset of stall, flow disturbances at the tunnel wall-wing root junction and flow disturbances of the wing support bracket at the 80 percent span location. The tufted wing is shown in Figure A-10. The tunnel air velocity was 50 ft/sec for these tests. A low tunnel air velocity was chosen because the effects would be more pronounced at lower speeds. The flow disturbances at the wall-model interface were apparent at about 8 degrees. The disturbance at the wall never extended outside the tunnel wall boundary layer, which is approximately 2 inches thick. The effects of the wall interface can be accounted for by assuming a reduction in the wing span (Ref. A-4). Based on the velocity profile through the boundary layer at the wall, a reduction in span of 1 inch was used in the data analysis.

The flow disturbance at the wire support bracket was not appreciable until an angle of attack of 10 degrees was reached. The effects of the wire were not accounted for in the data since they were minor in the angle of attack range of interest.

Onset of stall was noted at about 12 to 13 degrees and was oscillatory in nature. Also, it was observed that at higher angles of attack the flow disturbances near the tunnel wall and behind the support bracket became quite pronounced. For angles of attack between 0 and $\pm$ 10 degrees, the flow field over the upper surface was fairly uniform. Based on these results, the dynamic tests were limited to angles of attack between 0 and $\pm$ 10 degrees.

Data were obtained at various times during the dynamic test phase to ensure that the bearings were not deteriorating. The error in angle of attack was measured for tunnel wind speeds of 50, 80, and 120 ft/sec. The measurements were performed by first setting a trim angle of attack between 0 and $\pm$ 10 degrees and then physically disturbing the wing from trim and releasing it. The aerodynamic moment forced the wing back to either a new trim or the original trim angle. This was repeated a number of times to obtain an accurate estimate of the scatter band. All the data obtained was within a scatter band of $\pm$ 0.30 degrees.

Steady-state aerodynamic data were obtained for the pitch model at three tunnel velocities. These data are compared with published data to establish the validity of the results.

The aerodynamic moment as a function of angle of attack was measured by applying a known external moment and measuring the resulting angle of attack.

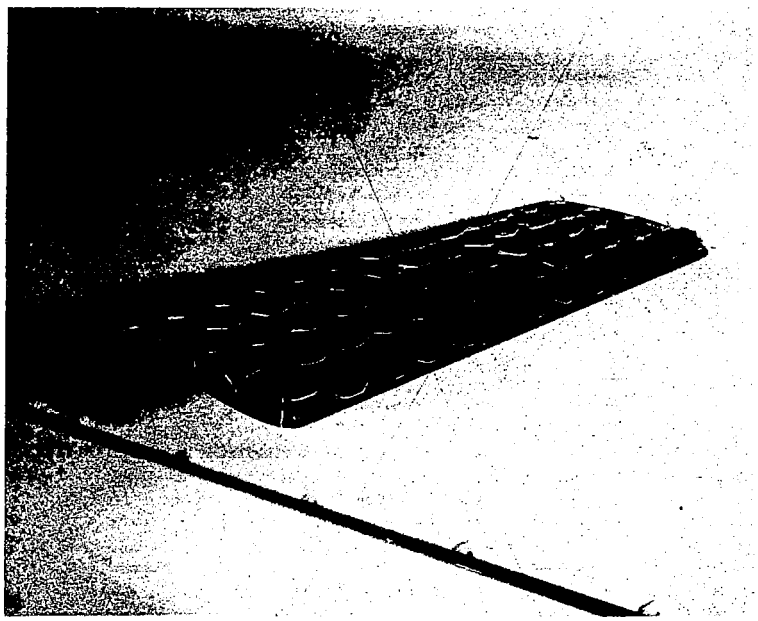

FIGURE A-10. PITCH MODEL INSTALLED IN TEST CABIN

The moment coefficient about some pitch axis is given by

$$C_{m_p} = \frac{M}{q'S'c} \quad , \tag{A-44}$$

where q' and S' are corrected values of tunnel dynamic pressure and wing area, and c is wing chord length. The moment, M, is given in terms of the applied force and distance from the pitch axis of the applied force by

$$M = Fr \cos \alpha \quad , \tag{A-45}$$

where r is equal to 0.5 feet, F is the applied weight, and α is the measured angle of attack.

Substituting Equation A-45 into Equation A-44 and assuming small angles (less than 10 degrees) gives

$$C_{m_p} = \frac{0.5F}{q'S'c} \quad . \tag{A-46}$$

The aerodynamic moment data for all the pitch axes can be compared if the moments are reference to a specific pitch axis location. Using the 10 percent pitch axis as the reference axis, moment data from the other pitch axes locations are transferred to the 10 percent by the following equation:

$$C_{m_{10\%}} = C_{m_p} \frac{\bar{X}'_{sm}}{\bar{X}_{sm}} \quad , \tag{A-47}$$

where $\bar{X}'_{sm}$ is the static margin for the 10 percent axis location and $\bar{X}_{sm}$ is the static margin for selected axis location. Figure A-11 is a plot of moment coefficient for all the data referenced to the 10 percent pitch axis. The angles of attack have been corrected for lift interference due to the tunnel walls. The moment data is within 15 percent of the data presented in Reference A-1. The results of these tests indicate that the model adequately simulates the NACA 0015 airfoil.

Since the aerodynamic moment was measured for three different pitch axes, the moment data was cross-plotted against pitch axis to estimate the location of aerodynamic center. The results are in general agreement with the results obtained in Reference A-1 and indicates that the aerodynamic center is between 19 and 23 percent chord. The static margin was calculated for the various model configurations using a value of 22.5 percent chord for the aerodynamic center.

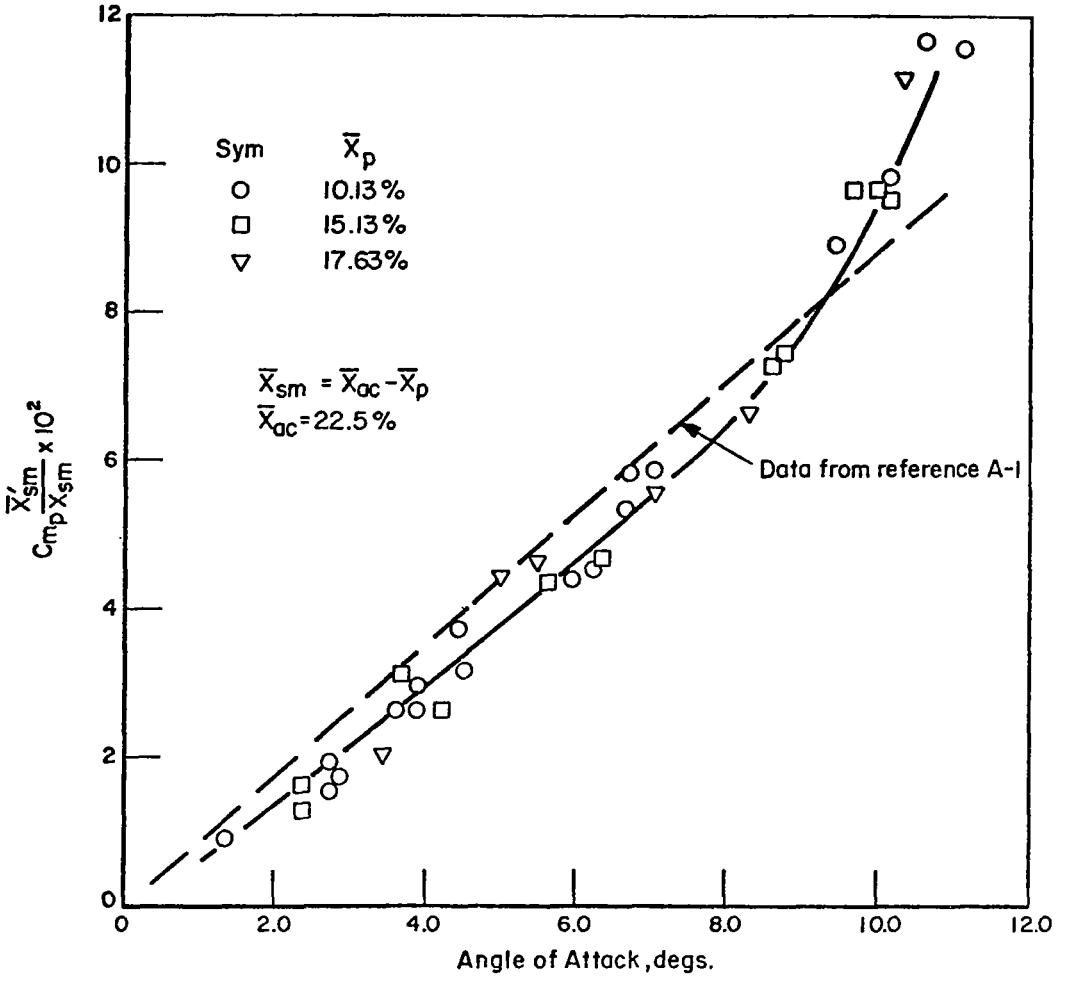

FIGURE A-11. MOMENT COEFFICIENT REFERENCED TO 10% PITCH AXIS

Yaw Model

A special calibration plate was designed to calibrate the potentiometers that were installed in the wing tips of this model. The potentiometers were found to be linear to within 1.0 percent for $\pm$ 10 degrees.

Tufts were taped to the wing panels to visually observe stall. The tunnel air velocity was adjusted to 80 ft/sec for the stall test. It was observed that stall occurred at about 11 to 12 degrees. Based on these results, panel angles of attack were limited to a maximum of 8 degrees during the yaw test.

The effect due to bearing force in each of the wing panels was measured in a similar manner that was followed in the pitch model test. Enough data were obtained to determine the maximum deviations in angle of attack due to these forces. The maximum deviation for both panels was found to be $\pm$ 0.35 degrees.

Prior to performing the yaw angle test, the panel deflections caused by selected tab angle settings was measured at zero yaw angle. The tunnel velocity for the initial tab angle test series was 80 ft/sec. Tab angles could be accurately set to within 1/4 degree. Figures A-12 and A-13 are plots of the individual panel angle of attack as a function of tab angle for tunnel velocities of 80, 120, and 160 ft/sec. Similarity of the panel response curves indicate that the two wing panels were geometrically similar. Symmetry of the response curves about zero tab angle indicates that the panels were symmetrical.

TEST PROCEDURE

The information presented in this section includes installation of the models and the procedure that was followed during the wing tunnel experiments. The section is subdivided into sections entitled "Pitch Model Test" and "Yaw Model Test".

Pitch Model Test

The model is shown installed in the test cabin in Figure A-10. The model pitch axis was aligned in the test section with the use of permanent reference points that are located in the side walls of the tunnel. The model pitch axis extended through the west tunnel wall and was attached to the model support mechanism on roller bearings. This mounting technique has two advantages: first, angle of attack can be measured by measuring the rotation of the pitch axis; and, secondly, the inertia and center of gravity of the wing can be varied from outside the tunnel. The pitch bar was isolated from the tunnel wall so that tunnel vibrations would not excite the model.

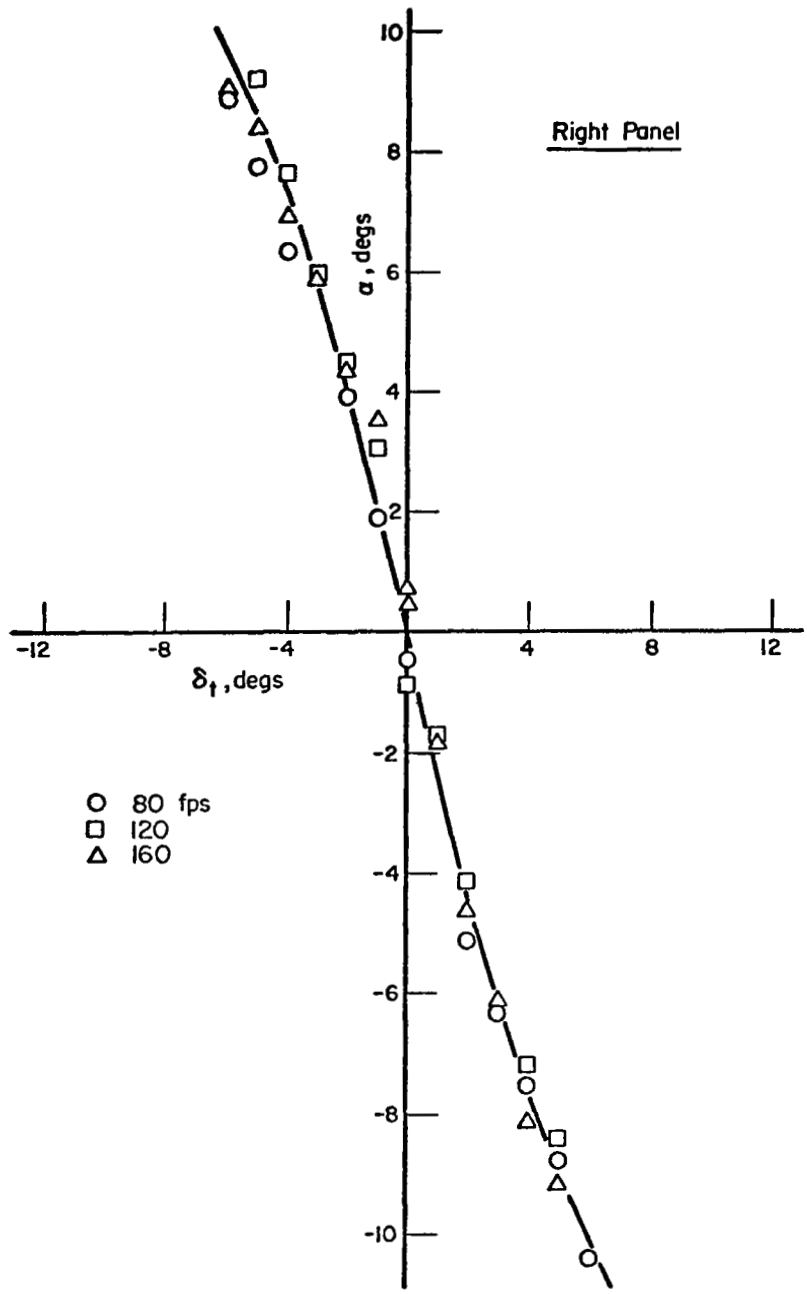

FIGURE A-12. RIGHT PANEL ANGLE OF ATTACK AS A FUNCTION OF TAB ANGLE

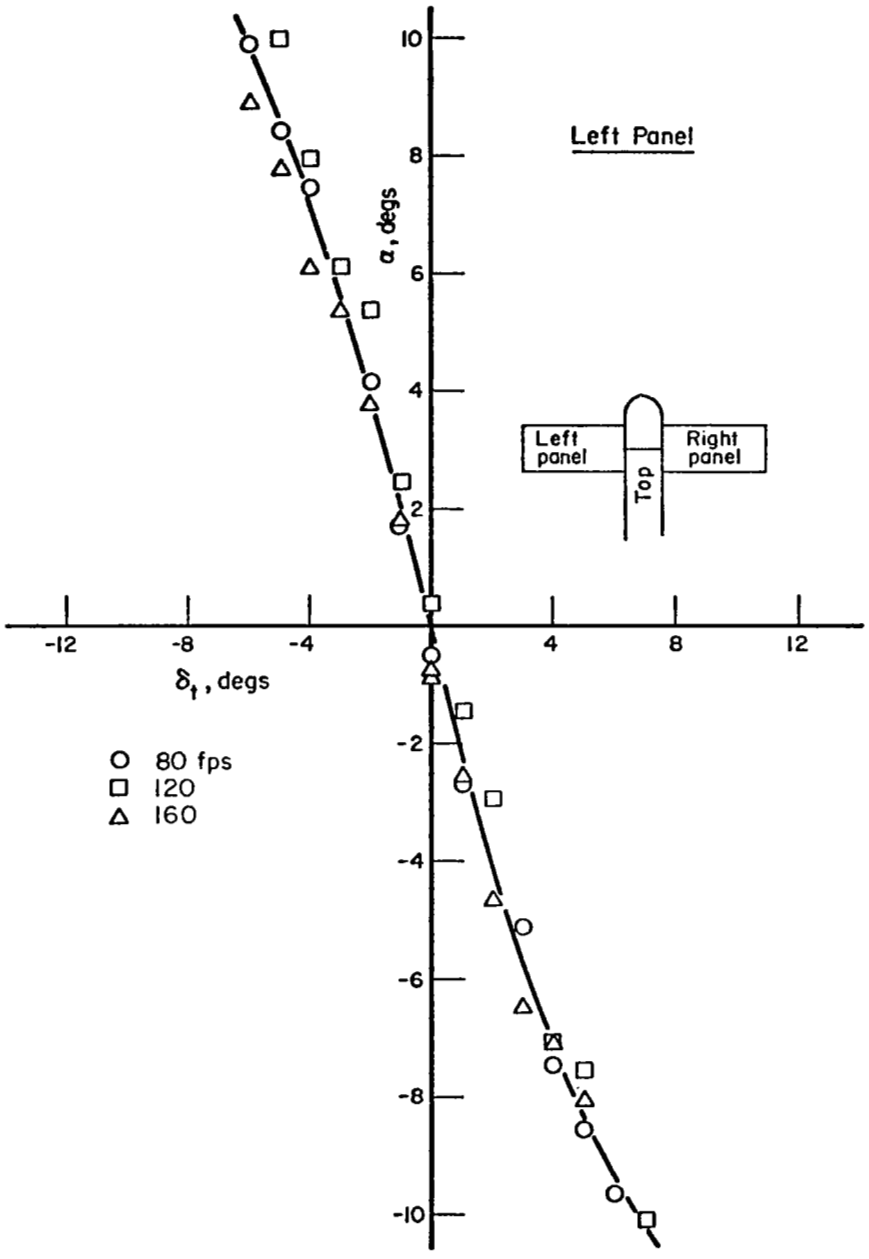

FIGURE A-13. LEFT PANEL ANGLE OF ATTACK AS A FUNCTION OF TAB ANGLE

Additional support wires were used to reduce wing deflections due to span-wise moments. The wires were attached to the model at the 75 percent span location. The wires were brought through small holes in the tunnel ceiling and floor and were attached rigidly to the building structure. Four independent wires were used so that alignment of the model pitch axis could be maintained when the wires were pulled taut.

The potentiometer signal, which indicated angular positions of the model, was recorded on a strip chart recorder. The maximum frequency response of this recorder is 100 cps. This response is well above the panel frequencies that were observed. The parameters that were varied during the dynamic test were:

- wind tunnel velocity
- wing inertia
- center of gravity of the wing
- pitch axis location.

The test matrix that was run included three tunnel velocities, three wing inertias, two center of gravity locations and three pitch axis locations. The test conditions that were run are listed in Table A-3.

The potentiometer was checked before and after every pitch axis change. This was accomplished by setting the wing at selected angles of attack (0, $\pm$ 10) and noting the potentiometer signal.

The dynamic tests were performed by disturbing the wing from its trim angle of attack by mechanically displacing it to $\pm$ 10 degrees. A mechanical holding device was used to ensure that the initial conditions (angular displacement and velocity) upon release were identical for all tests. It was determined during the shake-down test that it was impossible to hold the wing steady enough by hand at $\pm$ 10 degrees.

A few steady-state data points were repeated during the dynamic test, for each pitch axis setting and tunnel velocity for comparison with the calibration data. These spot checks were made to ensure that the model was not out of adjustment in any way.

Yaw Model Test

As stated earlier, the main support bar of this model was aligned in the tunnel using the tunnel wall reference points so that the model was actually vertical in the tunnel. The main support bar extended through a clearance in the tunnel wall. This bar was connected to the model support mechanism outside the

TABLE A-3. TEST MATRIX FOR PITCH MODEL

Run Number	Tunnel Velocity ft/sec	Model Configuration			Mass Parameter $\bar{I}$
		$\bar{X}_p$ % chord	I_y slug in.^{2}	α trim degrees	
13	120	10.13	.585	0	17.5
	120	10.13	.880	0	26.3
	120	10.13	1.205	-3.5	36.0
	120	10.13	1.625	-4.2	48.6
	120	10.13	1.625	+4.2	48.6
16	120	17.63	.363	0	10.8
	120	17.63	.518	0	15.5
	120	17.63	.983	0	29.4
	120	17.63	.426	-3.0	12.7
	120	17.63	1.237	-5.8	37.0
	120	17.63	.717	+6.5	21.4
	120	17.63	1.237	+6.7	37.0
17	120	15.13	.390	0	11.70
	120	15.13	.545	0	16.3
	120	15.13	1.010	0	30.2
	120	15.13	.487	-1.0	14.6
	120	15.13	1.264	-3.0	37.8
	120	15.13	.644	-4.0	19.3
	120	15.13	1.169	+8.0	35.0
	120	15.13	.869	+6.0	26.0
	120	15.13	1.489	+6.0	44.5
18	80	15.13	.487	0	14.6
	80	15.13	.441	0	13.2
	80	15.13	1.061	0	31.8
	80	15.13	.642	-1.0	19.2
	80	15.13	1.107	-1.0	33.1
	80	15.13	.869	-6.0	26.0
	80	15.13	.359	+4.0	10.7
	80	15.13	.869	+6.0	26.0
19	80	10.13	.625	0	18.7
	80	10.13	.780	0	23.4
	80	10.13	1.245	0	37.2
	80	10.13	.425	4.0	12.7
	80	10.13	1.045	4.0	31.3
	80	10.13	.458	3.0	13.7
	80	10.13	1.078	5.6	32.2
	80	10.13	1.325	-4.0	39.6

Run Number	Tunnel Velocity ft/sec	Model Configuration			Mass Parameter $\bar{I}$
		$\bar{X}_p$ % chord	I_y slug in.^{2}	α trim degrees	
20	80	17.63	.332	5.0	10.0
	80	17.63	.365	6.0	10.9
	80	17.63	.520	6.0	15.6
	80	17.63	.430	-4.0	12.9
	80	17.63	.585	-2.0	17.5
	80	17.63	1.050	-2.0	31.4
	80	17.63	.396	-3.0	11.8
	80	17.63	.551	-3.0	16.5
	80	17.63	1.016	-3.0	30.4
	80	17.63	.722	-7.0	21.6
	80	17.63	.997	-7.0	29.8
21	50	17.63	1.028	0	30.7
	50	17.63	.563	0	16.8
	50	17.63	.408	0	12.2
	50	17.63	.363	-5.0	10.9
	50	17.63	.518	-5.0	15.5
	50	17.63	.983	-5.0	29.4
	50	17.63	.430	-3.0	12.9
	50	17.63	.585	-3.0	17.5
	50	17.63	1.050	-3.0	31.4
	50	17.63	.442	5.0	13.2
	50	17.63	.562	5.0	16.8
	50	17.63	.597	5.0	17.8
22	40	15.13	.453	0	13.5
	40	15.13	1.073	0	32.1
	40	15.13	.608	0	18.2
	40	15.13	.390	4.0	11.7
	40	15.13	.545	4.0	16.3
	40	15.13	1.010	4.0	30.2
	40	15.13	.489	-3.0	14.6
	40	15.13	.644	-3.0	19.2
	40	15.13	1.109	-3.0	33.1
	40	15.13	.559	-6.0	16.7
	40	15.13	1.179	-6.0	35.2
	40	15.13	.724	-6.0	21.6
23	40	10.13	1.215	0	36.4
	40	10.13	.715	0	21.4
	40	10.13	.560	1.0	16.8
	40	10.13	1.180	1.0	35.3
	40	10.13	.456	6.0	13.6

Run Number	Tunnel Velocity ft/sec	Model Configuration			Mass Parameter $\bar{I}$
		$\bar{X}_p$ % chord	I_y slug in.^{2}	α trim degrees	
23	40	10.13	.611	6.0	18.3
	40	10.13	1.076	5.0	32.2
	40	10.13	.425	7.0	12.7
	40	10.13	.595	-1.0	17.8
	40	10.13	.750	-1.0	22.4
	40	10.13	.710	-4.0	21.2
	40	10.13	1.330	-4.0	39.8
	40	10.13	.785	-5.0	23.5

tunnel on roller bearings so the model could be rotated in the yaw direction. Zero yaw angle was established with reference to the tunnel floor and ceiling.

The instrumentation leads from the individual potentiometers in the wing tips were brought outside the tunnel through a center hole in the support bar. A strip chart recorder was used to record the potentiometer signals which represented angles of attack for the individual wing panels. The yaw angle was mechanically set by hand using a pointer and protractor. The pointer was attached to the support bar outside the tunnel and the protractor was fixed to the model support structure. A clamping arrangement was used to rigidly set selected yaw angles.

The yaw angle was varied over $\pm$ 12 degrees in increments of 2 degrees for various tab angles and three tunnel velocities (80, 120, and 160 ft/sec).

A total of 144 data points were run in this phase with additional points to check repeatability of the results.

Test Results

The results of the wind tunnel experiments for each of the models are presented in this section. The results of the pitch model will be presented first. Each of the traces were analyzed using techniques defined in Reference A-5 to obtain damping ratio and frequency response. A summary of the data is contained in Figure 3 of the main body of this report.

Yaw model results were recorded on strip charts. The individual panel angles of attack were recorded simultaneously and the yaw angle noted on each of the traces.

All of the data from the yaw tests indicated a linear relationship between panel angle of attack and yaw angle. The data from all the runs are plotted in Figure A-14. Panel angle of attack was referenced to panel trim angle at zero yaw in Figure A-14 so that all the data could be compared. All the data lie within $\pm$ 15 percent of an average linear variation.

The slope of the individual data curves were calculated and plotted in Figure A-15. The slope $\Delta\alpha/\Delta\beta$ is plotted as a function of trim angle at zero yaw, $\alpha_{\beta=0}$.

Data Reduction

As previously mentioned, the oscillatory responses of the pitch model were analyzed using standard methods found in Appendix III of Reference A-5. A discussion is found in the main body of this report.

For the yaw model, panel equilibrium is reached when, for zero sideslip,

$$C_{m_{\delta_t}} \delta_t + C_{m_{\delta_p}} \delta_p = 0$$

where

δ_t = control tab deflection, radians

δ_p = wing panel deflection, radians

$C_{m_{\delta_t}}$ = slope of panel pitching moment versus tab deflection

$C_{m_{\delta_p}}$ = slope of panel pitching moment versus panel deflection .

From Figures A-12 and A-13,

$$\left|\frac{\delta_p}{\delta_t}\right| \simeq 2 \quad . \tag{A-48}$$

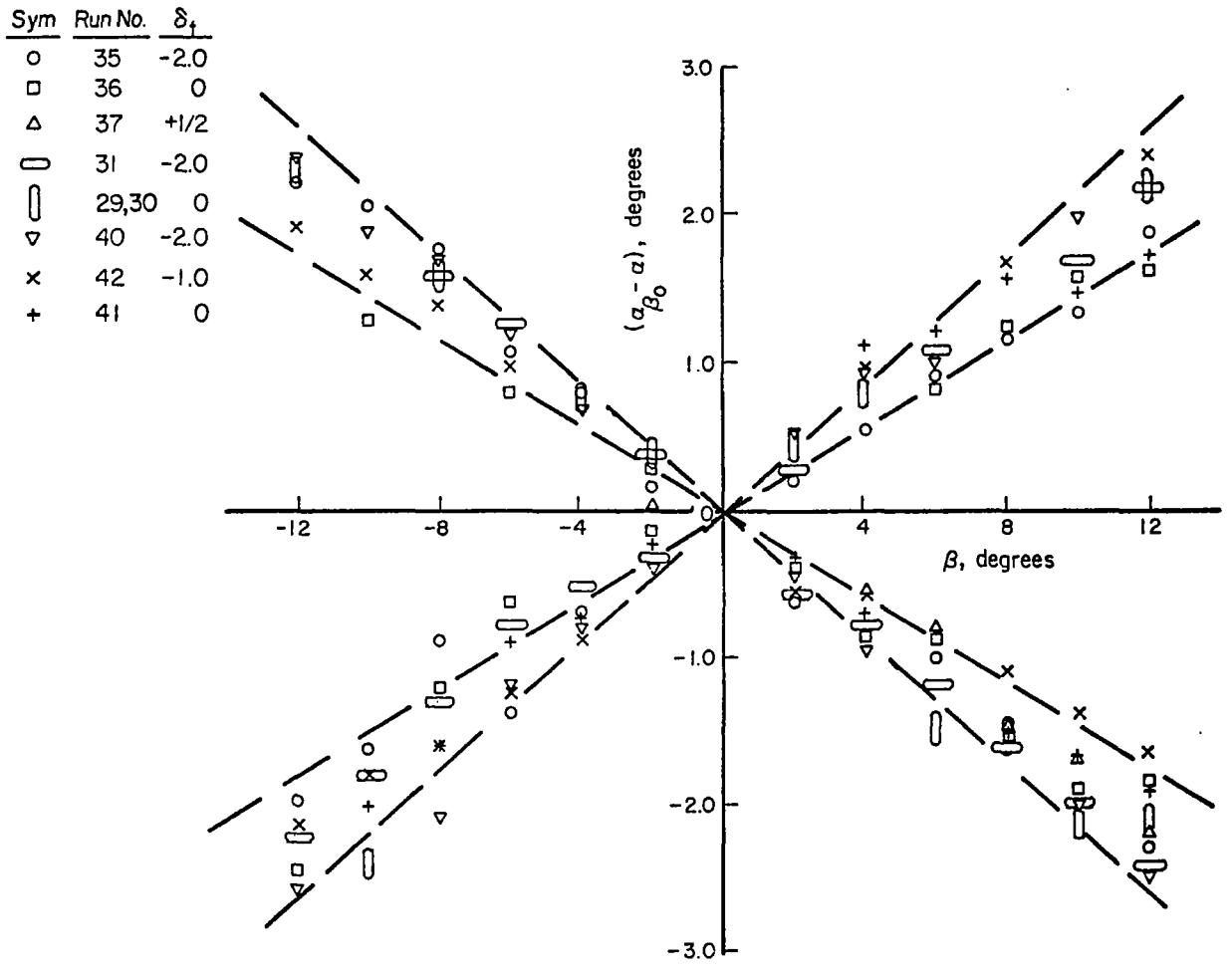

FIGURE A-14. WING PANEL DISPLACEMENT VERSUS SIDESLIP ANGLE

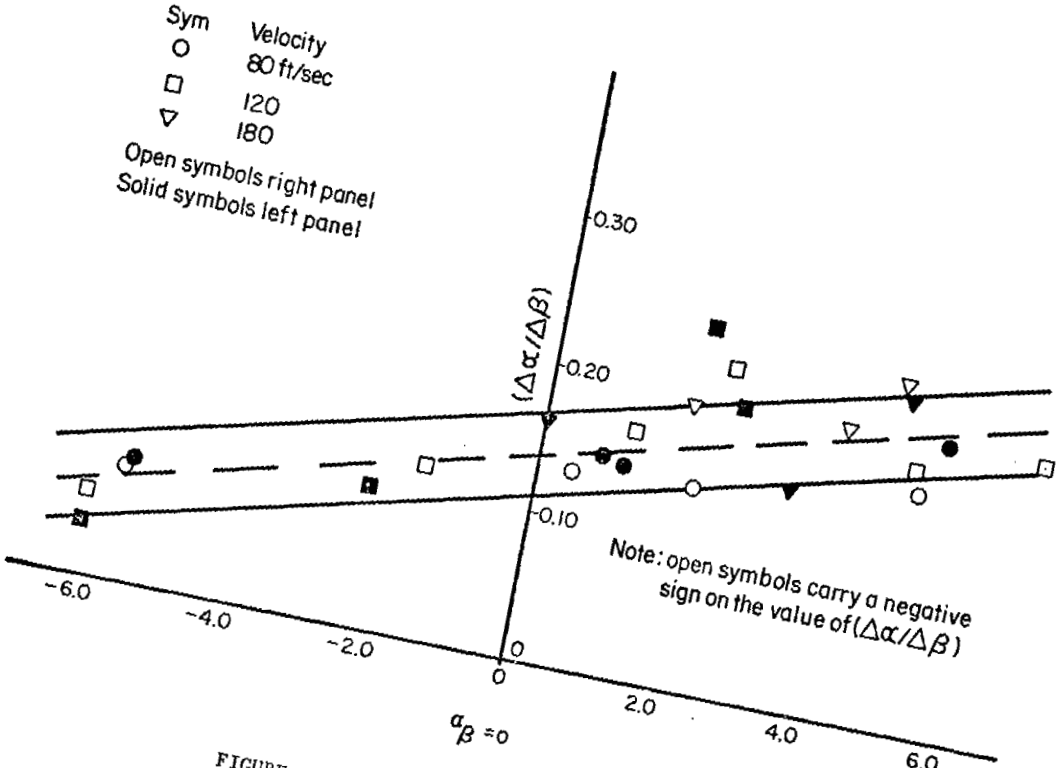

FIGURE A-15. SLOPE VARIATION WITH TRIM ANGLE

Using the lifting-line computer program described in Appendix B of Reference A-2, and the geometry of the yaw model wing panels, an effective hinge margin of 5.6 percent of chord was computed based on the above ratio. This would place the aerodynamic center of the wing panels at 20.6 percent chord, assuming that the hinge axis of the model was precisely located at 15 percent. This is in good agreement with the previously mentioned aerodynamic center positions extracted from the pitch model data, the variation being from 19 to 23 percent of chord.

The lifting-line program was used to compute values of the slope of life coefficient versus tab deflection and panel deflection, respectively. These values were then used to compute the slope of trimmed lift coefficient versus panel deflection. Then, using the trim curves of Figure A-12 and A-13, the trimmed lift curve slope of the free-panels was computed.

Using the average-slope line of Figure A-15, the variation of panel deflection with sideslip angle was then determined. This was, for the right wing panel,

$$\frac{\Delta\delta_p}{\Delta\beta} = - .231\ C_L - .162 \qquad \text{(A-49)}$$

The desired derivative, relating panel pitching moment to sideslip angle was then computed from,

$$C_{m_\beta} = - \frac{\left(C_{m_{R_{\delta_p}}} - C_{m_{R_{\delta_L}}} \right)}{2} \frac{\Delta\delta_p}{\Delta\beta} \quad . \qquad \text{(A-50)}$$

Where

$C_{m_{R_{\delta_p}}}$ = slope of right panel pitching moment due to right panel displacement

$C_{m_{R_{\delta_L}}}$ = slope of right panel pitching moment due to left panel displacement

C_{m_β} = slope of right panel pitching moment due to sideslip.

Values of $C_{m_{R_{\delta_p}}}$ and $C_{m_{R_{\delta_L}}}$ were computed from the lifting-line program and were -.183 and -.016, respectively. Substituting these values in Equation A-50 yielded the variation of C_{m_β} with sideslip,

$$C_{m_\beta} = -.0192\ C_L - .0135 \quad . \qquad \text{(A-51)}$$

References

A-1. Jacobs, E. N. and Sherman, A.: Airfoil Section Characteristics as Affected by Variations of the Reynolds Number. NACA Report 586, 1937.

A-2. Porter, Richard F. and Brown, Joe H., Jr.: Evaluation of the Gust Alleviation Characteristics and Handling Qualities of a Free-Wing Aircraft. NASA CR-1523, April, 1970.

A-3. Garner, H. C., Rogers, E. W. E., Acum, W. E. A., and Mashel, E. C.: Subsonic Wind Tunnel Wall Corrections. AGARD ograph 109, October, 1966.

A-4. Pope, Alan: Wind Tunnel Testing. 2nd Edition, John Wiley & Sons, New York, 1954.

A-5. Chalk, C. R., et al: Background Information and User Guide for MIL-F-8785B (ASG), Military Specification--Flying Qualities of Piloted Airplanes. AFFDL-TR-69-72, August, 1969.

APPENDIX B

MATHEMATICAL MODELS

Introduction

The equations of motion for free-wing aircraft were developed, for the controls-fixed case, in Appendix A of Reference B-4. These equations were first developed in complete nonlinear form and then linearized about a straight and level flight condition.

For the present analysis, only slight modifications were made to the original set of linearized equations; consequently, the development is not repeated here. On the other hand, some additional relations were developed for this study; specifically, the dynamic equations of motion of the longitudinal control system, and the equations used to simulate the takeoff and landing behavior of the aircraft.

The mathematical models discussed here required the estimation of numerous aerodynamic and inertial parameters. These were computed or obtained through many sources, notably References B-1, B-2, and B-3, as well as unpublished communications with the Cessna Aircraft Company and personnel at North Carolina State University, Department of Mechanical and Aerospace Engineering.

Symbols

The following symbols are used in this Appendix. More detailed definition of several of these quantities are found in Reference B-4. Those quantities defined explicitly in Equations B-8 are not repeated here.

C_e = chord length of control surface aft of hinge; feet

C_{h_α} = control surface hinge moment derivative with respect to angle of attack

C_{h_δ} = control surface hinge moment derivative with respect to control surface displacement

$C_{h_{\dot{\delta}}}$ = control surface hinge moment derivative with respect to rate of control deflection

C_p = gain constant, aileron deflection per unit roll rate, seconds

C_φ = gain constant, aileron deflection per unit roll rate angle

D_y = lateral path displacement, feet

e_e = location of control surface c.g. aft of control hinge, feet

g = acceleration of gravity, feet/sec^2

h = vertical path displacement, feet

I_s = moment of inertia of control column, slug-feet^2

I_{XX_T} = total moment of inertia about roll axis, slug=ft^2

I_{XY_P} = X - Y product of inertia of right wing panel, slug-ft^2

I_{XZ_T} = X - Z total product of inertia, slug-ft^2

$I_{y'}$ = moment of inertia of each wing panel about hinge axis, slug-ft^2

I_{YZ_P} = Y - Z product of inertia of right wing panel, slug-ft^2

I_{ZZ_T} = total moment of inertia about yaw axis, slug-ft^2

I_{δ_e} = combined moment of inertia of both control surfaces about their hinges, slug-ft^2

K_g = gearing ratio between control column and control surface displacement

K_θ = gain constant, elevator deflection per unit pitch angle

L = rolling moment, ft-lb

ℓ_h = distance from wing axis to control surface hinge, feet

M = pitching moment on fuselage, ft-lb

m_b = mass of bobweight, slugs

m_e = total mass of control surfaces, slugs

M_R = right wing panel pitching moment in lateral-directional equations, ft-lb

N = yawing moment, ft-lb

P = area of each free-wing panel, feet^2; and wing panel pitching moment in longitudinal equations, ft-lb

p = roll rate, radians/second

q = pitch rate, radians/second

r = yaw rate, radians/second

U = true airspeed, feet/second

u = dimensionless airspeed variable, $\Delta U/U$

V_g = vertical-gust velocity, feet/second

X = longitudinal force, lb

Y = lateral force, lb

Z = normal force, lb

α_f = inertial angle of attack of fuselage, angle between longitudinal axis and projection of inertial velocity vector in plane of symmetry, radians

β = inertial sideslip angle, angle between longitudinal axis and projection of inertial velocity vector in horizontal plane, radians

β_g = sideslip gust velocity, lateral gust velocity divided by airspeed

δ_a = aileron deflection, or asymmetric control surface deflection, numerically equal to displacement of right surface, radians

δ_e = elevator deflection, or symmetrical surface deflection, radians

δ_P = displacement angle of right wing panel with respect to fuselage axis, radians

$\delta_{t_R}, \delta_{t_L}$ = right and left control surface displacements, radians

θ = pitch angle of longitudinal fuselage axis with respect to horizon, radians

λ = Laplace operator, 1/second

φ = roll angle, radians

φ_g = rolling gust, 1/second

ψ = yaw angle, radians

Linearized Equations of Motion

Lateral-Directional Equations.- As derived in Reference B-4, the linearized set of equations describing the lateral-directional motion of the aircraft system is shown as Equation (B-1).

$$[B]\begin{bmatrix} \varphi \\ \Psi \\ \beta \\ \\ \delta_P \\ \delta_a \\ D_y \end{bmatrix} = \begin{bmatrix} -L_{p_w} \\ -N_{p_w} \\ 0 \\ \\ -M_{R_p} \\ 0 \\ 0 \end{bmatrix} \dot{\varphi}_g + \begin{bmatrix} -L_\beta \\ -N_\beta - N_r\lambda \\ -Y_\beta \\ \\ -2M_{R_\beta} \\ 0 \\ 0 \end{bmatrix} \beta_g \qquad \text{(B-1)}$$

The matrix of coefficients of the homogeneous equations [B], is given by Equation (B-2).

$$[B] = \begin{bmatrix} (-\lambda^2 + L_p\lambda) & (\frac{I_{XZ_T}}{I_{XX_T}}\lambda^2 + L_r\lambda) & L_\beta & 2(\frac{I_{XY_P}}{I_{XX_T}}\lambda^2 + L_{\delta_P}) & 2L_{\delta_{t_R}} & 0 \\ (\frac{I_{XZ_T}}{I_{ZZ_T}}\lambda^2 + N_p\lambda) & (-\lambda^2 + N_r\lambda) & N_\beta & 2(\frac{I_{YZ_P}}{I_{ZZ_T}}\lambda^2 + N_{\delta_P}) & 2N_{\delta_{t_R}} & 0 \\ (Y_p\lambda + \frac{g}{U}) & (Y_r - 1)\lambda & (-\lambda + Y_\beta) & 2Y_{\delta_P} & 0 & 0 \\ (\frac{I_{XY_P}}{I_{y'}}\lambda^2 + M_{R_p}\lambda) & \frac{I_{YZ_P}}{I_{y'}}\lambda^2 & 2M_{R_\beta} & (-\lambda^2 + M_{R_{\dot\delta}}\lambda + M_{R_{\delta_P}} - M_{R_{\delta_L}}) & (M_{R_{\delta_{t_R}}} - M_{R_{\delta_{t_L}}}) & 0 \\ (C_p\lambda + C_\varphi) & 0 & 0 & 0 & -1 & 0 \\ 0 & U & U & 0 & 0 & -\lambda \end{bmatrix} \qquad \text{(B-2)}$$

For simulation of the various linkages involved in the study of the passive mechanical stability augmentation schemes, appropriate additional elements were added, on an ad hoc basis to these fundamental equations.

As written, these equations include differential panel freedom. To simulate the rigid wing aircraft, without such freedom, all elements of the fourth column of matrix [B], with the exception of that in the fourth row, were set equal to zero. This effectively removed the influence of differential panel motion on the other variables.

A part of this investigation involved the assessment of control deflections required to maintain steady sideslip with constant heading. To accomplish this, the basic equations were modified to include the rudder control, and all rate and acceleration terms were set equal to zero. With rudder deflection considered as the independent variable, the static values of bank angle, sideslip, differential panel deflection, and aileron control deflection were obtained through the solution of Equation (B-3).

$$\begin{bmatrix} \varphi \\ \beta \\ \delta_P \\ \delta_a \end{bmatrix} = \begin{bmatrix} 0 & L_\beta & 2L_{\delta_P} & 2L_{\delta t_R} \\ 0 & N\beta & 2N_{\delta_P} & 2N_{\delta t_R} \\ \frac{g}{U} & Y_\beta & 0 & 0 \\ 0 & 2M_{R_\beta} & (M_{R_{\delta_P}} - M_{R_{\delta_L}}) & (M_{R_{\delta t_R}} - M_{R_{\delta t_L}}) \end{bmatrix}^{-1} \begin{bmatrix} -L_{\delta_R} \\ -N_{\delta_R} \\ -Y_{\delta_R} \\ 0 \end{bmatrix} \delta_R \qquad \text{(B-3)}$$

Longitudinal Equations.- The linearized set of equations describing the longitudinal motion of the aircraft, with controls fixed, in response to vertical gust velocities, was derived in Reference B-4 and appears below as Equation (B-4).

$$[A] \begin{bmatrix} \alpha_f \\ \theta \\ \delta_P \\ u \\ \delta_e \\ h \end{bmatrix} = \begin{bmatrix} -Z_{v_g} \\ -M_{\dot{v}_g}\lambda - M_{v_g} \\ -P_{v_g} \\ -X_{v_g} \\ 0 \\ 0 \end{bmatrix} V_{g_v} \qquad \text{(B-4)}$$

The matrix of coefficients [A] is,

$$[A] = \begin{bmatrix} (-Z_{\dot{\alpha}}\lambda + Z_{\alpha}) & (Z_{\dot{q}}\lambda^2 + Z_q\lambda) & (Z_{\ddot{\delta}_P}\lambda^2 + Z_{\dot{\delta}_P}\lambda + Z_{\delta_P}) & Z_u & Z_{\delta_e} & 0 \\ (M_{\dot{\alpha}}\lambda + M_{\alpha}) & (-\lambda^2 + M_q\lambda) & (M_{\ddot{\delta}_P}\lambda^2 + M_{\delta_P}) & 0 & 0 & 0 \\ (P_{\dot{\alpha}}\lambda + P_{\alpha}) & (P_{\dot{q}}\lambda^2 + P_q\lambda) & [(-1 + P_{\ddot{\delta}_P})\lambda^2 + P_{\dot{\delta}_P}\lambda + P_{\delta_P})] & P_{\dot{u}}\lambda & P_{\delta_e} & 0 \\ X_{\alpha} & X_{\theta} & X_{\delta_P} & -\lambda + X_u & 0 & 0 \\ 0 & K_{\theta} & 0 & 0 & -1 & 0 \\ -U & U & 0 & 0 & 0 & -\lambda \end{bmatrix} \qquad \text{(B-5)}$$

In Equation (B-5), as originally derived in Reference B-4, a simple algebraic expression was used to define the elevator (symmetrical control) displacement, as seen in the fifth row of the matrix. This was modified in the current study to include the dynamic characteristics of the longitudinal control system. This equation is,

$$-H_{\ddot{\delta}_e}\ddot{\delta}_e = H_{\dot{\delta}_e}\dot{\delta}_e + H_{\delta_e}\delta_e + H_{\dot{\alpha}}\dot{\alpha}, + H_{\alpha}\alpha + H_{\dot{q}}\dot{q} + H_q q + H_{\ddot{\delta}_P}\ddot{\delta}_P + H_{\delta_P}\delta_P + H_{com} \qquad \text{(B-6)}$$

where

$$H_{\ddot{\delta}_e} = = -\left(\frac{I_s}{K_g} + K_g I_{\delta_e}\right)$$

$$H_{\dot{\delta}_e} = \left(\frac{\rho U^2}{2} S_e C_e K_g\right) C_{h_{\dot{\delta}}}$$

$$H_{\delta_e} = \left(\frac{\rho U^2}{2} S_e C_e K_g\right) C_{h_{\delta}}$$

$$H_{\dot{\alpha}} = -x_b m_b - K_g m_e e_e \qquad \text{(B-7)}$$

$$H_{\alpha} = \left(\frac{\rho U^2}{2} S_e C_e K_g\right) C_{h_{\alpha}}$$

$$H_{\dot{q}} = -K_g m_e e_e \ell_h - I_{\delta_e} K_g$$

$$H_q = U(x_b m_b + K_g m_e e_e)$$

$$H_{\ddot{\delta}_P} = H_{\dot{q}}$$

$$H_{\delta_P} = \left(\frac{\rho U^2}{2} S_e C_e K_g\right) C_{h_{\alpha}}$$

The values of C_{h_δ} and C_{h_α} were obtained from Appendix B of Reference B-2. However, these values so obtained are two dimensional section data. To account for finite wing effects, a lifting line computer program was used to obtain correction factors for local flow effects on the C_{h_α} derivative. This was necessary because the local average angle of attack at the control surface depends not only on the free-stream angle of attack but wing panel and control surface deflections as well. The remaining hinge moment derivative, $C_{h_{\dot{\delta}}}$, was obtained from Reference B-5. The mass and inertia data for control elements were obtained by comparison with similar information contained in an unpublished communication from the Cessna Aircraft Company.

Takeoff and Landing Equations.- For the study of landing and takeoff dynamic behavior, several modifications and additions were made to the fundamental longitudinal set of Equation (B-4). Specifically, the reaction forces from contact with the runway surface were included in the vertical force and fuselage moment equations, the effect of the reduced downwash at the horizontal tail due to ground effect was included as was the weight moment caused by displacement of the fuselage assembly center of gravity from that of the total aircraft.

The landing gear forces were computed on the assumption that the landing gear behave as simple linear springs with a force proportional to the distance that the wheel would be below the runway level if the ground were not present.

The reduction in downwash caused by ground effect was taken from Appendix B.7 of Reference B-2.

References

(B-1) USAF Stability and Control DATCOM. Air Force Flight Dynamics Laboratory, Wright-Patterson Air Force Base, Ohio, Revised November 1965.

(B-2) Etkin, Bernard: Dynamics of Flight. John Wiley and Sons, Inc., New York, 1959.

(B-3) Dommasch, D. O., Sherby, S. S., and Connolly, T. F.: Airplane Aerodynamics. Putnam Publishing Corporation, New York, Third Edition, 1961.

(B-4) Porter, Richard F. and Brown, Joe H., Jr.: Evaluation of the Gust Alleviation Characteristics and Handling Qualities of a Free-Wing Aircraft. NASA CR-1523, 1970.

(B-5) Cohen, Doris: A Theoretical Investigation of the Rolling Oscillations of an Airplane With Ailerons Free. NACA Report 787, 1943.

APPENDIX C

REVIEW OF GUST ALLEVIATION SYSTEMS FOR COMPARISON WITH THE FREE-WING AIRCRAFT'S PERFORMANCE

Longitudinal turbulence may induce both pitch accelerations and normal accelerations. Depending on the position in the aircraft where these accelerations are recorded, the pitching motion may be sensed as normal acceleration. In the comparisons to follow, the acceleration reductions are with reference to a mid-position in the aircraft or to the c.g. location. In one case, the work that is discussed deals with only an isolated wing.

It is convenient to classify longitudinal gust alleviation systems according to which of the following techniques is used:

(1) Pitching the entire aircraft by use of the elevators to maintain constant angle of attack

(2) Variation of wing incidence to maintain constant angle of attack

(3) Operation of flaps, spoilers, or deflectors to offset the lift increments on the wing.

A broad classification of the free-wing concept might place it in category (2). However, its gust alleviation performance is considerably superior to that achievable by direct mechanical control of the wing incidence.

Table C-1 shows a comparison of some notable examples of analyses and experiments on longitudinal gust alleviation systems. The correlation of these examples with the suggested classifications is as follows:

Example I	Class 3
Example II	Class 1
Example III	Use of fixed spoilers is a minor method and is outside the three major classes of systems.
Example IV	Class 2
Example V	Class 3
Example VI	Class 3.

It is difficult to find examples of substantial analytical and experimental efforts in which quantitative RMS load factor reduction results are presented and in which the principal objective was to reduce the RMS load factor.

Two of the examples presented in Table C-1 are based only on discrete gust models and thus only peak load reduction results are available. These results are of little value in judging the potential of these methods for improved ride quality. They are included only for their possible value in giving a general idea of the effectiveness of the methods.

A bibliography of the literature that was surveyed in compiling these examples is included at the end of this section. The sources of the results reported in Table C-1 are also indicated in the Table.

From Table C-1, it may be noted that the greatest reduction in RMS load factor, achieved in an experimental flight investigation, was 35 percent. This is the Example I case, which was a relatively long-term and widely reported NACA program. Many NACA TN publications have dealt with the various phases of that program. The figure of 60 percent reduction in load factor has been reported in some non-NACA sources as representative of the overall results. This is misleading for, as will be noted in Table C-1, the 60 percent reduction is in peak load factor and is at the natural frequency of the test aircraft.

No evidence was found in this survey to indicate that a RMS load factor reduction better than 35 percent has ever been demonstrated. Example V, based on analyses rather than flight experiments, suggests the possibility of 50-70 percent RMS reductions. Of course, theoretically, 100 percent reduction is possible. The Example V study report cites several potential problems and practical constraints that would likely prevent the achievement of the 50-70 percent reduction. The Example V analytical model involved an advanced technology, low-wing loading STOL aircraft system and modern stability augmentation system techniques. If this system comes to a hardware demonstration stage, it might prove a new performance for RMS load factor reduction. However, it is not likely to greatly exceed the 35 percent reduction that has been demonstrated in the Example I and Example VI cases.

Each of the three classes of gust alleviation methods has some characteristic limitation. These limitations are summarized as follows:

Class I

(a) High values of pitching velocity are required, resulting in large accelerations at points away from the c.g. position

(b) Prediction of lag effects.

Class 2

(a) Longitudinal control problem--see Example I comments, Table C-1

(b) Large control forces are required to directly control wing incidence

(c) Prediction of lag effects.

Class 3

(a) Longitudinal control problem as in Class 2

(b) Downwash from conventional flaps produces additional adverse pitching motion since its action on the tail can be in the same direction as the gust

(c) Prediction of lag effects.

TABLE C-1. COMPARISONS OF GUST ALLEVIATION SYSTEMS

Description of Gust/Acceleration Alleviating Device	Source of Results Reported	Nature of Gust or Turbulence Encounter	Percent Reduction in Peak Load Factor	Percent Reduction in RMS Load Factor	Notable System or Exp. Procedure Lim.	Comments
I. Wing flaps are actuated by an automatic control system to oppose changes in lift due to angle of attack changes produced by gusts. The system is actuated by indication of an angle of attack vane located on a probe ahead of the aircraft. Part of the elevator was geared to the wing flaps to balance pitching moment. Two motion alleviation configurations were used: (1) Fixed auxiliary flaps--The in-board flaps (auxiliary flaps) remained fixed. (2) Actuated auxiliary flaps--The in-board flaps were geared to move in opposition to the main flaps to produce downwash to compensate for the gust velocity at the tail.	Flight investigations by NASA using Beech C-45. Experimental and theoretical results are reported in NASA TN D-643, NACA TN 2415, NACA TN 2416, NASA TN D-532, NACA TN 3612, NACA TN 3597, NACA TN 3746.	Experimental flight investigation. Flights were made in clear air turbulence at 2,500 ft at 130 Kt.	60 percent at the natural frequency of the airplane (0.6 cps). 40 percent at 2 cps. Using an accelerometer as the gust sensor rather than the gust vane, the normal acceleration alleviation was reported to be about 40-45 percent.	Flap type (1) 16 percent Flap type (2) 35 percent	Was effective in reducing the accelerations at all frequencies up to about 2 cps. Typical of systems that operate flaps or other controls to offset lift--if the lift increment due to change of angle of attack is eliminated, the elevators will be ineffective for producing a change in the direction of the flight path.	In the system described, deflection of the control column produced a deflection of the in-board elevator and through the automatic control system, a flap deflection to produce lift and pitching moment in the desired direction to change attitude. The vane, sensing the change in angle of attack, caused the flaps to return to neutral so that the aircraft remained at the new angle of attack.
II. A mass-overbalanced viscously restrained elevator is used to alter the longitudinal motions (increasing the short-period damping ratio) induced by the direct effect of the gust loads.	Analytical investigation for a lightly damped airplane model flying at M = 0.7 at S.L. NACA TN 4173.	Continuous random turbulence/PSD techniques.	48 percent at the natural frequency of the airplane.	20 percent	Simplified representation of response to unit step gust input is not valid for all aircraft. No provision was made for elevator control. Elevator occupied the entire exposed trailing edge of the tail.	Aircraft model had relatively large pitching inertia and static margin. In a sharp edge gust the system has negligible effect until the first a_n peak has been reached.
III. Fixed spoilers, 2.5 percent of the local chord in height, extending along 90 percent of the wing span and mounted perpendicular to the upper surface of the wing at a position 12 percent of the local chord aft of the leading edge.	Aircraft model tested in Langley gust tunnel. NACA 0012 airfoil. NACA TN 1753 (1948) 88 fps forward speed and 10 fps max. gust velocity.	Sharp edge gust Gradient gust with gradient distance of 12 chords.	No reduction, response slightly worse with the spoilers than without. 30 percent	Not determined.	Spoiler caused appreciable pitching motion in the gusts but the incremental angle of pitch was small at the time of maximum a_n and the correction for its effect did not radically change the acceleration increments.	Test covered only the possibilities of an up-gust. Action in a negative gust is subject to conjecture--probably not so effective.

TABLE C-1. COMPARISONS OF GUST ALLEVIATION SYSTEMS
(Cont'd)

Description of Gust/Acceleration Alleviating Device	Source of Results Reported	Nature of Gust or Turbulence Encounter	Percent Reduction in Peak Load Factor	Percent Reduction in RMS Load Factor	Notable System or Exp. Procedure Lim.	Comments
IV. Torsionally flexible wing with the torsion axis ahead of the locus of the section aerodynamic centers. The torsion axis was located at 10 percent of the chord.	NACA TN 802 (1941)	Sharp edge gust Gradient gusts with gradients from 0 to 16 chord lengths. Velocity maximum = 6 fps.	5 percent 17 percent for gust with gradients between 7 and 15 chord lengths.	Not determined.	Experiment is outdated. Wing concept is not pertinent to modern requirements. Very low tunnel speeds (60 fps) were used.	Control problems not considered.
V. A 30 percent chord elevator and 18 percent chord rear segment of a full span, double slotted flap were used to affect gust alleviation in the longitudinal mode under the control of a special ride smoothing stability augmentation system. The SAS system consists of two feedback loops: vertical acceleration driving the aft segment of the full span flap and pitch angular rate driving the elevator for satisfactory handling qualities. Gain scheduling, as a function of flight condition, may be required, but it was not included in this analytical study. A lateral SAS load reduction system was also evaluated in this study.	Low-Wing-Loading STOL Transport Ride Smoothing Feasibility Study, The Boeing Company, Final Report, D3-8514-2, January, 1971.	Continuous random turbulence/PSD techniques.	Not determined.	Descent: 70 percent at mid-craft position. Landing Approach: 44 percent at mid-craft position. Cruise: 50 percent at mid-craft position.	Pitch rate response would not meet handling qualities requirements without the pitch rate feedback. Structural flexibility may prevent the reduction in rms load factor to the extent indicated with the rigid body model used in this study. Control system nonlinearities during heavy turbulence can cause excessive structural loading and reduced stability.	Discrete 1-cos gusts were also used in the analyses to define surface rate and displacement limit effects. The results of the study dealing with the lateral loads reduction indicate the possibility of 60 percent maximum reductions (rms) at the aft position in the aircraft.
VI. A concept originated by a Frenchman, René Hirsch, circa 1938. A flight article was built and flown successfully in 1954. Many flights were made thereafter and Hirsch was promoting the concept as late as 1967. In this scheme the horizontal tail is freed to rotate about a chordwise hinge axis. When the gust forces on the horizontal tail cause it to move, a trailing edge wing flap is driven through mechanical linkage to offset the lift increment. Hirsch recognized the importance of the long wave length gusts and conceived the idea of a rearward sensor (the horizontal tail) instead of a forward sensor. Hirsch's demonstration aircraft was a small twin engine aircraft having this feature and others for lateral gust alleviation. This involved movable wing tips linkad to the rudder.	NASA SP 258 (1971) DOCAERO No. 42, January, 1957, pp 13-28. DOC-AIR-ESPACE, No. 105, July, 1967, pp 41-56.	Experimental flight investigation.	Not determined.	Results are similar to Example I. 35 percent	The mechanical complexity of the system is an apparent limitation although Hirsch's aircraft did make numerous successful flights.	Hirsch's system has the advantage that the stability problem described in I above is corrected automatically. An up elevator input will generate a downward force on the horizontal tail, driving it down. Through the mechanical linkage the wing flap will be driven down, increasing wing lift and giving proper control.

BIBLIOGRAPHY

C-1. Donely, P. and Shufflebarger, C.C.: Test of a Gust Alleviating Flap in the Gust Tunnel. NACA TN 745, 1940.

C-2. Shufflebarger, C. C.: Test of a Gust-Alleviating Wing in the Gust Tunnel. NACA TN 802, 1941.

C-3. Mickelboro, H. C.: Evaluation of a Fixed Spoiler as a Gust Alleviator. NACA TN 1753, 1948.

C-4. Phillips, W. H. and Kraft, C. C., Jr.: Theoretical Study of Some Methods for Increasing the Smoothness of Flight Through Rough Air. NACA TN 2416, 1951.

C-5. Kraft, C. C., Jr. and Assadourian, A.: Experimental Study of an Angle-of-Attack Vane Mounted Ahead of the Nose of an Airplane for Use as a Sensing Device for an Acceleration Alleviator. NACA TN 2415, 1951.

C-6. Boucher, R. W. and Kraft, C. C., Jr.: Analysis of a Vane-Controlled Gust-Alleviation System. NACA TN 3597, 1956.

C-7. Kraft, C. C., Jr.: Initial Results of a Flight Investigation of a Gust-Alleviation System. NACA TN 3612, 1956.

C-8. Croom, D. R., Shufflebarger, C. C., and Huffman, J. K.: An Investigation of Forward-Located Fixed Spoilers and Deflectors as Gust Alleviators on an Upswept-Wing Model. NACA TN 3705, 1956.

C-9. Cooney, T. V. and Schott, R. L.: Initial Results of a Flight Investigation of the Wing and Tail Loads on an Airplane Equipped with a Vane-Controlled Gust Alleviation System. NACA TN 3746, 1956.

C-10. Hirsch, René: Studies and Tests of an Airplane Gust Absorber. DOCAERO, no. 42, Jan. 1957, pp 13-28.

C-11. Phillips, W. H.: Loads Implications of Gust-Alleviation Systems. NACA TN 4056, 1957.

C-12. Croom, D. R. and Huffman, J. K.: Investigation at Transonic Speeds of Deflectors and Spoilers as Gust Alleviators on a 35° Swept Wing Transonic-Bump Method. NACA TN 4006, 1957.

C-13. Croom, D. R. and Huffman, J. K.: Investigation at Low Speeds of Deflectors and Spoilers as Gust Alleviators on a Model of the Bell X-5 Airplane With 35° Swept Wings and on a High-Aspect-Ratio 35° Swept-Wing Fuselage Model. NACA TN 4057, 1957.

C-14. Tobak, M.: On the Minimization of Airplane Responses to Random Gusts. NACA TN 3290, 1957.

C-15. Croom, D. R. and Huffman, J. K.: Investigation of Deflectors as Gust Alleviators on a 0.09-Scale Model of the Bell X-5 Airplane With Various Wing Sweep Angles From 20° to 60° at Mach Numbers from 0.40 to 0.90". NACA TN 4175, 1957.

C-16. Crabill, N. L.: An Analytical Investigation of the Gust-Alleviating Properties of a Simple Pitch Damper. NACA TN 4173, 1957.

C-17. Hunter, P. A., Kraft, C. C., Jr., and Alford, W. L.: A Flight Investigation of an Automatic Gust-Alleviation System in a Transport Airplane. NASA TN D-532, 1961.

C-18. Schott, R. L. and Hamer, H. A.: Flight Investigation of Some Effects of a Vane-Controlled Gust Alleviation System on the Wing and Tail Loads of a Transport Airplane. NASA TN D-643, 1961.

C-19. Hurt, George J., Jr.: Rough-Air Effect on Crew Performance During a Simulated Low-Altitude, High-Speed Surveillance Mission. NASA TN D-1924, 1963.

C-20. Hirsch, René: Gust Absorption on Aircraft and Results of Flight Tests of an Experimental Device. DOC-AIR-ESPACE, no. 105, July 1967, pp 41-56.

C-21. Rustenburg, J. W.: A Technique for the Evaluation of Aircraft Ride Quality. ASD-TR-68-18, June 1968.

C-22. Anon.: Low Wing Loading STOL Transport Ride Smoothing Feasibility Study. The Boeing Company, D3-8514-2, January 1971.

C-23. Phillips, W. H.: Gust Alleviation, Performance and Dynamics of Aerospace Vehicles. NASA SP-258, 1971.

APPENDIX D

INERTIAL COUPLING MOMENTS ON FREE-WING PANELS

Introduction

Although inertial coupling effects are generally insignificant for light aircraft, the unique pitch freedom of the wing panels prompted a limited investigation of these phenomena. The objective was to assess the probability of encountering large inertial pitching moments which might overpower the control surfaces and result in an uncontrollable maneuver.

Symbols

$I_{x'}$, $I_{y'}$, $I_{z'}$ = moments of inertia of right wing panel measured in panel axis system, slug-feet^2

$I_{x'y'}$, $I_{x'z'}$, $I_{y'z'}$ = products of inertia of right wing panel measured in panel axis system, slug-feet^2

m_p = mass of one wing panel, slugs

p,q,r = roll rate, pitch rate, and yaw rate, respectively, measured about aircraft body axes, radians/sec

R = radial distance from spin axis to aircraft center of gravity, feet

U,V,W = components of aircraft velocity along the aircraft body axes, feet/second

$\bar{X}$ = longitudinal coordinate of hinge axis measured in aircraft body axes system, feet

X'_{cg}, Z'_{cg} = longitudinal and normal coordinates of wing panel center of gravity measured in panel fixed axes, feet

$\bar{Z}$ = coordinate of hinge axis measured along aircraft Z body axis, feet

α = angle of attack between airflow and reference chord line of wing section, radians

δ_e = symmetrical control surface displacement, positive trailing edge down, radians

δ_p = displacement of wing panel with respect to fuselage, positive leading edge up, radians

θ = pitch angle of longitudinal fuselage axis with respect to horizon, radians

φ = roll angle, positive right wing down, radians

Ω = angular rate about spin axis, radians/second

$\omega_{x'}$, $\omega_{z'}$ = rolling and yawing angular rates, respectively, measured in panel fixed axes, radians/second

Wing-Panel Pitching Equation

The development of the complete nonlinear equations of motion is contained in Appendix A of Reference D-1. Using that development, the pitching moment equation for each wing panel can be expressed as Equation (D-1).

$$
\begin{aligned}
&I_{y'}(\ddot{\delta}_p + \dot{q}) = \\
&\left.\begin{aligned}
&m_p(X'_{cg}\sin\delta_p - z'_{cg}\sin\delta_p)\left[\dot{U} + (\dot{q}+rp)\bar{Z} - (r^2+q^2)\bar{X} - rV + qW\right] \\
&+ m_p(X'_{cg}\cos\delta_p + z'_{cg}\sin\delta_p)\left[\dot{W} - (\dot{q}-pr)\bar{X} - (q^2+p^2)\bar{Z} - qU + pV\right]
\end{aligned}\right\} \text{Offset c.g.} \\
&\left.\begin{aligned}
&+ I_{y'z'}\left[(\dot{r}-qp)\cos\delta_p + (\dot{p}+qr)\sin\delta_p\right] \\
&+ I_{x'y'}\left[(\dot{p}+qr)\cos\delta_p - (\dot{r}-qp)\sin\delta_p\right] \\
&+ I_{x'z'}\left[(r^2-p^2)\cos 2\delta_p + 2pr\sin 2\delta_p\right]
\end{aligned}\right\} \text{Products of Inertia} \\
&+ (I_{z'}-I_{x'})\left[(p^2-r^2)\frac{\sin 2\delta_p}{2} + pr\cos 2\delta_p\right] \Big\} \text{Gyroscopic Precession} \\
&+ \text{Aerodynamic Pitching Moment}
\end{aligned}
\qquad \text{(D-1)}
$$

The moments and products of inertia are with respect to a right-hand orthogonal coordinate system, fixed to the wing panel. The origin is on the wing hinge axis and lies in the plane of symmetry of the aircraft. The x' axis coincides with the reference chord line of the wing panel with positive direction toward the leading edge. The positive y axis coincides with the hinge axis of the right wing panel. This coordinate system is identical to the panel axis system described in Appendix A of Reference D-1.

Product of Inertia Terms.- Equation (D-1) applies to either the right or left wing panel, the difference being that the $I_{y'z'}$ and $I_{x'y'}$ products of inertia are of opposite sign for the left panel. It follows that if the wing panels were to have differential freedom (which they are not, in this investigation) the only asymmetric effect of inertial coupling would be through the influence of these terms.

For the primary case of interest, differential panel freedom is not permitted. Consequently, the effects of the aforementioned product of inertia terms can be disregarded because the contributions on the left and right panels are of opposite sign and counteract each other.

The remaining product of inertia term only exists if the reference chord line is not a principal axis. This term is always small and can be eliminated entirely either by proper mass arrangement or by a slight rotation of the reference x' axis to coincide with the chordwise principal axis of the average wing cross section.

Elimination of the product of inertia terms permits concentration on the two remaining inertial terms; those due to wing panel imbalance about the hinge line and the gyroscopic term.

Normal Maneuvers

Because of the complexity of the individual terms of Equation (D-1), generalization of the magnitudes is difficult; these being dependent upon the maneuver being conducted and the wing panel deflection with respect to the aircraft body axis.

Gyroscopic Term.- Attention is first confined to the gyroscopic term since it cannot be eliminated even if the wing panels are balanced. In fact, for near-planar object such as wing panels,

$$I_{z'}-I_{x'} \cong I_{y'} \qquad \text{(D-2)}$$

Physically, this term represents the tendency for the wing panels to assume an attitude in which either the rolling or yawing velocity (with respect to the wing panels themselves) is zero. This observation is certainly not obvious from Equation (D-1), but it is clear from Equation (A-19) of Reference D-1. In that reference, the term is given by

$$\text{Moment increment} = (I_{x'} - I_{z'})\omega_{x'}\,\omega_{z'} \qquad \text{(D-3)}$$

In Equation (D-1), the simplified form of Equation (D-3) has been modified to express the angular rates in terms of airplane body axis rates and panel deflection with respect to the fuselage longitudinal axis. This was done to provide a better means of estimating the potential magnitudes of the pertinent factors.

First of all, it was established that the aircraft roll and yaw rates experienced in normal maneuvers in light aircraft are not of sufficient magnitude to cause a significant effect from this term. Consider for example a full deflection aileron roll. A typical maximum roll rate for an aircraft of this type is not expected to exceed 90 deg/sec. In addition, the wing panel deflection could be expected to be reasonably small; but, taking the worst hypothetical case with $\delta p = 45$ degrees, but no yawing rate, the pitching moment caused by the entire term would be about 8.35 ft-lb for the selected nominal aircraft.

Furthermore, in normal maneuvers, the largest products of rolling and yawing rates take place in climbing or descending turns. Considering a spiral maneuver with the pitch angle at 45 degrees, the maximum product occurs at limit load factor at the maneuvering speed* of the aircraft. The resulting panel pitching moment is less than 2 ft-lb.

Wing-Panel Imbalance.- For those terms in Equation (D-1) which depend on wing panel imbalance, larger inertial moments are possible. Again assuming a roll rate of 90 degrees per second, the vertical displacement of the hinge axis from the aircraft c.g., for the nominal aircraft, would cause a centrifugal effect producing wing pitching moments of the order of 3.1 ft-lb per inch of panel c.g. displacement from the hinge axis, if the panel displacement is small such that $\cos\delta_p \simeq 1$.

Fortunately, the aerodynamic pitching moment dominates. The aerodynamic pitch stiffness of each wing panel at the cruise condition is about 130 ft-lb per degree. At the absolute minimum speed, with the reduced effective hinge margin with slats extended, the aerodynamic moment per degree is only about 13 ft-lb, but even this value is more than sufficient to dominate the gyroscopic term.

*The maneuvering speed is defined here as the lowest equivalent airspeed at which it is possible to reach the design limit load factor of +3.8 g's.

To envision the most extreme adverse condition, perhaps the most significant inertial effects in normal operations could be encountered if the aircraft suffered a sharp lateral gust upset at minimum speed and no corrective aileron control was used to stop the roll. If the panels are balanced in the clean configuration, the panel c.g. would be slightly forward of the hinge axis with slats extended. This displacement is expected to be small, perhaps one inch. If the assumed lateral upset produced a steady roll rate of 90 deg/sec, as used in the previous example, the inertial moment would scarcely be noticeable.

Autorotational Maneuvers

The largest angular rates, and presumably the most pronounced inertial coupling effects, are experienced in autorotational maneuvers (spins and snap rolls) for aircraft in the class being considered.

Although it is most unlikely that the free-wing aircraft could be brought to a complete stall, a prerequisite for the type of motion considered in this section, the analysis could not be considered complete without a cursory examination of the panel pitching moments if such a condition were experienced.

For this purpose, it was assumed that the aircraft was in a steady spinning motion about a vertical spin axis (dynamically, a snap roll is a similar maneuver, so no loss of generality is involved). In this maneuver, the angular rates about the aircraft body axes are:

$$p = -\Omega \sin\theta$$

$$q = \Omega \sin\varphi \cos\theta \qquad \text{(D-4)}$$

$$r = \Omega \cos\varphi \cos\theta$$

In a steady spin, the pitching rate is generally small because the bank angle (φ) is small. Furthermore, the primary inertial term of interest is the gyroscopic effect which does not depend upon the pitch rate. For these reasons, the analysis was simplified by assuming zero bank angle, resulting in:

$$p = -\Omega \sin\theta$$

$$q = 0 \qquad \text{(D-5)}$$

$$r = \Omega \cos\theta$$

Gyroscopic Term.- Equations (D-5) may be substituted into the gyroscopic term of Equation (D-1); and, using the relations below,

$$(\alpha - 90^o) = \theta + \delta_p \tag{D-6}$$

$$I_{z'} - I_{x'} = I_{y'} \tag{D-7}$$

The gyroscopic term then becomes,

$$\text{Gyroscopic moment} = I_{y'} \frac{\Omega^2}{2} \sin 2\alpha \tag{D-8}$$

If Equation (D-8) is plotted versus angle of attack, four equilibrium angles of attack will be noted. Only two of these are stable, as indicated by the negative slopes at angles of attack of $\pm 90^o$ in Figure D-1.

For a rate of spin of 1 revolution per second, the maximum magnitude of the gyroscopic moment for the selected nominal aircraft is only,

$$I_{y'} \frac{\Omega^2}{2} = 134. \text{ ft-lb} \tag{D-9}$$

Physically, the gyroscopic term tends to rotate the wing panels into a plane normal to the axis of spin ($\alpha = \pm 90^o$), with no preference as to whether or not the leading edge of the wing is pointed toward or away from the spin axis. The other two positions of equilibrium are at $\alpha = 0$ and $\alpha = 180$ degrees, but these are unstable under the effect of this inertial term alone.

Fortunately, the aerodynamic pitching moment completely dominates the gyroscopic term, even at very low dynamic pressure. The wing panel is only stable, under the influence of the aerodynamic moment, at the angle of attack commanded by the control surface deflection. Particularly in the range of useful lift coefficients (relatively small angles of attack), the gyroscopic moment is insignificant, even in this rapid spinning maneuver.

Wing Panel Imbalance.- Unlike the gyroscopic term, the wing panel imbalance effect depends upon the radius of the spin. In the offset c.g. terms of Equation (D-1), it can be shown that the factors containing $\bar{X}$ and $\bar{Z}$ represent the contribution of these quantities to the radial distance from the spin axis to the hinge line. The analysis is greatly simplified if these quantities are ignored, implying that the difference in radial distance from the spin axis, R, is the same for the airplane center of gravity and the hinge axis.

Since the offset of the wing c.g. normal to the chord line is bound to be very small, only the chordwise displacement, X'cg, is considered. After appropriate substitutions similar to those made previously, the pitching moment contribution is,

$$\text{Imbalance moment} = -m_P X'_{cg} R\Omega^2 \cos\alpha \qquad \text{(D-10)}$$

The radial distance, R, is difficult to estimate with precision, but it is usually a fraction of the span of the airplane (ref. D-2). For this analysis, it was chosen as 10 feet. Again using one revolution per second as the spin rate, the maximum value of the offset c.g. term is 214. ft-lbs per inch of displacement from the hinge axis. Furthermore, this maximum value occurs at zero angle of attack as shown in Figure D-2.

As mentioned previously, the wing panel should be balanced with slats retracted, but with slats extended, X'_{cg} will have a positive value; and, from Equation (D-10), the effect of this offset is a tendency for the wing panel to rotate to a plane normal to the axis of spin with the leading edge pointed away from the spin axis. This can be seen in Figure D-2 where the only stable equilibrium, as indicated by the negative slope, is at an angle of attack of -90 degrees.

Total Effect of Combined Moments.- Despite the rather severe nature of the prescribed spinning maneuver, the aerodynamic control power is more than adequate to bring the wing panels out of stall even at an assumed low airspeed of 59 knots.

Figure D-3 shows the inertial and aerodynamic contributions as well as the total pitching moment variation with angle of attack. For the inertial terms, the curves of Figures D-1 and D-2 were combined, with a mass imbalance of one slug foot (X'_{cg} = 1.9 inches forward of the hinge axis). The control surface deflection of -8.3 degrees was selected to establish an arbitrary trim angle of attack of 10 degrees to demonstrate the ability of the aerodynamic moments to overpower the inertial effects.

References

(D-1) Porter, Richard F., and Brown, Joe H., Jr.: Evaluation of the Gust Alleviation Characteristics and Handling Qualities of a Free-Wing Aircraft. NASA CR-1523, 1970.

(D-2) Duncan, W. J.: The Principles of the Control and Stability of Aircraft. Cambridge University Press, 1952.

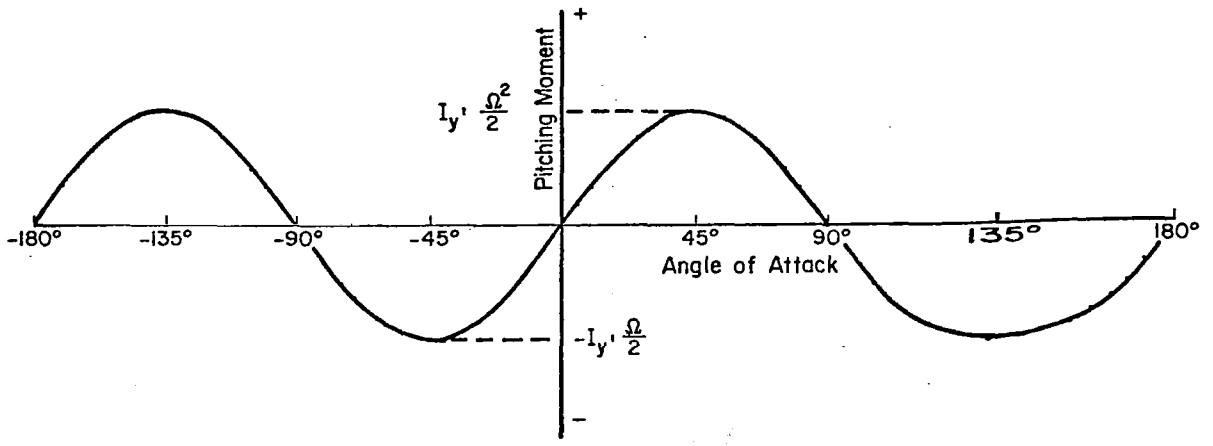

FIGURE D-1. GYROSCOPIC WING PITCHING MOMENT IN STEADY SPIN

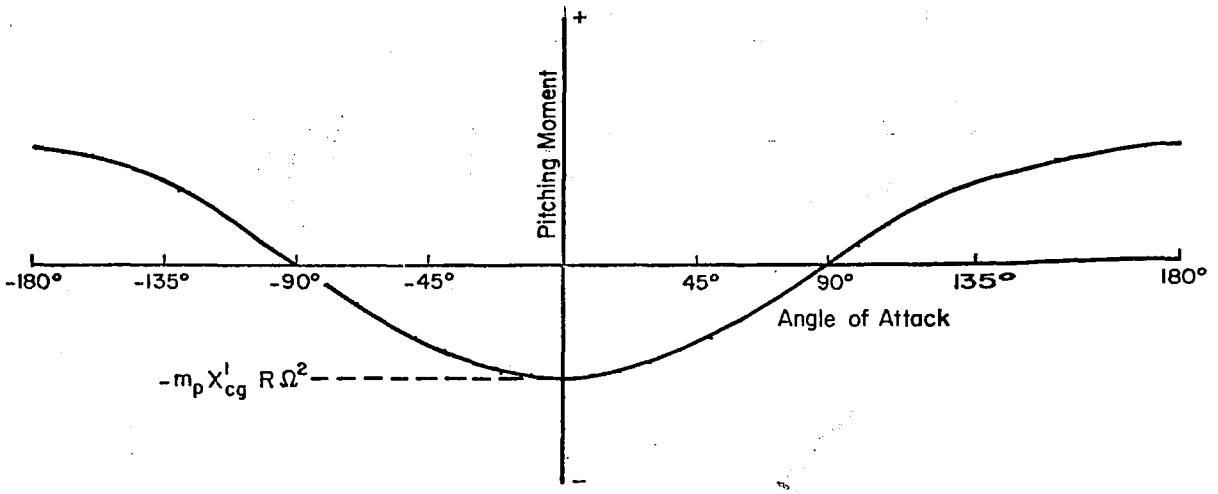

FIGURE D-2. WING PITCHING MOMENT CAUSED BY IMBALANCE ABOUT HINGE AXIS, STEADY SPIN